The Dissertation Committee for Jacob Michael Goran Certifies that this is the approved version of the following dissertation:

The Bioelectrochemistry of Enzymes and their Cofactors at Carbon Nanotube and Nitrogen-Doped Carbon Nanotube Electrodes

Committee:

Keith J. Stevenson, Supervisor

Richard M. Crooks

Mary J. Kirisits

Adrian T. Keatinge-Clay

Jennifer S. Brodbelt

The Bioelectrochemistry of Enzymes and their Cofactors at Carbon Nanotube and Nitrogen-Doped Carbon Nanotube Electrodes

by

Jacob Michael Goran, B.A.; B.S.

Dissertation

Presented to the Faculty of the Graduate School of

The University of Texas at Austin

in Partial Fulfillment

of the Requirements

for the Degree of

Doctor of Philosophy

The University of Texas at Austin

May 2014

Dedication

To my parents, William and Jennifer Goran

Acknowledgements

I would like to acknowledge those grads/post-docs who have overlapped with me during my time in the Stevenson Lab, but have since moved on: Jing Wu, Marisa Sheffer, Srinivas Beeram, Katie Walker, Salome Ngatia, Nick Delone, and Cori Atkinson. A special thanks to Jaclyn Wiggins-Camacho who not only taught me the nanotube way, but has always been available for my questions. To the post-docs Sankar Murugesan, Alex Veneman and Tony Dylla, we all got to Austin about the same time, I thank you for sharing your time, energy, and wisdom. To the lifting crew from the Crooks group: Jim Loussaert, Paul DeGregory, Kyle Knust, Morgan Anderson, and especially Stephen Fosdick, thanks for many fruitful discussions. I have had the opportunity to work with some very bright undergraduates such as Sandra Mantilla and Ethan "Huy" Phan. I give a special thanks to Carlos Favela for working so hard, your publication record speaks for itself. To Daniel Redman and Nellymar Membreno, thanks for allowing me to talk your ears off, and breaking up the day with random musings. To my Johnston cousins Will Hardin and Tyler Mefford, keep that Perovskite research train a moving. To my old cubicle roomie, Kjell Schroder, a chipotle lunch. Donald Robinson, your wife did a great job decorating your desk! Radhika Dasari, Cardinal Village will always have a special place in my heart. In the spirit of Katie Walker, I wish Matthew Charlton and Janine Elliott the best of luck with PPFs. To the post-docs Jonathon Duay and Aoife O'Mahony, we now all have electrode arrays in common. Ian Rust, I am glad to see you are picking up the enzyme work, may there be many fruitful investigations in your future. I have enjoyed my time here, especially working on projects with others. To Keith, thanks for your guidance, and the whiskey shot when I joined your lab.

The Bioelectrochemistry of Enzymes and their Cofactors at Carbon Nanotube and Nitrogen-Doped Carbon Nanotube Electrodes

Jacob Michael Goran, Ph. D.

The University of Texas at Austin, 2014

Supervisor: Keith J. Stevenson

This dissertation explores the electrochemical behavior of enzymes and their cofactors at carbon nanotube (CNT) and nitrogen-doped carbon nanotube (N-CNT) electrodes. Two common types of oxidoreductases are considered: flavin adenine dinucleotide (FAD)-dependent oxidases and nicotinamide adenine dinucleotide-dependent (NAD^+)-dehydrogenases. Chapter 1 presents the oxygen reduction reaction (ORR) at N-CNT electrodes as a way to electrochemically measure enzymatic turnover at the electrode surface. The unique peroxide pathway at N-CNT electrodes, which catalytically disproportionates hydrogen peroxide (H_2O_2) back into oxygen, provides an increased ORR current directly proportional to the rate of enzymatic turnover for H_2O_2 producing enzymes, even in an oxygen saturated solution. Biosensing of L-lactate using the increased ORR current is demonstrated using L-lactate oxidase. Chapter 2 explores the surface bound electrochemical signal of FAD when FAD-dependent enzyme or free FAD is allowed to spontaneously adsorb onto the CNT/N-CNT surface. Specifically, the origin of the enzymatically generated FAD signal and the rate constant of the electron

transfer are elucidated. Chapter 3 continues the discussion of the cofactor FAD by demonstrating its use as an informative surface specific redox probe for graphitic carbon surfaces. Primarily, FAD can be used to determine the electroactive surface area and the relative hydrophobicity/hydrophilicity of graphitic surfaces. Chapter 4 changes gears to NAD^+-dependent dehydrogenases by investigating the electrocatalytic oxidation of NADH at N-CNTs in comparison with conventional carbon electrodes or nondoped CNTs. Biosensing of glucose through the oxidation of NADH is demonstrated using glucose dehydrogenase adsorbed onto the N-CNT surface. Chapter 5 continues the discussion of NAD^+-dependent dehydrogenases by addressing the reaction kinetics of NADH oxidation at N-CNTs as a tool to measure the enzymatic reduction of NAD^+.

Table of Contents

List of Tables

List of Figures

CHAPTER 1

Amperometric Detection of L-lactate using Nitrogen-Doped Carbon Nanotubes modified with Lactate Oxidase*

1.1 INTRODUCTION

Ever since the pioneering work of Clark and Lyons in 1962, electrochemical biosensing schemes have incorporated the inherent selectivity of enzymes.[1] Initial studies electrochemically measured oxygen (O_2), a cofactor for many enzymatic reactions, but the variability and limitations of O_2 levels caused a shift towards the enzymatic byproduct, hydrogen peroxide (H_2O_2). Unfortunately, large overpotentials are necessary for the direct detection of H_2O_2 by either oxidation or reduction at the electrode surface.[2–5] In order to lower the operating potential, additional peroxidases[6–12] and/or redox mediators[13–18] have been employed. Electrochemical enzyme biosensors that measure a change in O_2 or H_2O_2 are classified as first generation biosensors. Redox mediators, which shuttle electrons between the enzyme's active center and the electrode, provide the basis for second generation biosensors. Although these first and second generation biosensors are still the most widely used and studied, there is a need to develop third generation biosensors where the enzyme's active center has a direct electrical connection to the transducer. Third generation biosensors would operate close to the redox potential of the enzyme, eliminating the need for diffusional redox mediators, peroxidases, or additional redox shuttles for signal transduction. While certain immobilized enzymes have exhibited direct electron transfer characteristics,[11,12,19–22] most schemes suffer from slow electron transfer kinetics, and inefficient utilization of active enzymes, due to the

*Portions of this chapter were published in Goran, J. M.; Lyon, J. L.; Stevenson, K. J. *Anal. Chem.* **2011**, *83*, 8123-8129. (Lyon supplied the initial idea, Stevenson supervised this work)

inaccessibility of the redox active site.[22,23] Steps have been taken to overcome these barriers, such as novel approaches to "wire" the enzyme's active center to promote facile electron transfer processes via a redox hydrogel,[24–27] conducting polymer, [28–32] or reconstituted enzyme[33,34] methods.

Carbon nanotubes (CNTs) are a relatively recent addition to vast array of biosensing schemes and materials, but possess attractive physicochemical properties such as their unique electronic structure, high electronic conductivity, and increased resistance to surface fouling.[35] Additionally, the rigidity of CNTs have been reported to facilitate direct electron transfer between the enzyme's active site and the electrode.[36–43] CNTs have also displayed intrinsic electrocatalytic behavior towards common enzymatic byproducts such as H_2O_2 or dihydronicotinamide adenine dinucleotide (NADH).[3,35,44–46] The electrocatalytic behavior of CNTs is often attributed to their edge plane character, which facilitates fast electron transfer kinetics.[47–51] The inclusion of heteroatoms, such as nitrogen, creates turbostratic disorder, further increasing the edge plane character of CNTs.[52] Thus, heteroatom doped CNTs and nitrogen-doped CNTs (N-CNTs) in particular have received considerable attention for biosensor applications.[37,53,54] Our group has developed synthetic procedures for N-CNTs and assessed their unique properties.[55–59] We have also demonstrated that the oxygen reduction reaction (ORR) at N-CNTs proceeds through a peroxide pathway,[60,61] where a fast catalytic disproportionation of peroxide provides an alternative to the traditional peroxidase-based detection schemes.[62] In this chapter, we report the use of N-CNTs as a "peroxidase mimetic" for biogenic analyte detection in lieu of the peroxidase or redox mediating approaches. We note here that though we refer to our N-CNTs as a peroxidase mimetic, they do not truly mimic a peroxidase-catalyzed reduction pathway, i.e., they do not reduce hydrogen peroxide to

water via a 2-electron transfer. Instead, the N-CNTs are used to detect hydrogen peroxide at a low potential through a catalytic feedback mechanism associated with the ORR.[62] The effectiveness of this biosensing scheme, including necessary figures of merit, is demonstrated herein with lactate oxidase.

1.2 Results and Discussion

1.2.1 Enzyme and Chemicals

Lactate oxidase (from *Pediococcus sp*. E.C. 1.1.3.2, lyophilized powder at 40 U/mg) and L-cysteine (≥98%) were purchased from Sigma-Aldrich. L-(-)-lactate acid lithium salt (99%), uric acid (99+%), L-(+)-ascorbic acid (99+%), and 4-acetamidophenol (98%) were purchased from Acros Organics. Bis(cyclopentadienyl)iron (ferrocene, 99%) was obtained from Alfa Aesar. Tetrabutylammonium bromide (TBABr) was purchased from Fluka Analytical (>99.0%). Sodium phosphate dibasic (Na_2HPO_4), sodium phosphate monobasic (NaH_2PO_4), and H_2O_2 (30 wt% in H_2O) were purchased from Fisher. Nafion® 117 Solution (5 wt% in lower aliphatic alcohols) and α-D-glucose were purchased from Aldrich.

1.2.2 CNT/N-CNT Preparation

CNTs/N-CNTs were produced in-house via a floating catalyst chemical vapor deposition (CVD) technique using a quartz tube housed inside of two adjacent single-zone tube furnaces (Carbolite Model HST 12/35/200/2416CG) as previously described.[52,60,62] A customized LabVIEW program interfaced the furnaces, two electronic gas mass flow controllers (MKS type 1179A), and a programmable syringe pump (New Era Pump Systems NE-1000). Ferrocene, used as the growth catalyst, was dissolved in either *m*-xylene (nondoped) or pyridine (N-doped) at a concentration of 20 mg mL^{-1}. The

ferrocene precursor solution was placed in a gastight glass syringe (Hamilton 81320), which was fitted into a programmable syringe pump. The syringe pump was connected to the quartz tube via stainless steel lines, which also introduced argon (Ar) and either hydrogen (H_2, nondoped) or ammonia (NH_3, N-doped) via the gas mass flow controllers. After an initial Ar purge (200 sccm for 15 minutes), the second furnace was heated to either 700 °C (nondoped) or 800 °C (N-doped). Upon reaching temperature, the first furnace was heated to either 150 °C (m-xylene) or 130 °C (pyridine), whereby the programmable syringe pump introduced the precursor solution at a rate of 0.1 mL min^{-1}, along with either H_2 (nondoped) or NH_3 (N-doped) at a total gas flow rate (including Ar) of 575 sccm. Nitrogen doping levels were selected based upon the flow rate of NH_3 as previously described.[52] Once 1 mL of the precursor solution was pumped into the heated quartz tube (10 minutes), flow of the precursor solution and the co-injected gas was stopped. Ar continued to flow at a rate of 200 sccm, in order to cool the resulting multiwalled carbon nanotubes along the inner wall of the quartz tube (in the second furnace).

1.2.3 Lactate Biosensor Construction

Biosensor construction parameters were optimized for L-lactate signal sensitivity (shown in the supporting information). The 7.4 at.% N-CNTs were used to prepare the biosensors, since they had the highest current response to H_2O_2 (Table 1). N-CNTs were stored in airtight vials prior to use, and used within two weeks of synthesis to minimize oxidation effects. A 2 mg mL^{-1} nanotube solution in absolute ethanol was sonicated for 2 hours to ensure a homogeneous mixture. 12 μL of the N-CNT/ethanol mixture was drop cast on a 0.5 cm diameter glassy carbon (PINE Instruments AFE2M050GC) rotating disk electrode (RDE), and allowed to dry for 15 minutes. This time duration allowed N-CNTs

to dry only partially; completely dry nanotubes regained a hydrophobic character and thus made subsequent aqueous additions difficult. 5 μL of a 0.5 U LOx μL^{-1} solution (solution activity was based off the manufacturer's assay) in 0.1 M sodium phosphate buffer (SPB) at pH 7.0 was drop cast on the partially dry nanotubes creating a N-CNT/LOx mixture. The N-CNT/LOx mixture was again allowed to partially dry before 2 μL of a modified Nafion® solution was drop cast on top of the mixture. Nafion® was modified with tetrabutylammonium bromide (TBABr) to improve the biocompatibility of the perfluorosulfonated ionomer by increasing the pore size and decreasing the local acidity of the enzyme's environment.[63] A 3:1 ratio (moles of TBABr to moles of sulfonic acid sites)[63,64] was mixed with the 5 wt.% Nafion® solution and diluted to 0.075 wt.% in pure ethanol. The constructed electrode was allowed to dry completely (about 15-30 min in air at room temp) before a final coat of 2.5 μL of the modified Nafion® was applied. CNT/N-CNT modified electrodes were also made without enzyme, exactly as outlined above, with 5 μL of SPB replacing the 5 μL of LOx solution. These electrodes were used to determine the ORR peak positions (E_p) and the H_2O_2 sensitivity to CNTs and N-CNTs. Electrodes were used within 30 minutes of construction and stored in SPB at 4 °C for subsequent investigations.

1.2.4 Cyclic Voltammetry and Chronomaperometry

Electrochemical experiments were performed using an Autolab™ PGSTAT30 potentiostat interfaced with Autolab™ GPES software (version 4.9). A five neck 125 mL glass cell was outfitted with a 0.5 cm diameter glassy carbon (GC) rotating disk electrode. The electrode was polished with 0.05 μm alumina slurry on microcloth (Buehler) and sonicated in 18.2 MΩ water prior to use. A 0.1 M SPB (pH 7.0) was used as the supporting electrolyte (100 mL for all experiments). All cyclic voltammetry (CV)

was performed with a quiescent solution. For rotating disk experiments, a PINE Instruments AFMSRX analytical rotator was set at a rotation rate of 1000 rpm. Aliquots of H_2O_2 or L-lactate were injected directly into the stirred solution using a pipette. Electrode assemblies were not cycled (to remove the electroactive $Fe^{2+/3+}$ species remaining from CNT/N-CNT synthesis) prior to chronoamperometric or steady state kinetic experiments. All experiments were conducted using a Hg/Hg_2SO_4 reference electrode (CH Instruments, +0.64 V vs. SHE; +0.40 vs. SCE; +0.44 vs. Ag/AgCl) and a Au wire counter electrode.

1.3 RESULTS AND DISCUSSION

1.3.1 Oxygen Reduction Reaction at N-CNT Electrodes

The first electrochemical step for oxygen reduction at both CNTs and N-CNTs involves the two-electron reduction of O_2 to produce hydrogen peroxide/hydroperoxide (H_2O_2/HO_2^-)*, as shown in equation 1.1.

$$O_2 + H_2O + 2e^- \rightarrow HO_2^- + OH^- \qquad (1.1)$$

This first step may be followed either by a second two-electron electrochemical reduction step with HO_2^- to produce OH^- (eq. 1.2),

$$HO_2^- + H_2O + 2e^- \rightarrow 3\ OH^- \qquad (1.2)$$

or, by a rapid chemical step associated with the decomposition (disproportionation) of HO_2^- to regenerate O_2 and form OH^- (eq. 1.3).

---

* We note that since the pK_a of hydrogen peroxide is 11.62, the principal form at neutral pH is hydrogen peroxide and not hydroperoxide; however, in order to maintain continuity and simplicity, we also note that the disproportionation rate of hydrogen peroxide is the same in both basic and neutral pH conditions.[29] In this context, hydroperoxide and hydrogen peroxide will be used synonymously.

$$2\ HO_2^- \leftrightarrow O_2 + 2\ OH^- \qquad (1.3)$$

At CNTs, the electrochemical reduction to OH^- occurs by successive two-electron electrochemical reduction steps (eq. 1.1 and eq. 1.2); whereas at N-CNTs the electrochemical reduction to OH^- occurs by a two-electron electrochemical reduction of O_2 to HO_2^-, followed by the chemical step associated with the disproportionation of HO_2^- (eq. 1.1 and eq. 1.3) to produce O_2 and OH^-, commonly referred to as a catalytic electrochemical-chemical (EC') mechanism to indicate that both electrochemical and chemical steps are involved. A more detailed explanation of the mechanistic details of the ORR at N-CNTs is given elsewhere.[29] The reduction of O_2 and disproportionation of the HO_2^- intermediate at a low overpotential is the key to the use of N-CNTs for oxidase-coupled first generation biosensors.

The disproportionation of HO_2^- (H_2O_2) at N-CNTs (eq. 1.3) occurs rapidly[60,61] manifested by the presence of a single ORR peak in cyclic voltammograms. Figure 1.1 displays cyclic voltammograms (CVs) of the ORR for 7.4 at.%, 6.3 at.%, 5.0 at.%, 4.0 at.% N-CNTs, and nondoped CNTs in oxygen saturated 0.1 M SPB (pH 7.0). The reduction peak shifts positive as the amount of incorporated nitrogen increases, displaying catalytic enhancement due to nitrogen doping. The measured oxygen reduction half wave potentials (E_p) as a function of nitrogen doping are indicated in Table 1.1. ORR at nondoped CNTs presents an initial two-electron reduction peak at -0.814 ± 0.011 V and a second two-electron reduction peak at -1.17 ± 0.02 V, corresponding to the sequential electrochemical reduction of oxygen to hydroperoxide (hydrogen peroxide) then to hydroxide (2 X 2 pathway). The ORR peak in the presence of H_2O_2 at 7.4 at.% N-CNTs, shown in Figure 1.2, displays an increased ORR peak current, giving further support to the chemical disproportionation of H_2O_2 and subsequent increase in oxygen.

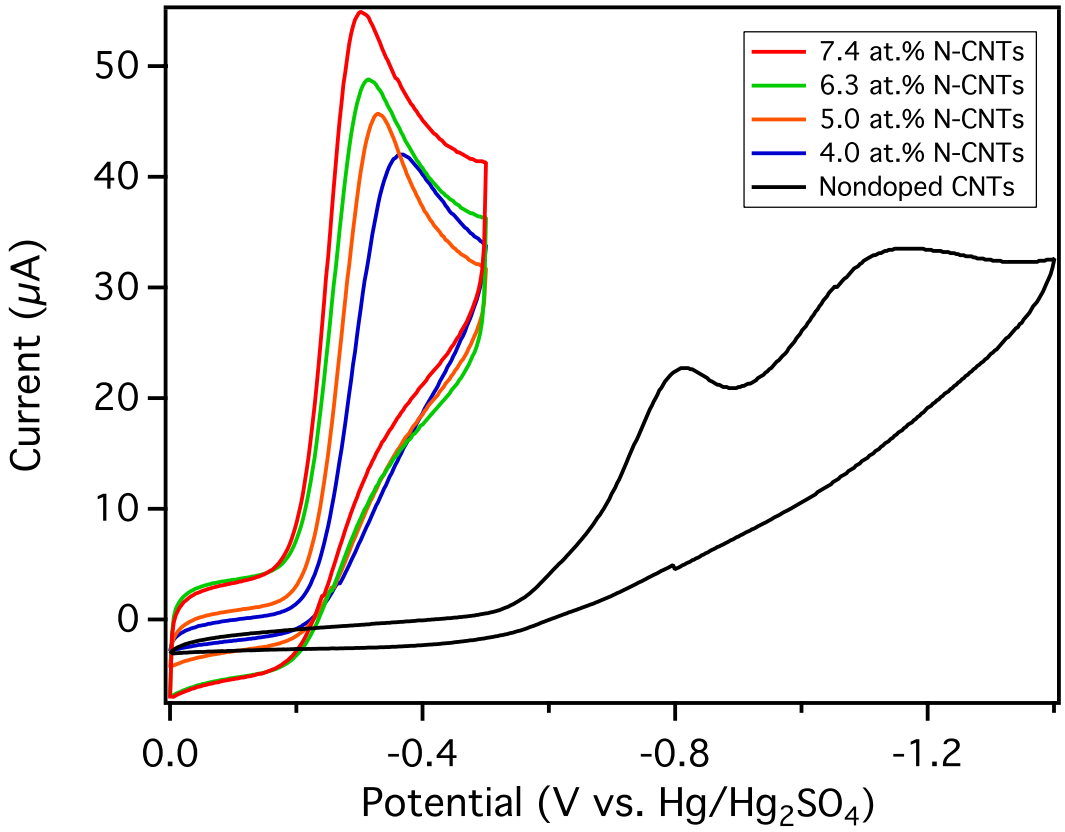

Figure 1.1. CVs of the ORR for 7.4 at.%, 6.3 at.%, 5.0 at.%, 4.0 at.% N-CNT and nondoped CNT modified electrodes in 0.1 M SPB at pH 7.0 (scan rate 20 mV/s)

Table 1.1. Measured ORR E_p and hydroperoxide sensitivities for the CNT/N-CNT modified electrodes.

Type	ORR E_p (V)	Poised Potential (V)	HO_2^- Sensitivity ($A\ M^{-1}\ cm^{-2}$)
CNTs	-0.814 ± 0.011	-1.08	Not detected
4.0 at.% N-CNTs	-0.365 ± 0.002	-0.29	0.16 ± 0.01
5.0 at.% N-CNTs	-0.330 ± 0.002	-0.26	0.23 ± 0.03
6.3 at.% N-CNTs	-0.315 ± 0.001	-0.24	0.24 ± 0.01
7.4 at.% N-CNTs	-0.302 ± 0.002	-0.23	0.25 ± 0.01

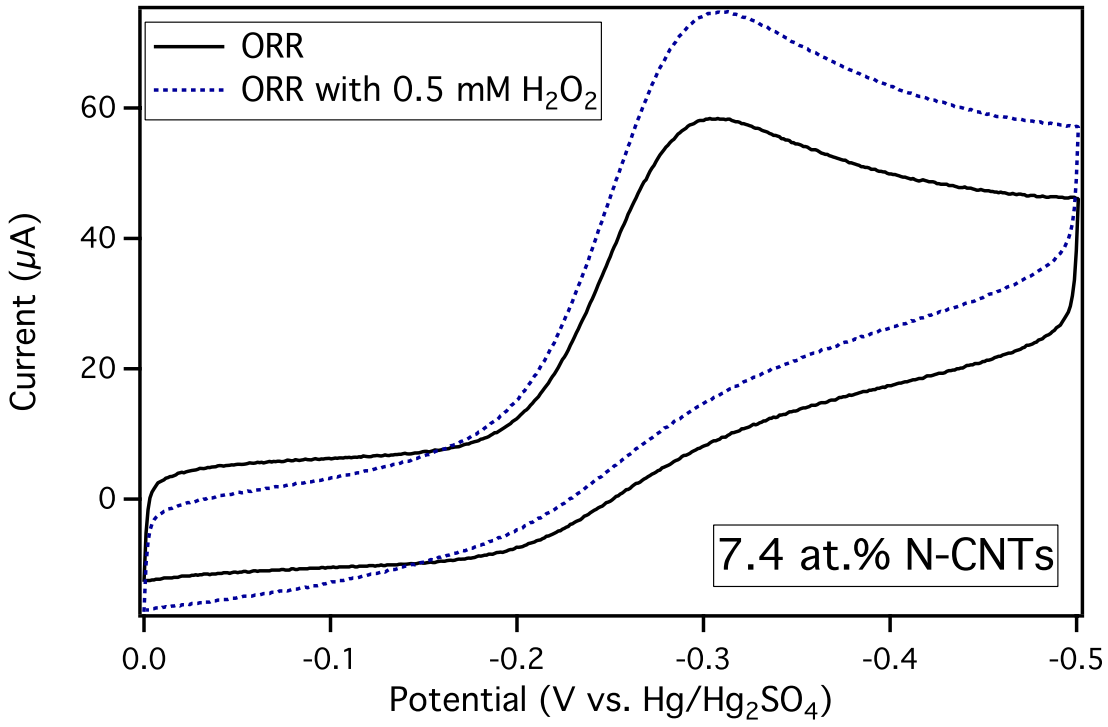

Figure 1.2. Cyclic voltammograms of the ORR in the presence and absence of 0.5 mM H_2O_2 (7.4 at.% N-CNT, scan rate 20 mV/s, 0.1 M SPB pH 7.0)

The fast chemical disproportionation of H_2O_2 at N-CNTs provides ample opportunity for quantitative detection of H_2O_2; however, in order to use this sensing technique, the current response to H_2O_2 in the presence of O_2 must be assessed, since O_2 is needed for the enzymatic reaction. The current response to $H_2O_2^-$ for CNT and N-CNT electrodes was measured by rotating disk amperometry (RDA) in the presence of a saturated oxygen solution (0.1 M SPB). The CNT/N-CNT modified GC electrodes were set at a rotation rate of 1000 rpm while H_2O_2 was introduced in 25 μM increments up to 500 μM (O_2 was constantly bubbled during experiments). The working electrode was poised between 70-80 mV positive of the peak apex for the ORR, as this potential range gave the highest current response, shown in Figure 1.3 for 6.3 at.% N-CNTs. The linear slope from 0-250 μM provided the basis for determining the sensitivity of our CNTs to H_2O_2 at the selected poised potentials, displayed in Table 1.1. The response is linear for the entire 500 μM range ($R^2 > 0.999$) and displays H_2O_2 sensitivities increasing concurrently with nitrogen content. The largest increases are seen from the nondoped CNTs to the 4.0 at.% N-CNTs, where pyridine is used as the N-CNT growth precursor instead of *m*-xylene, and from the 4.0 at.% N-CNTs to the 5.0 at.% N-CNTs, where NH_3 gas is introduced during nantube formation to increase N-doping. All types of N-CNT modified electrodes display pronounced sensitivity to H_2O_2, and are clearly differentiable from the background oxygen in solution.

1.3.2 Application of Lactate Oxidase to N-CNT Modified Electrodes

Oxidase enzymes producing hydrogen peroxide as a byproduct are traditionally coupled with peroxidases in order to obtain an electrochemical signal for quantitative analyte detection.[6–12] N-CNTs can replace this bi-enzymatic approach by use of the fast

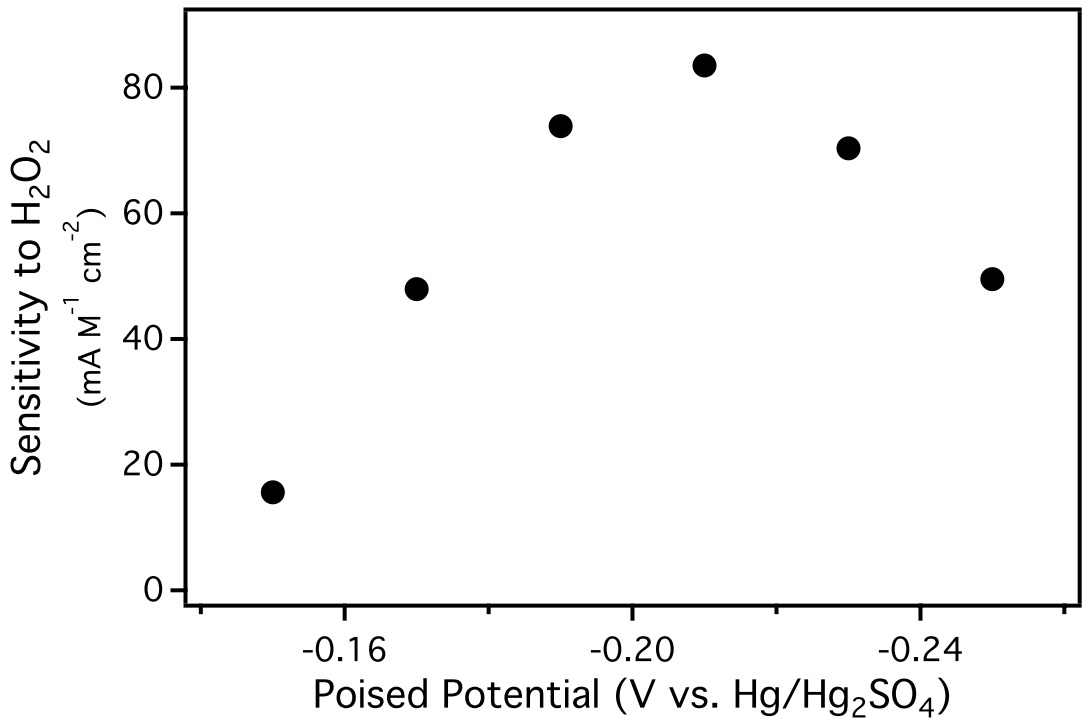

Figure 1.3. Sensitivity to H_2O_2 as a function of poised potential (5 μL of 2 mg mL^{-1} 6.3 at.% N-CNT in a modified Nafion® solution applied to a glassy carbon electrode, 0.5 cm diameter).

catalytic disproportionation of hydrogen peroxide on N-CNTs, resulting in increased ORR.[62] Lactate oxidase (LOx) is a flavoenzyme catalyzing the reaction shown below (eq. 1.4).

$$\text{L-lactate} + O_2 \rightarrow \text{Pyruvate} + H_2O_2 \qquad (1.4)$$

In a biosensor constructed with N-CNTs and LOx, the enzymatically produced H_2O_2 provides a reduction current response directly proportional to the amount of lactate in solution. Figure 1.4A provides an example of the reduction current response as additions of 25 μM of L-lactate are added to a N-CNT/LOx assembly in O_2 saturated SPB solution. Figure 1.4B displays the resulting amperometric response versus the lactate concentration. The response is fast ($\leq$ 2s), indicating that lactate is not diffusionally hindered from reaching the enzyme due to the modified Nafion® binder. Since O_2 is required to initiate the enzymatic reaction (eq. 4), a biosensor was tested in the absence of oxygen (by bubbling Ar instead of O_2) and did not exhibit a detectable response to lactate, indicating that the observed current was due to enzymatically generated H_2O_2 (shown in Figure 1.5A). Figure 1.5B displays the background oxygen reduction current as additions of electrolyte (SPB) are added to solution in contrast to additions of L-lactate. Spatial dependence of the enzyme's location with respect to the N-CNTs was determined by placing 10 μL of the LOx solution in the supporting electrolye, rather than being immobilized on the N-CNT surface. Upon addition of lactate, only an indistinct, slow onset deviation from the initial background was observed as H_2O_2 was formed in solution, indicating that enzymatically generated H_2O_2 must be in close proximity to the N-CNTs for functional responses, shown in Figure 1.6.

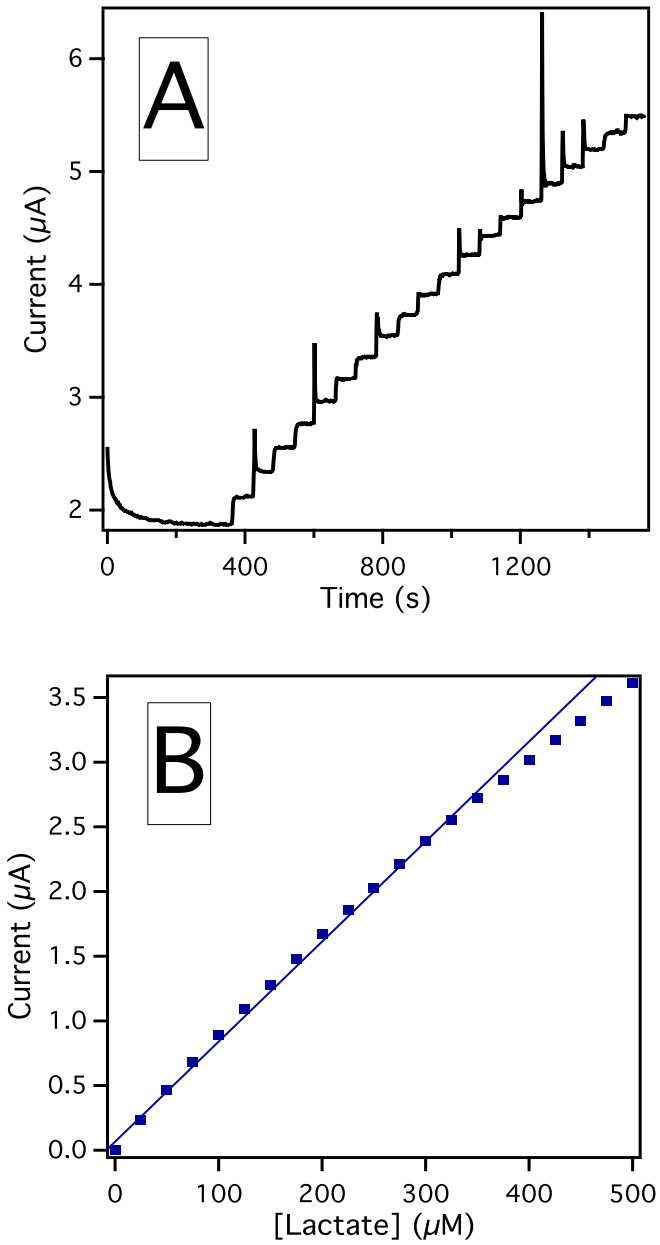

Figure 1.4. (A) Rotating disk chronoamperometric data for a typical biosensor displaying the reduction current response to L-lactate (rotation rate 1000 rpm). Aliquots of 25 μM L-lactate were introduced at 360 s, and added every 60 s (Poised potential -0.23 V vs. Hg/Hg_2SO_4). (B) The resulting amperometric response versus lactate concentration (line added to display linear range).

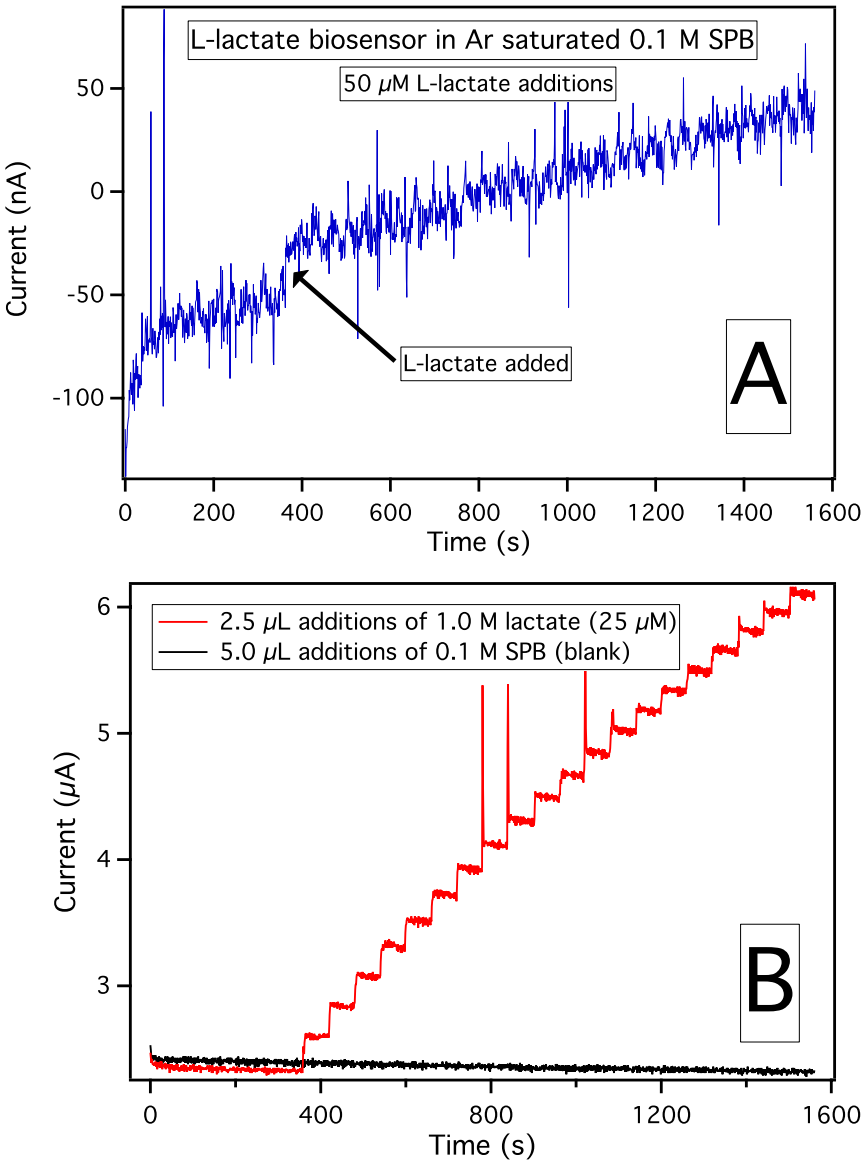

Figure 1.5. Rotating disk chronoamperometric data for (A) a L-lactate biosensor displaying the response to 50 μM L-lactate in the absence of oxygen (bubbling argon) and (B) a L-lactate biosensor displaying the response to 2.5 μL of L-lactate (25 μM) or 5 μL 0.1 M SPB as a blank. Aliquots were introduced at 360 s, and added every 60 s thereafter (rotation rate 1000 rpm, poised potential -0.23 V vs. Hg/Hg_2SO_4).

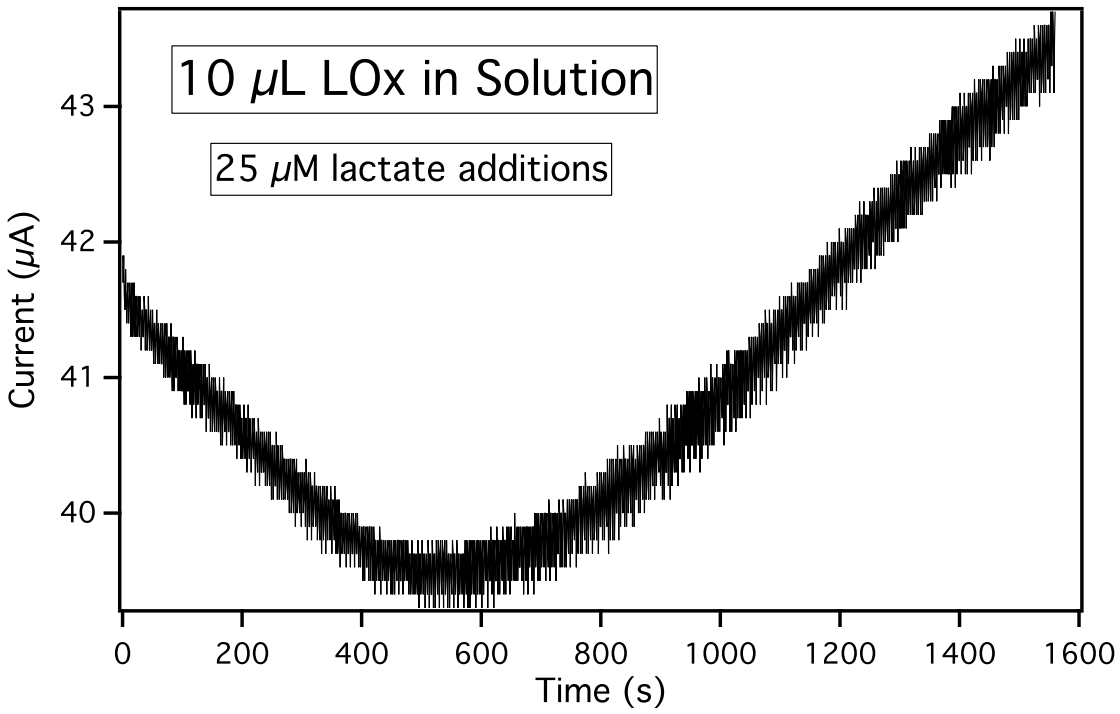

Figure 1.6. Rotating disk chronoamperometric data for a 7.4 at.% N-CNT modified electrode with 10 μL of the LOx solution in the supporting electrolyte. Aliquots of 25 μM of L-lactate were introduced at 360 s, and added every 60 s thereafter (rotation rate 1000 rpm, poised potential -0.23 V vs. Hg/Hg_2SO_4).

The poised potential during chronoamperometric experiments plays a large role in the magnitude of the signal sensitivity. Surprisingly, the potential is optimal near the onset of the reduction peak (about 70-80 mV positive of the peak apex) rather than being at or after the peak apex; such pre-onset sensitivities have been observed before by us and others.[62,65] Figure 1.7 presents the measured sensitivity to lactate as a function of the poised potential. The potential is optimal at -0.23 V, which is 70 mV more positive than the ORR E_p for 7.4 at.% N-CNT (Table 1.1). Optimization of the biosensor's sensitivity to lactate as a function of the amount of applied LOx or N-CNTs are shown in Figure 1.8. After optimization of the N-CNT/LOx assemblies to the specification outlined in the experimental section, the average sensitivity to L-lactate, based on the slope of the linear range ($R^2 \geq 0.995$) for seven independently constructed biosensors, was determined to be 0.040 ± 0.002 A M^{-1} cm^{-2}. Table 1.2 shows some analytical figures of merit for other CNT-based lactate sensors using LOx. One notable difference is the operating potential, of which this work presents the lowest potential at -0.23 V (vs. Hg/Hg_2SO_4) for a reduction current response. Most first generation biosensor schemes produce oxidation currents and must maintain a low operating potential to mitigate interference from easily oxidizable interferents such as ascorbic acid and uric acid. Reduction current detection schemes eliminate interference from oxidizable species, but often at the cost of a high negative operating potential. This biosensing scheme produces a reduction current while still maintaining a low operating potential. Furthermore, this is the first work, to our knowledge, where N-CNTs are coupled with LOx.

The repeatability for ten separately prepared 200 μM samples of lactate was 1.6% (RSD), with a fabrication reproducibility between seven independently constructed

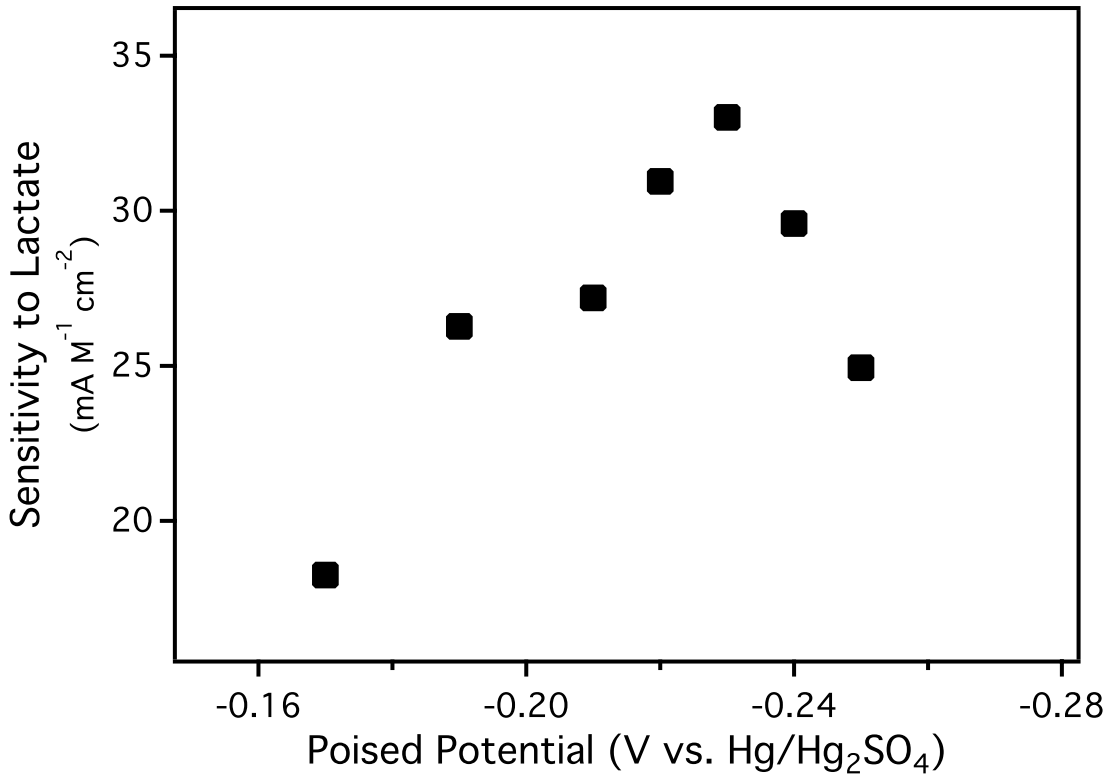

Figure 1.7. L-lactate sensitivity (mA M^{-1} cm^{-2}) as a function of the poised potential.

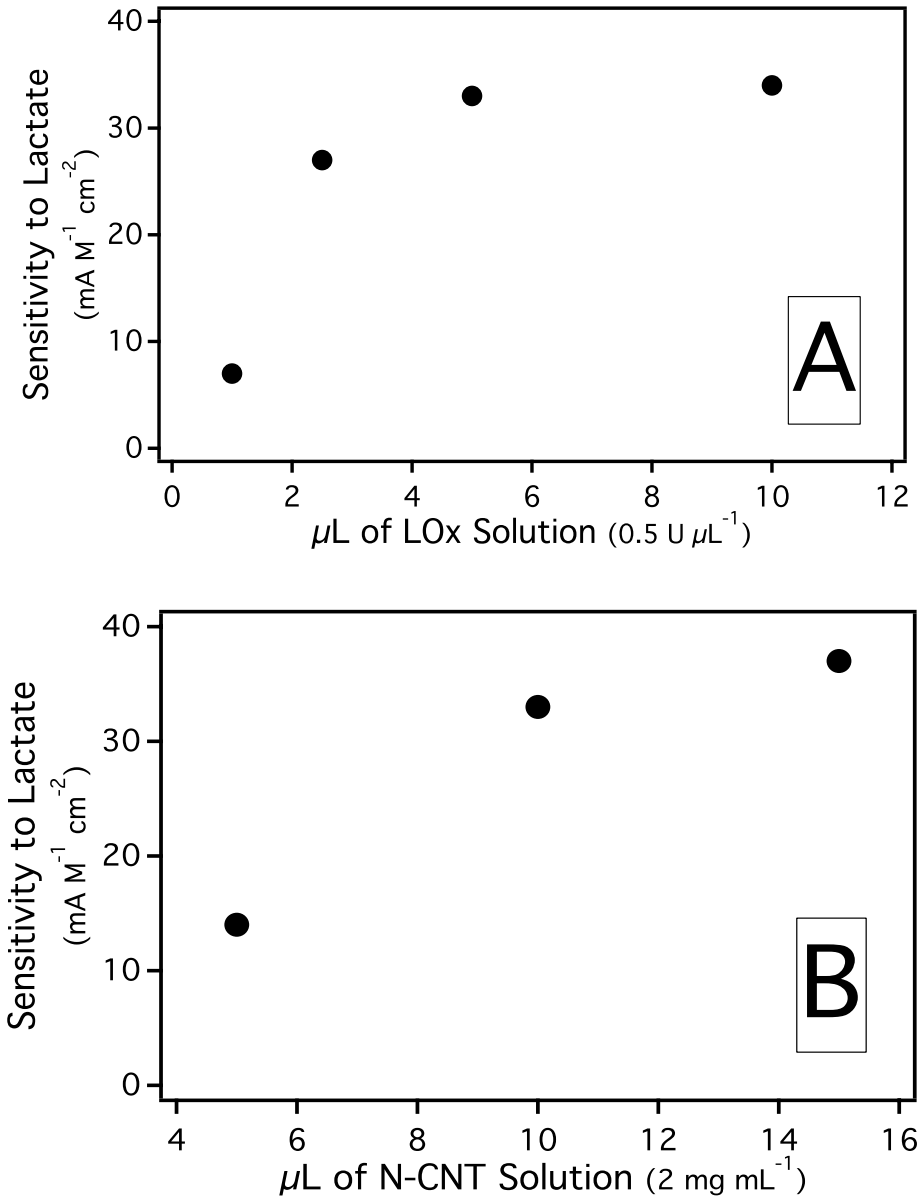

Figure 1.8. Sensitivity to lactate as a function of the (A) volume of LOx solution or the (B) volume of 7.4 at.% N-CNT solution applied to the biosensor.

Table 1.2. Comparison of Analytical Figures of Merit for CNT/LOx based lactate sensors found in the Literature

Sensor	Linear Range (mM)	Limit of Detection (μM)	Sensitivity ($A\ M^{-1}\ cm^{-2}$)	Operating Potential (V vs. Hg/Hg_2SO_4)	Repeatability (RSD)	Reproducibility (RSD)	Reference
N-CNT/LOx/Modified Nafion on GC	0.014-0.325	4.1	0.040	-0.23 V (reduction current)	1.6%	5.0%	This Work
CNT/LOx in Sol-gel on GC	0.2-2.0	0.3	0.006 A/M*	+0.11 V (oxidation current)	0.5%	3.6%	[66]
Chitosan/PVI-Os/CNT/LOx on Au	0-1.0	5	0.0197	-0.14 V (oxidation current)	4.9%	NR	[67]
CNT/Pt nanoparticles/LOx in Sol-gel on GC	0.2-2.0	0.3	0.0064 A/M*	+0.06 V (oxidation current)	0.4%	<2%	[68]
CNT/Pt nanoparticles/LOx on GC	0-0.10	0.25	0.426	+0.26 V (oxidation current)	7-9%	NR	[69]
CNT/HRP/LOx on GC	NR	NR	0.0013	-0.74 V (reduction current)	NR	NR	[70]
CNT/LOx paste electrode	0-7.0	300	0.00020	-0.54 V (reduction current)	NR	NR	[71]

NR = Not Reported, *Area of electrode was not given, Area is Geometric Area

biosensors of 5.0% (RSD) based on the standard deviation of the average sensitivity. The limit of detection, defined as three times the standard deviation of the background signal, was calculated at 4.1 ± 1.6 μM (N = 7), with a linear range of 14-325 μM, based on the initial limit of quantitation as ten times the standard deviation of the background signal. The biosensors were tested in the presence of five common interferents: ascorbic acid, paracetamol, uric acid, L-cysteine, and glucose. The biosensor's response to a 200 μM aliquot of L-lactate in the presence of 100 μM of each of the five interferents caused a 14% decrease in the signal response. Although Nafion® is known to mitigate or eliminate electroactive interferents,[72–76] modification with TBABr attenuates the natural selectivity to increase biocompatibility.[63,64] Thus, some interferent effect is expected.

The long term stability of the N-CNT/LOx assembly was monitored by measuring the sensitivity (response current versus lactate concentration from 0-250 μM) and the repeatability (response to 200 μM samples of lactate) at selected days over a 3 month period, displayed in Figure 1.9. When not in use, the biosensor was immersed in 0.1 M SPB and stored at 4° C. The overall sensitivity dropped slowly during the 3 month span; however, over the entire time course, the repeatability for 200 μM samples of lactate (N = 5) remained below 3.4% (RSD). It should be noted that the N-CNT/enzyme biosensing assembly developed here is compatible with both larger more active enzymes such as glucose oxidase (MW 160 kDa, activity of 100-250 U/mg)[62] and smaller, less active enzymes such as LOx used in this work (MW 80 kDa, activity of 40 U/mg). Thus, the N-CNT/enzyme/modified Nafion® assembly is a versatile biosensing platform, where different enzymes are effectively immobilized, while still maintaining enzymatic activity.

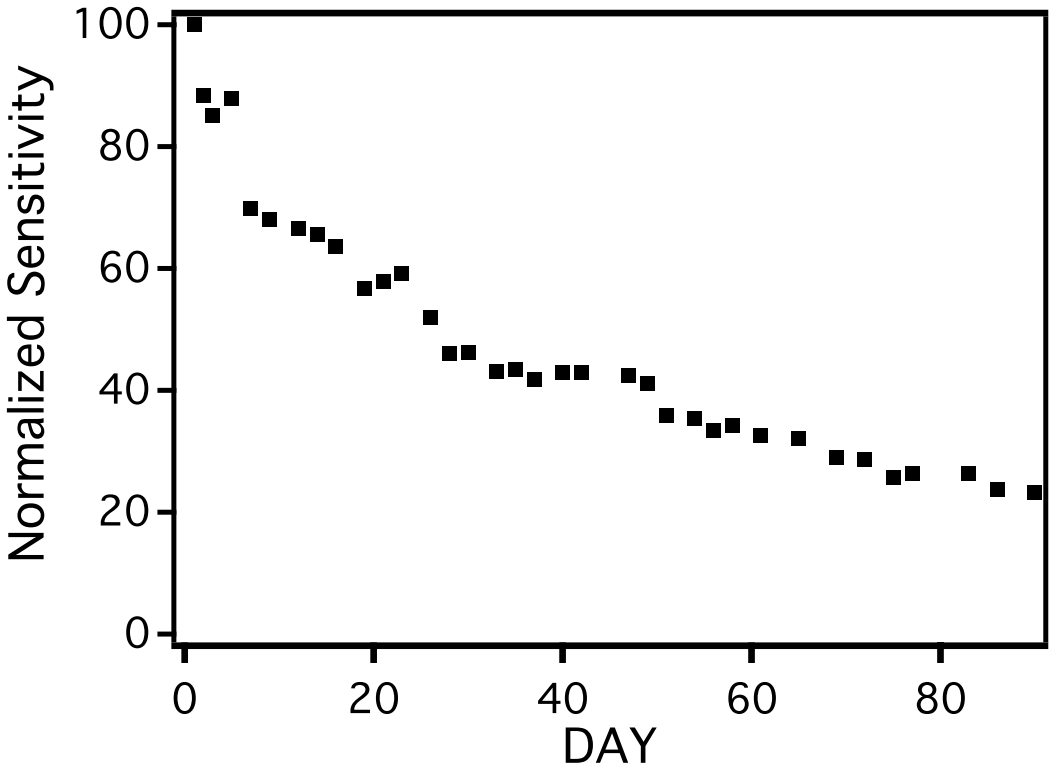

Figure 1.9. The change in sensitivity to lactate, monitored over 90 days (Normalized to the initial sensitivity at day 1, 0.041 A M^{-1} cm^{-2}).

1.3.3 Steady State Enzyme Kinetics

At higher substrate concentrations, the lactate biosensors displayed substrate saturation curves, where steady state kinetic parameters could be extracted. Both the apparent Michaelis constant (K_M^{app}, the concentration where the enzymatic reaction has reached half of its maximum velocity) and the maximum velocity (V_{max}) were determined by Lineweaver-Burk (double reciprocal) plots. Figure 1.10A displays a representative saturation curve. The assemblies were poised at -0.23 (V vs Hg/Hg_2SO_4) and rotated at 1000 rpm while measuring the response current to lactate. The resulting Lineweaver-Burk plot, where the inverse of the response current is plotted against the inverse of the lactate concentration, is shown in Figure 1.10B. The Lineweaver-Burk plots display excellent linearity (R^2>0.9995), described by the following relationship (eq. 1.5),

$$1/i = (K_M^{app}/ i_{max})(1/[Lactate]) + 1/i_{max} \quad (1.5)$$

where i is the current response, i_{max} is the saturation current, and [Lactate] is the lactate concentration. The calculated K_M^{app} of 1.60 ± 0.34 mM (N = 10) is in good agreement with other constants found in the literature.[77–81] K_M^{app} is well above the linear range and given the fast response time (≤ 2 s), indicates that immobilization does not appreciably affect enzyme activity and lactate is not diffusionally hindered from reaching the enzyme. The maximum velocity was calculated from the following equation (eq. 1.6),

$$V_{max} = i_{max}/(nF) \quad (1.6)$$

where n is the number of electrons (n = 1) transferred in the HO_2^- disproportionation

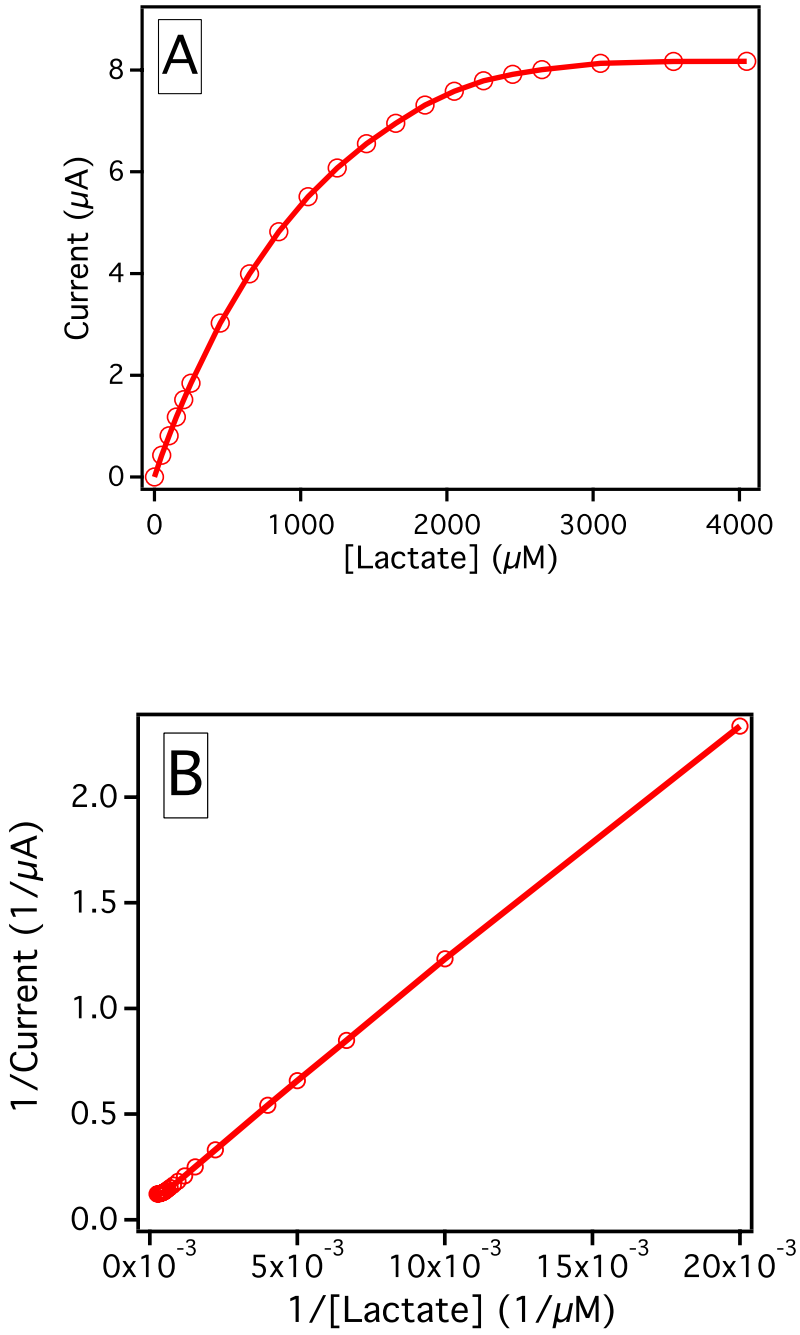

Figure 1.10. (A) A Michaelis-Menten saturation curve for a typical biosensor (poised potential at -0.23 V vs. Hg/Hg_2SO_4). (B) The resulting Lineweaver-Burk plot (double-reciprocal plot).

reaction[62] and F is Faraday's constant (96485 C mol^{-1}). The V_{max} of 132 ± 35 pmol/s (N = 10) is well below the linear range, indicating that the act of measuring has little effect on the overall concentration of lactate in solution.

The sensor response attenuates slightly with each subsequent addition of lactate, suggesting that the accumulation of product (i.e. pyruvate) might be inhibiting the forward enzymatic reaction. The maximum velocity (132 ± 35 pmol/s) over the entire experiment's time course (1560 s) would cause approximately 0.20 μM of pyruvate to accumulate. In order to determine if product inhibition was causing attenuation, K_M^{app} and V_{max} were measured in the presence of 0.40 μM, 3 mM, and 10 mM of pyruvate. No difference was detected in K_M^{app} or V_{max} for any of the pyruvate levels, providing evidence that product inhibition does not affect sensor performance.

1.3.4 Electroactivity of the Redox Center of LOx.

Figure 1.11 presents the CV response of immobilized LOx on N-CNTs with modified Nafion® binder immersed in Ar purged buffer (SPB) before and after being cycled. The initial scan (solid line in Figure 1.11) displays a redox peak centered at $E_{1/2}$ = -0.86 V, associated with the redox center of LOx. A second redox peak centered at $E_{1/2}$ = -0.60 V is due to an electroactive $Fe^{2+/3+}$ redox species, present from the iron precursor used during CNT synthesis. The $Fe^{2+/3+}$ redox response has been investigated before[55] and can be electrochemically passivated by cycling. Repeated cycling does not affect the N-CNTs redox response to H_2O_2 (or O_2), as no statistical difference was found after passivation of the surface immobilized Fe. After cycling the N-CNT/LOx electrode assembly about 20 times, only the redox center of LOx remain electrochemically active (dotted line in Figure 1.11). The electroactive surface coverage (Γ) was calculated from the following equation (eq. 1.7).

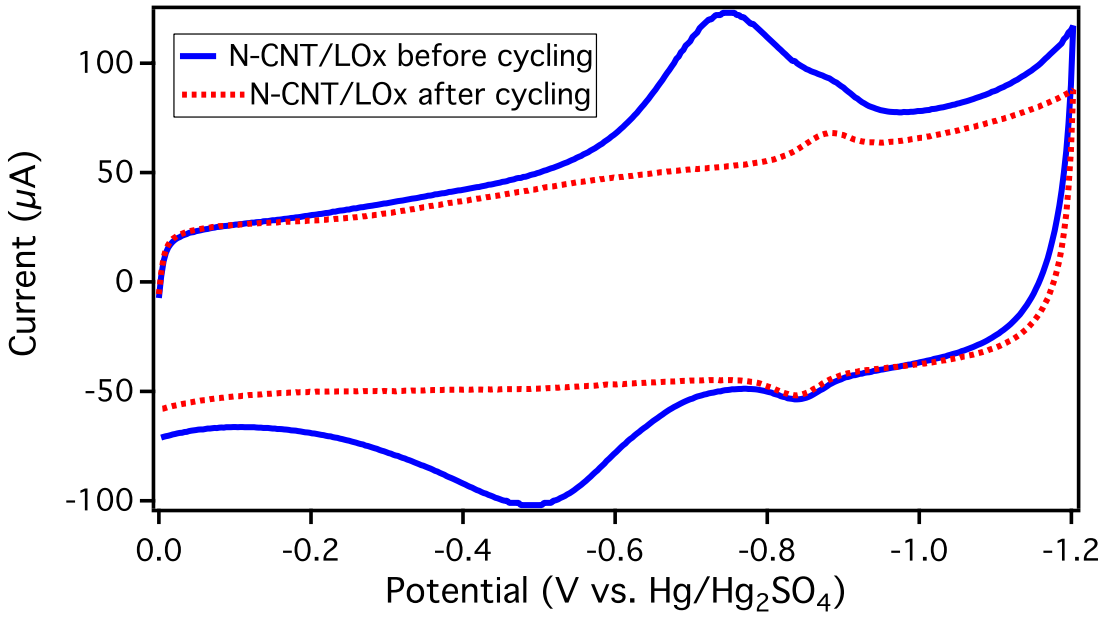

Figure 1.11. CVs of a N-CNT/LOx modified electrode before and after being cycled (20 cycles) in Ar purged 0.1 M SPB (pH 7.0), scan rate 50 mV/s.

$$\Gamma = Q/nFA \quad (1.7)$$

Where Q is the charge (in C) calculated from the area under the cathodic or anodic peak, n is the number of electrons transferred (n = 2) in the flavin/dihydroflavin ($FAD/FADH_2$) redox couple,[40,82] F is Faraday's constant (96485 C mol^{-1}), A is the geometric area of the electrode (0.196 cm^2), and Γ is the surface coverage measured at 0.27 nmol cm^{-2} for the lactate biosensors (Figure 1.13 and Table 1.3).

Direct electrical connection between CNTs and enzymes have been observed before[36–43] and is mostly due to the rigid nature of the CNTs (i.e., their ability to penetrate the enzyme and get close enough to the redox active center to allow tunneling to occur).[43] In order to verify electrical connection to the active center of LOx, N-CNTs were cycled (to remove the electroactive $Fe^{2+/3+}$ species) prior to the application of LOx, without the addition of modified Nafion®. Figure 1.12 displays CVs of cycled N-CNT modified electrodes before and after the application of LOx, in Ar saturated electrolyte (SPB). The before scan shows just the background capacitive current of the N-CNTs (dotted line Figure 1.12). After application of the LOx (solid line Figure 1.12), the background capacitive current decreases slightly, indicative of adsorption, and the peak at $E_{1/2}$ of -0.86 V appears. The measured potential is consistent with the formal potential of the cofactor for LOx, flavin adenine dinucleotide (FAD).[42,43,82,83] Additionally, the measured potential is also consistent with the formal potential of electrically connected glucose oxidase, which also uses FAD as a cofactor.[36,37,41] The surface coverage for the N-CNT/LOx modified electrodes without

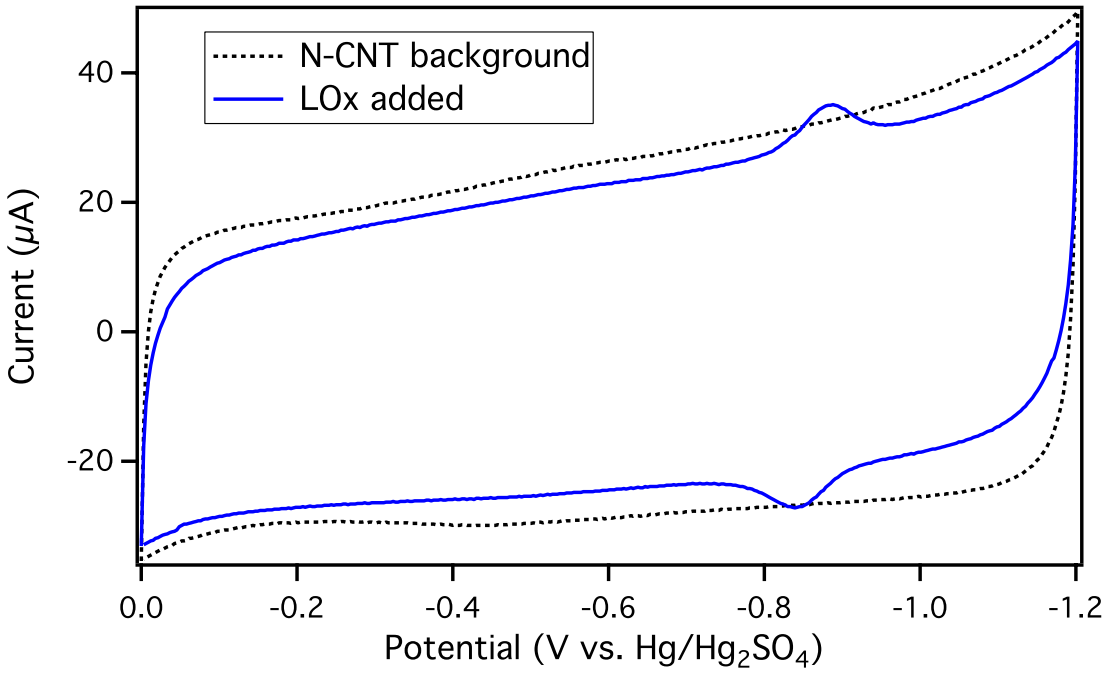

Figure 1.12. CV of N-CNT and N-CNT/LOx modified electrodes without modified Nafion® in Ar saturated 0.1 M SPB (pH 7.0), scan rate 50 mV/s.

modified Nafion® was found to be nearly identical to the surface coverage with modified Nafion®, shown in Figure 1.13 and Table 1.3, suggesting that Nafion® doesn't play a role in the observed electrical connection to the redox center of LOx. The peak current has a linear correlation with scan rate, indicative of a surface confined reaction (Figure 1.13 and Table 1.3).[42]

1.4 CONCLUSION

The unique first generation biosensing scheme outlined above eliminates the need for additional peroxidases or redox mediators. The ability of N-CNTs to disproportionate hydrogen peroxide/hydroperoxide, which subsequently produces a local increase of oxygen, provides a reduction current response to L-lactate at the lowest known operating potential, -0.23 V (vs. Hg/Hg_2SO_4), for an amperometric lactate biosensor constructed using CNTs. This biogenic detection system can be applied to any enzyme producing hydrogen peroxide as a byproduct, or simply for the detection of hydrogen peroxide alone.[56,61,62] The simplified lactate sensor displays a sensitivity of 0.040 ± 0.002 A M^{-1} cm^{-2}, a limit of detection of 4.1 ± 1.6 μM, and a linear range of 14-325 μM, with opportunity for further improvements. For instance, the conversion efficiency of LOx, calculated by dividing the sensitivity of the biosensor to lactate over the N-CNTs' sensitivity to H_2O_2, is only 16%. N-CNTs also seem to display an apparent direct electron transfer to the redox active center of LOx, FAD. The electron transfer to FAD after adsorption of either FAD of FAD containing enzymes, such as glucose oxidase, will be further explored in chapter 2.

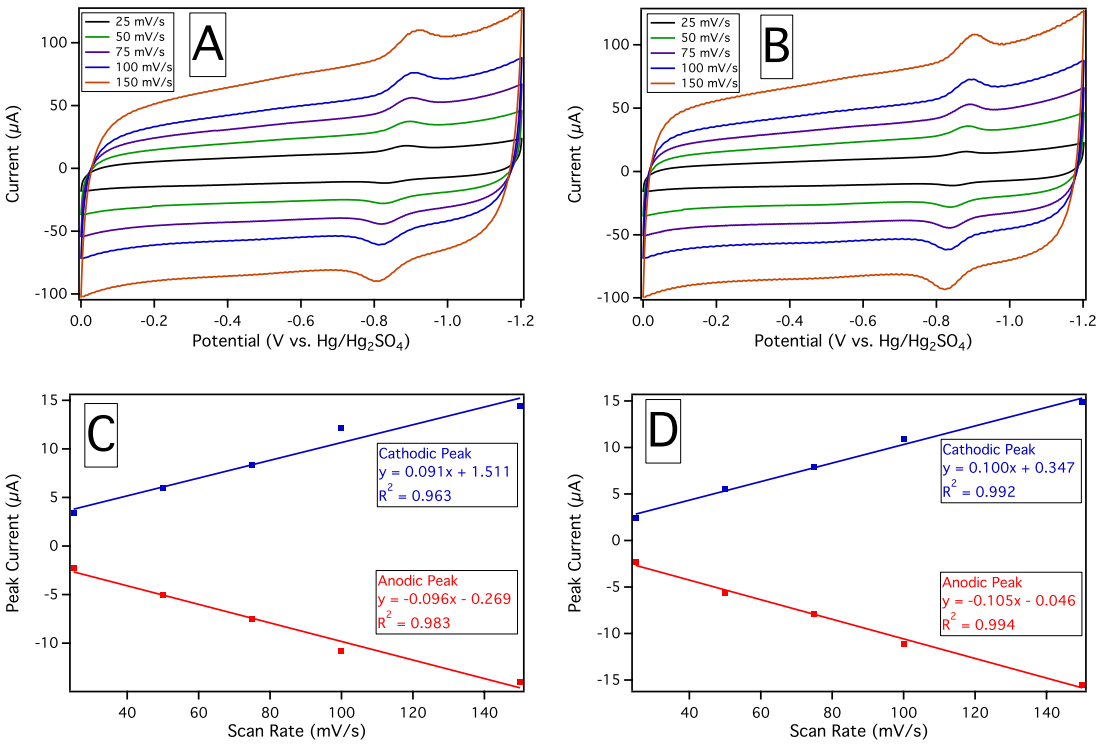

Figure 1.13. Cyclic voltammograms of a biosensor with (A) and without (B) the application of modified Nafion® in Ar purged SPB (pH 7.0) displaying the direct electron transfer to the redox center of LOx at selected scan rates (25, 50, 75, 100, and 150 mV/s). The peak current of the surface reaction as a function of scan with (C) and without (D) the modified Nafion®.

Table 1.3. Table of the calculated surface coverage of LOx for biosensors with or without the application of modified Nafion®.

Sample	Surface Coverage of LOx (Biosensor) (nmol/cm^2)	Surface Coverage of LOx (Biosensor without modified Nafion®)(nmol/cm^2)
1	0.269	0.240
2	0.273	0.260
3	0.257	0.264
Average	0.266 ± 0.008	0.255 ± 0.013

CHAPTER 2

Influence of Surface Adsorption on the Interfacial Electron Transfer of Flavin Adenine Dinucleotide and Glucose Oxidase at Carbon Nanotube and Nitrogen-Doped Carbon Nanotube Electrodes*

2.1. INTRODUCTION

Carbon nanotubes (CNTs) have been explored for a vast array of biosensing applications, either by themselves[45,46,84,85] or modified with enzymes such as glucose oxidase (GOx).[35,86–88] The ideal enzymatic biosensor would be a so-called "third" generation biosensor, where the electrode would have direct electrical access to the redox active center of a functioning enzyme. Given that the protein shell is designed to protect the redox active center and impart selectivity, only a few enzymes naturally exhibit this behavior on traditional electrode surfaces[12,20,21]; however, novel methods have been employed to facilitate direct electron transfer (DET) between electrode surfaces and other enzymes.[23,24,26,34,89,90] CNTs have been noted as an ideal material for direct electron transfer due to their small size and excellent electronic conductivity.[43] The literature contains many reports of DET between CNT electrodes and the enzyme glucose oxidase (GOx).[36,37,40–43,91–99] Flavin adenine dinucleotide (FAD), the redox active center of GOx, is tightly bound inside a deep pocket of GOx, but is not covalently bound.[100] A hypothesis of the DET process between CNTs and GOx is that the small diameter CNTs are able to penetrate into the protein or glycoprotein shell deep enough for electron tunneling to occur.[43] The electrochemical behavior of FAD has been studied on electrode materials such as mercury[82,101,102], glassy carbon (GC)[103,104], modified GC[105], gold[106], titanium[107],

---

*Portions of this chapter were published in Goran, J. M.; Mantilla, S. M.; Stevenson, K. J. *Anal. Chem.* **2013**, *85*, 1571-1581. (Mantilla performed experiments, Stevenson supervised this work)

TiO_2[108], and graphite[109,110], but has not been adequately investigated on CNTs. This chapter examines the spontaneous adsorption of FAD and GOx on CNTs and nitrogen-doped CNTs (N-CNTs), which offers a unique way to modify the surface and extend our understanding of the surface confined redox reaction. Our technique is unique in that oxidative acids such as sulfuric and nitric[42,43,93,94,98] are not used to create oxygen functionalities and assist in the dispersion of the hydrophobic CNTs into aqueous solutions. In addition, we do not employ surfactants like cetyltrimethylammonium bromide (CTAB, a cationic surfactant)[36], Triton X-100[99], or 3-aminopropyltriethoxysilane (APTES)[91] to assist suspension, or binders such as Nafion[36,37,95,98] to ensure adhesion of the FAD or GOx to the electrode. Furthermore, GOx or FAD was not covalently attached to the CNTs with carbodiimide coupling[93,99], dispersed in an immobilizing film[41], or constructed from layer-by-layer assembly with cationic films such as polyethylenimine (PEI)[94]. Our approach provides a more accurate understanding of the natural physical processes behind GOx and FAD adsorption and the influence of surface adsorption on the measured interfacial electron transfer rates. Conclusively, the electroactive FAD observed from the spontaneous adsorption of GOx to CNT and N-CNT electrodes is not associated with active enzyme, as bioelectrocatalytic current was not observed upon the addition of glucose, thereby demonstrating that DET is not occurring with GOx. FAD does, however, rapidly adsorb at CNT/N-CNT electrodes, even at low concentrations, to produce a significant and reversible redox response. The commonly used Laviron method, which takes the anodic and cathodic potential peak-to-peak splitting as a way to determine the heterogeneous electron transfer rate constant is also investigated; displaying the need to fully determine whether the measured potential peak splitting is

under the kinetic control of an electron transfer, or ohmic control due to uncompensated resistance.

2.2. EXPERIMENTAL

2.2.1 Chemicals

Sodium phosphate monobasic (NaH_2PO_4), sodium phosphate dibasic (Na_2HPO_4), sodium hydroxide (NaOH), potassium nitrate (KNO_3), *o*-phosphoric acid (85%), and pyridine were purchased from Fisher (all ACS Grade). Bis(cyclopentadienyl)iron (ferrocene, 99%) was obtained from Alfa Aesar. Flavin adenine dinucleotide disodium salt hydrate (≥95%), glucose oxidase (Type X-S from *Aspergillus niger* 100,00-250,00 U/g), α-D-Glucose, and *m*-xylene were purchased from Sigma-Aldrich.

2.2.2 CNT/N-CNT Synthesis

CNTs and N-CNTs were prepared by chemical vapor deposition (CVD) using ferrocene dissolved in either *m*-xylene (nondoped) or pyridine (N-doped) at a concentration of 20 mg mL^{-1} as described in previous reports. [52,59–61] Approximately 1 ml of the ferrocene solution was fed into a single quartz tube (at 0.1 mL min^{-1}) through a programmable syringe pump (New Era Pump Systems NE-1000) fitted with a glass syringe (Hamilton 81320). The quartz tube was placed lengthwise across two separate tube furnaces (Carbolite Model HST 12/35/200/2416CG), the first of which was set at a temperature to properly vaporize the organic solvent (150 °C for *m*-xylene and 130 °C for pyridine), while the second was set to ensure formation of multiwalled CNTs/N-CNTs (700 °C *m*-xylene and 800 °C for pyridine) on inside lining of the quartz tube. Argon gas was used to carry the vaporized ferrocene solution through the tube along with hydrogen (for nondoped CNTs) or ammonia to increase the amount of nitrogen incorporated into

the carbon lattice. The amount of incorporated nitrogen as a function of the flow rate of ammonia was shown in a prior report.[52]

2.2.3 Electrochemistry and Electrode Preparation

Cyclic voltammograms (CVs) and chronoamperograms (CAs) are presented with cathodic current being assigned a positive value and the anodic current given a negative value. CNT/N-CNT electrodes were prepared by drop casting 24 μg of CNTs/N-CNTs on a 0.5 cm diameter glassy carbon (PINE Instruments AFE2M050GC) electrode surface, without the use of binders, surfactants, or oxidizing agents. CNT/N-CNT solutions were sonicated (Branson ultrasonic cleaner, model 2510R-MTH) for 2 hours in absolute ethanol prior to drop casting to ensure a homogeneous mixture. The mass normalized 24 μg were drop cast from a single 12 μL aliquot of a 2 mg mL^{-1} solution of N-CNTs, while 6 aliquots of 10 μL were drop cast from a nondoped CNT solution of 0.4 mg mL^{-1}. The glassy carbon (GC) surface was polished with 0.05 μm alumina slurry on microcloth (Buehler) and sonicated in 18.2 MΩ cm water prior to CNT/N-CNT application. After drop casting, CNT/N-CNT electrodes were allowed to fully dry in air before "wetting" the electrode surface in a mixture of sodium phosphate buffer (SPB) and ethanol. CNT/N-CNT electrodes were cycled in SPB (from 0.00 to -1.20 V vs. Hg/Hg_2SO_4 100 times at 300 mV/s) to passivate electroactive iron prior to use.[55] Electrodes were then placed in an inverted position in SPB solutions containing varying concentrations of FAD or GOx. CVs were taken after specific exposure times to the FAD and GOx solutions (adsorption was always performed at open circuit potential). Electrodes were rinsed with the appropriate concentration of SPB to remove loosely adsorbed FAD or GOx prior to electrochemical measurements. Voltammograms were obtained by initially sweeping the potential negative (usually starting at 0.00 V vs. Hg/Hg_2SO_4) before reversing back in a

positive direction. The amount of FAD adsorbed was calculated from integration of the cathodic peak (coulometrically). A five neck 125 mL glass cell was outfitted with a Hg/Hg_2SO_4 reference electrode (CH Instruments, +0.64 V vs. SHE; +0.40 vs. SCE; +0.44 vs. Ag/AgCl) and a coiled Au wire counter electrode for all electrochemical experiments, in conjunction with a Autolab™ PGSTAT30 potentiostat interfaced with Autolab™ GPES software (version 4.9). Electron micrographs of the CNT/N-CNTs electrodes were obtained using a FEI Quanta 650 FEG with secondary electrons (electron energy of 30 keV).

2.3 Results and Discussion

2.3.1 Spontaneous Adsorption of GOx and FAD onto CNT/N-CNT Electrodes

Figure 2.1 presents electron micrographs of the CNTs/N-CNTs after sonication and solution drop casting on a GC electrode. All three morphologies are similar, comprised of a three-dimensional mesh of CNTs or N-CNTs; however, the 7.4 at.% N-CNTs still contain a substantial amount of bundled tubes. In addition to the many attractive physicochemical properties of CNTs, three-dimensional networks of CNTs can greatly enhance the spontaneous adsorption of adsorbates, especially in the case of enzymes.[111] Figure 2.2 shows CVs of CNT and N-CNT electrodes at increasing exposure times to solutions containing 6.5 μM FAD and 81.3 μM GOx in 0.1 M sodium phosphate buffer (SPB) at a pH of 7.0. Electrodes and solutions were kept in the dark at all times, except during electrochemical measurements (~3 minutes), to ensure that photolytic reactions did not occur.[112] The observed redox reaction is due to a surface confined electron transfer of FAD for both the adsorbed FAD and GOx via eq. 2.1:

$$FAD + 2H^+ + 2e^- \leftrightarrow FADH_2 \qquad (2.1)$$

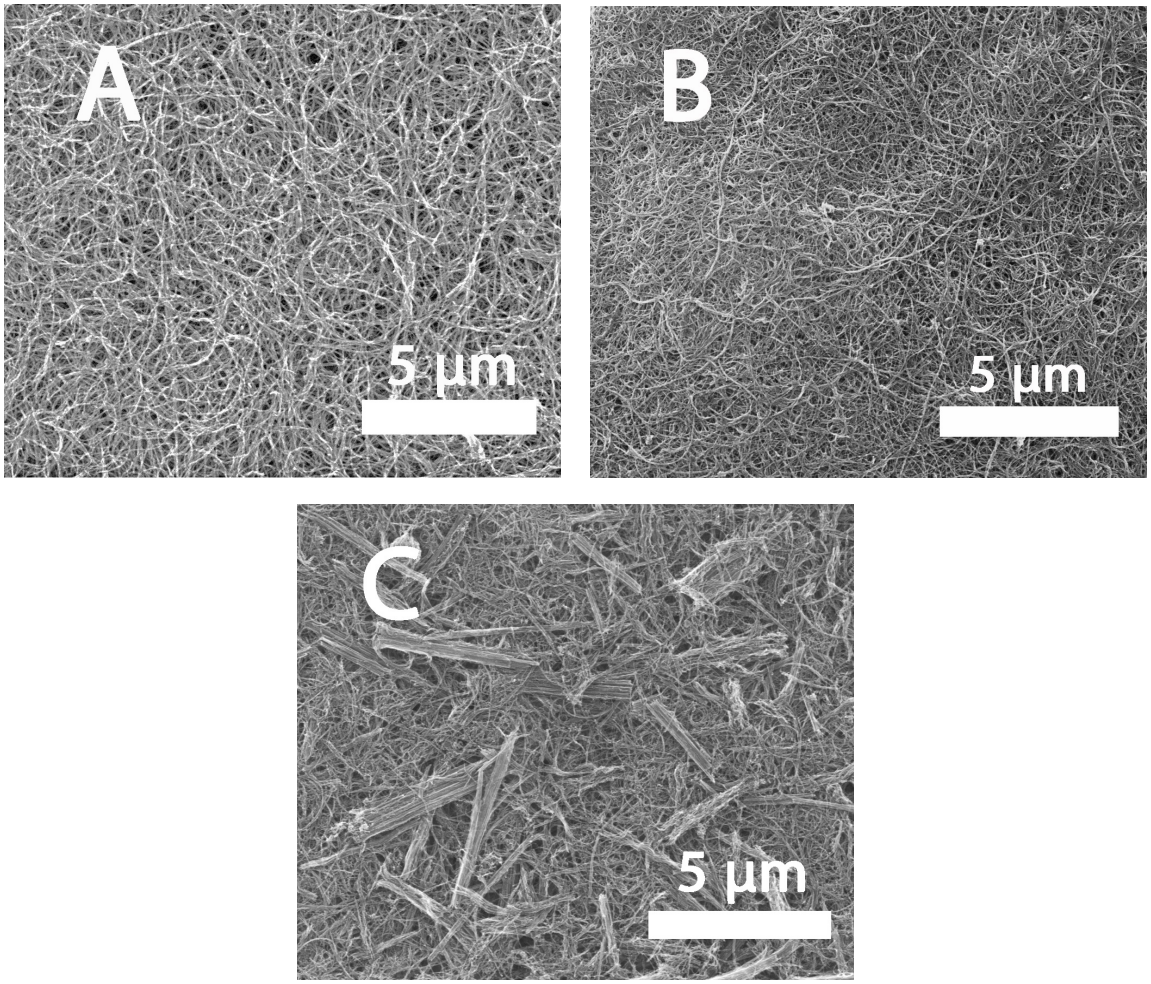

Figure 2.1. Scanning electron micrographs of the CNT/N-CNT electrodes: (A) nondoped CNTs (B) 4.0 at.% N-CNTs (C) 7.4 at.% N-CNTs

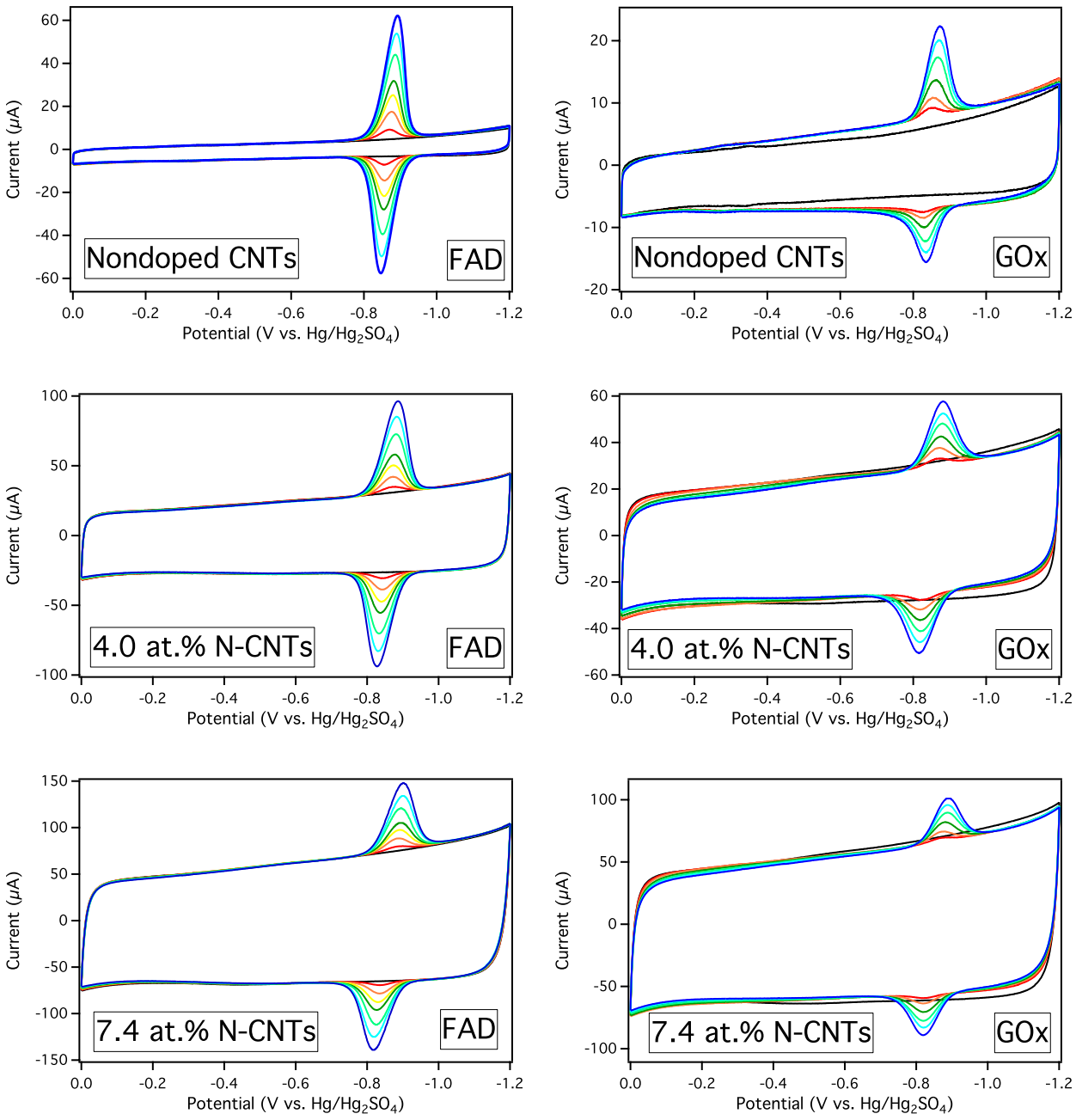

Figure 2.2. CVs of 6.5 μM FAD and 81.3 μM GOx in 0.1 M SPB *p*H 7.0 adsorbing onto CNTs/N-CNTs over 1 hour (black = background, red = 1 min, orange = 5 min, yellow = 10 min, green = 15 min, aqua = 30 min, light blue = 45 min, blue = 60 min) at a constant scan rate (100 mV/s).

The $E_{1/2}$ or formal potential of this reaction resides at -0.85 V for the N-CNT electrodes and -0.86 V for the CNT electrodes. Figure 2.3 displays overlaid CVs of FAD adsorbed at nondoped CNT, 4.0 at.% N-CNT, and 7.4 at.% N-CNT modified electrodes, showing the 10 mV more negative shift in the $E_{1/2}$ of FAD on nondoped CNTs. The difference between $E_{1/2}$ at CNTs and N-CNTs is reflective of the nitrogen incorporated into the carbon lattice, which subsequently produces positively charged nitrogen functionalities, decreases hydrophobicity, and creates more edge plane sites for facile electron transfer.[57] The background capacitive current increases with nitrogen doping of CNTs, as seen in the increase of non-faradaic current in the CVs of Figure 2.2. Adsorption of GOx causes the background capacitive current of N-CNTs to decrease with increasing amounts of adsorbed GOx. For nondoped CNTs, the initial adsorption of GOx appears to impart an increased capacitive current, suggesting that GOx interacts differently at the more hydrophobic CNT electrodes. In contrast, adsorbed FAD does not appreciably change the background capacitive current for either CNT or N-CNT electrodes. The rates of adsorption were found to be linear during the first 15 minutes for FAD, but not as monotonic for GOx. Initial adsorption rates are shown in Table 2.1. These values display an increase in the adsorption rate as a function of nitrogen doping, which is reflective of the increased surface area of the N-CNTs and the presence of more edge plane sites which can promote stronger and more facile adsorption.[57,59] Figure 2.4 presents the amount adsorbed from Figure 1.2 extended for 45 hours. The adsorption of FAD on CNT and N-CNT electrodes appears to reach a constant maximum around 25 hours (at 6.5 μM FAD in 0.1 SPB). The amount of GOx adsorbed also reaches a

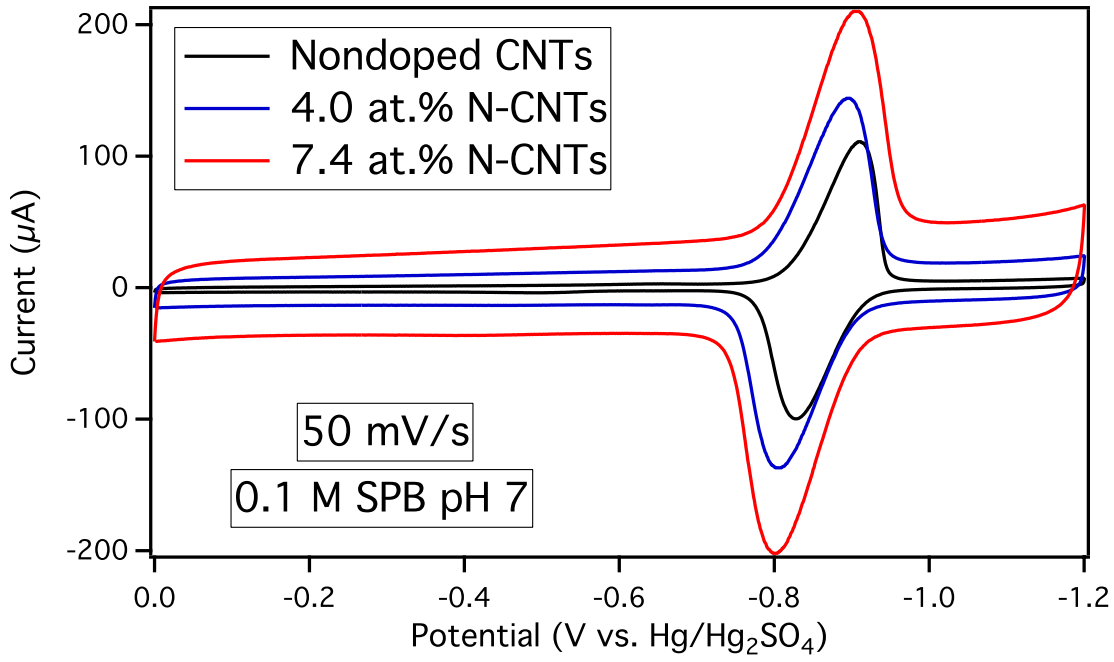

Figure 2.3. FAD adsorbed onto Nondoped CNT, 4.0 at.% N-CNT, and 7.4 at.% N-CNT modified electrodes displaying the 10 mV more negative shift in the $E_{1/2}$ for the redox reaction on Nondoped CNTs (scan rate 50 mV/s).

Table 2.1. Initial adsorption rates of FAD and GOx onto CNTs/N-CNTs

Type	FAD (pmol/min)	GOx (pmol/min)
Nondoped CNTs	5.0	1.1
4.0 at.% N-CNTs	6.6	2.9
7.4 at.% N-CNTs	7.6	3.6

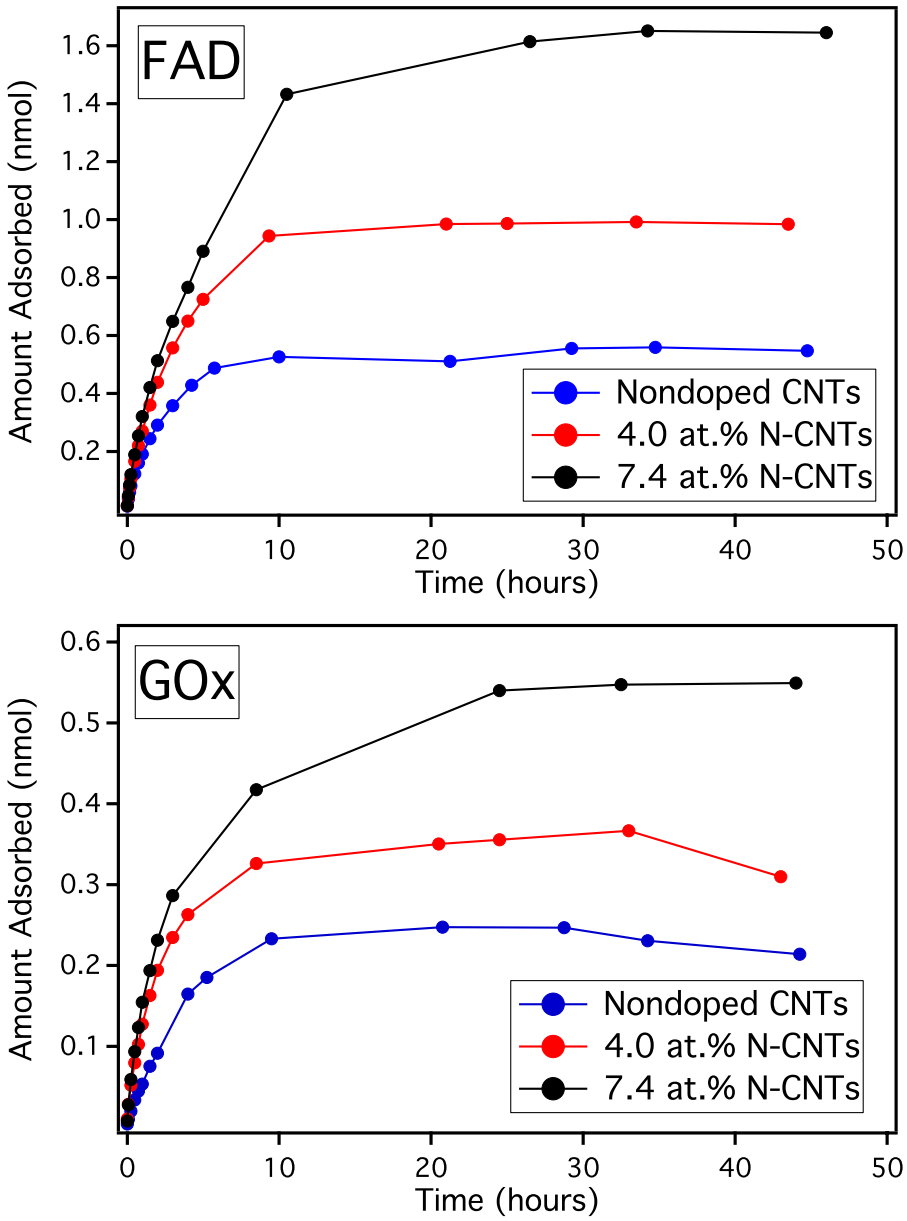

Figure 2.4. FAD and GOx adsorbed onto nondoped CNT, 4.0 at.% N-CNT, and 7.4 at.% N-CNT electrodes from Figure 2.2 extended for over 45 hours (0.1 M SPB pH 7.0).

maximum, but begins to decrease from that maximum within the measured timeframe. We believe this observed maximum for FAD and GOx is in fact a dynamic equilibrium based on the concentration of adsorbing species in solution and the available surface sites. In the case of FAD, the equilibrium is stable since any desorbing FAD will be quickly replaced by another FAD from solution. In the case of GOx, the desorbing FAD molecules can be replaced by non-electroactive GOx, whereby the electroactive amount adsorbed will decrease over time.

The FAD adsorption maximum increases concurrently with concentration, shown in Figure 2.5, indicating Langmuir adsorption behavior. This effect is not large between the concentrations used, and deviations in the amount of CNTs drop cast on the electrode can confound the trend, as observed for Figure 2.5A; however, if the same electrode is placed in increasing concentrations of FAD, the adsorption maximum also increases. Previous studies of FAD adsorbed onto TiO_2[108] and GC[103] have also shown that the FAD adsorption process displays Langmuir isotherm behavior.

2.3.2 Effect of Ionic Strength

For a surface confined redox reaction, the peak current should scale linearly with the scan rate according the equation (eq. 2.2) below[113]:

$$i_p = \nu \Gamma A(n^2F^2/(4RT)) \qquad (2.2)$$

Where i_p is the peak current (A), ν is the scan rate (V s^{-1}), Γ is the surface concentration (mol cm^{-2}), A is the electroactive surface area of the electrode (cm^2), n is the number of electrons transferred in the redox reaction, F is Faraday's constant (96485 C), R is the gas constant (8.314 J mol^{-1} K^{-1}), and T is the temperature (K). The ionic strength of the supporting electrolyte, however, plays a large role in determining the scan rates at which

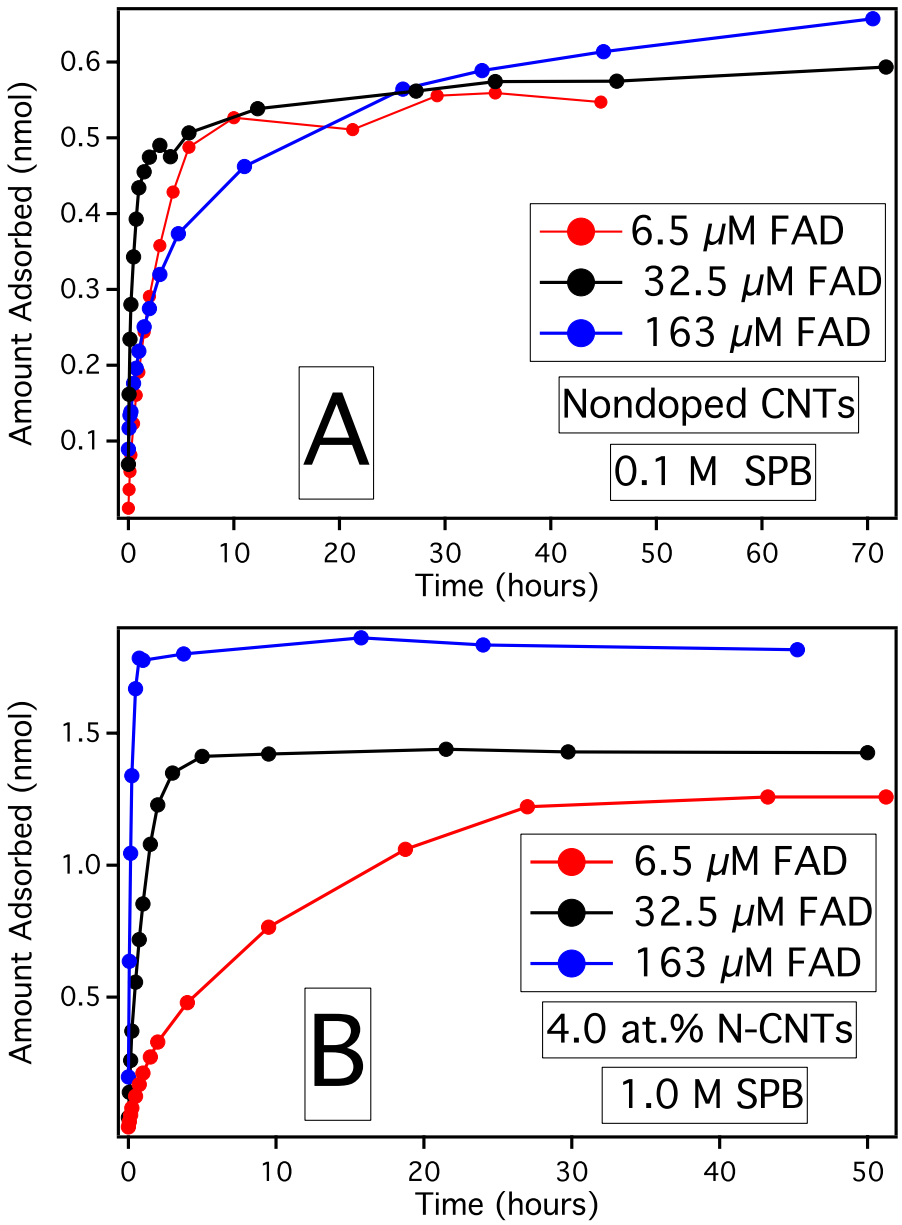

Figure 2.5. Solutions of 6.5 μM, 32.5 μM, and 163 μM FAD adsorbing onto (A) nondoped CNTs in 0.1 M SPB pH 7 or (B) 4.0 at.% N-CNTs in 1.0 M SPB pH 6.75.

a linear relationship is observed. A series of three different ionic strengths are shown in Figure 2.6, at varying scan rates. At lower scan rates the ionic strength of the supporting electrolyte plays less of a role in influencing the magnitude of the peak current; however, a difference is still observed. At high scan rates and low ionic strengths, the peak potentials are shifted (peak-to-peak potential splitting gets larger) and peak broadening occurs. It should be noted that although the peak-to-peak (cathodic and anodic) potential splitting (ΔE_p) gets larger at higher scan rates and lower ionic strengths, the $E_{1/2}$ or formal potential remains essentially constant. Although the linear relationship between the surface adsorbed FAD peak current and the scan rate also depends on the amount adsorbed, the limit of the linear relationship was determined to be 150 mV/s for 0.1 M, 250 mV/s for 0.5 M, and 400 mV/s for 1.0 M SPB.

The ionic strength also effects the maximum or equilibrium amount of FAD adsorbed onto the CNT/N-CNT surface. Analogous to a hydrophobic protein purification column, more FAD is adsorbed at higher ionic strengths, indicating that hydrophobic interactions play a role in the adsorption of FAD. This effect can be seen in Figure 2.7, which displays CVs of 4.0 at.% N-CNT electrodes at increasing exposure times to a 6.5 μM solution of FAD in 0.1 M or 1.0 M SPB. Figure 2.7 also displays the coordinating amount adsorbed as calculated from integration of the cathodic peak. Although the concentration of FAD is the same in each case, the maximum amount adsorbed is significantly higher in 1.0 M SPB as opposed to 0.1 M SPB. This effect can be seen when CVs are taken as a FAD loaded CNT/N-CNT electrode is transferred into increasing or decreasing ionic strength solutions. When FAD is adsorbed in 0.1 M SPB and transferred into higher ionic strength solutions, the amount adsorbed stays relatively constant. When FAD is adsorbed in 1.0 M SPB and transferred to lower ionic

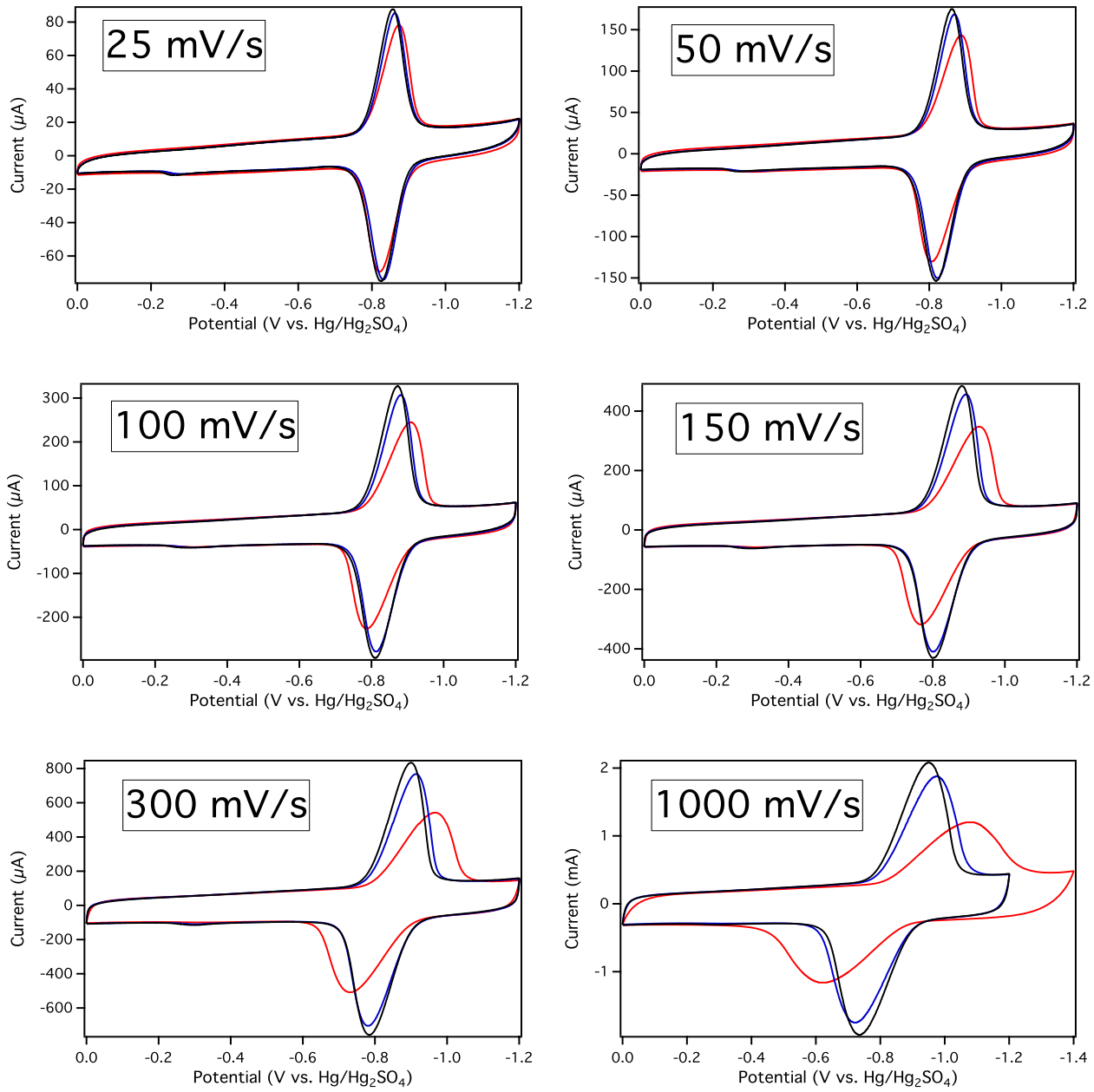

Figure 2.6. The observed surface confined redox reaction of FAD adsorbed onto 4.0 at.% N-CNTs as a function of scan rate and concentration of the supporting electrolyte (SPB pH 7.0; red = 0.1 M, blue = 0.5 M, black = 1.0 M)

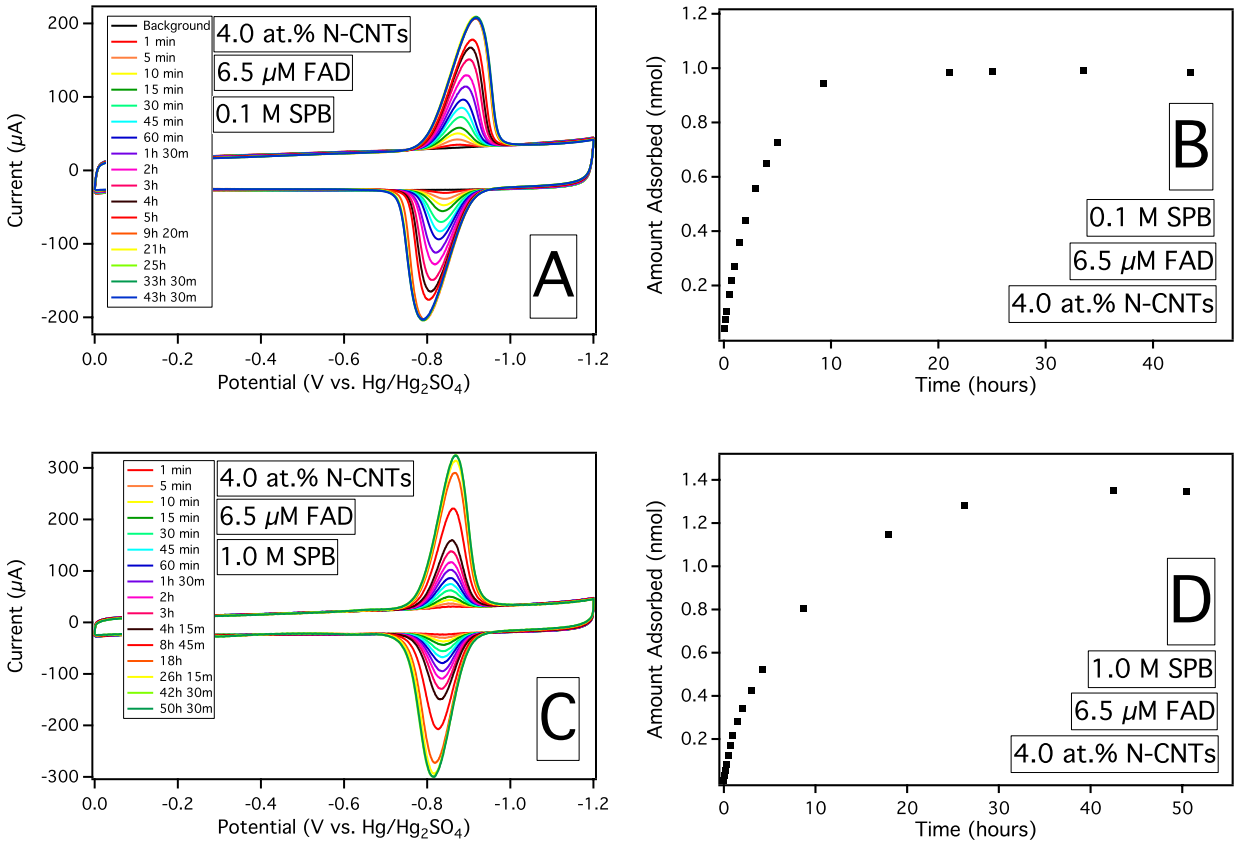

Figure 2.7. CVs of 6.5 μM FAD adsorbing onto 4.0 at.% N-CNTs in 0.1 M pH 7.0 (A) and 1.0 M pH 6.75 (C) SPB at increasing time points (scan rate 100 mV/s). The coordinating amount adsorbed (as calculated from the integration of the cathodic peak) is shown for each CV time point on the right (B and D).

strengths, the amount adsorbed decreases. It should also be noted that the measured ΔE_p is significantly smaller in 1.0 M SPB in comparison to values measured in 0.1 M SPB (Table 2.2).

The full width of the FAD peak at half the maximum (FWHM) peak current on nondoped CNTs during early adsorption times in 1.0 M SPB and a scan rate of 100 mV/s is close to 45 mV. The predicted FWHM for an ideal nerstian reaction under Langmuir conditions (90.6 mV/*n*) where *n* is a two-electron transfer process associated with eq. 2.1 is also 45 mV.[113] Although deviations from ideal behavior such as lateral interactions[113–115], inhomogeneity of adsorbate populations or surface sites[114,116], and ion interactions[117] can drastically effect peak shape, we note that the ideal FWHM occurs at low surface coverages, where intermolecular forces are minimal and initial adsorption sites are most likely identical. Additionally, the FWHM increases concurrently with increasing amounts of the adsorbing species (from 45 mV at low surface coverages to 95 mV at the maximum coverage), while the formal potential remains fairly constant. We cannot rule out, however, that the ideal FWHM is a composite of the aforementioned interactions. Adsorbed FAD on N-CNTs exhibit larger than ideal FWHM values due to the inhomogeneity of surface adsorption sites as nitrogen disrupts the carbon lattice.

2.3.3 Laviron's Method for Determining the Heterogeneous Electron Transfer Rate Constant and Uncompensated Resistance

In almost every reported heterogeneous electron transfer rate constant (k_s) between GOx and CNTs[36,40–43,92,93,95,96,98,99] the authors have employed Laviron's method to determine k_s.[118] This method uses the cathodic and anodic peak potential splitting, ΔE_p, as a way to determine k_s, which should be a function of the scan rate. Although this method is analytically sound, the uncompensated resistance (R_u) is not taken into account and this

aspect can drastically affect the outcome of observed measurements. In fact, Laviron's method is only valid if the electron transfer reaction (i.e. the kinetic part) is controlling ΔE_p. Figure 2.8 displays CVs of FAD adsorbed onto 4.0 at.% N-CNTs at different scan rates (2.8A), and during adsorption at a constant scan rate (2.8C) in 1.0 M SPB pH 6.75. At a constant scan rate, the ΔE_p should be independent of the amount adsorbed, and $E_{p,c}$ should concurrently remain constant.[119] Figure 2.8D displays a shift in the cathodic peak potential ($E_{p,c}$) as a function of the cathodic peak current ($i_{p,c}$), which is increasing concurrently with the amount adsorbed. Using Ohm's law (V = iR), the slope of Figure 2.8D is a measure of the resistance due to the increase in peak current as FAD is increasingly adsorbed. Figure 2.8B shows an identical plot, but of the $E_{p,c}$ shifting as the scan rate is changed. Interestingly, the slope or measured resistance in both plots are identical (67 Ω), indicating that resistance is controlling ΔE_p, and not the kinetics of heterogeneous electron transfer.

At nondoped CNTs in 1.0 M SPB and at low surface coverages of FAD, we observe a rate constant of 7.6 s^{-1} using Laviron's method. Since this value is under ohmic control, this is merely a lower limit, with the actual k_s being much faster. Given this measurement, it should be noted that every cited k_s is slower than this value, except when FAD is covalently attached to the ends of aligned single walled CNTs[42], or the "non-kinetic" peak splitting contribution is subtracted out.[40] Furthermore, our k_s was measured in 1.0 M SPB, but the majority of k_s were determined in 0.1 M solutions, where the ionic strength was already shown to play a large role in the observed electrochemical behavior and measured k_s. Table 2.2 presents the absorption time, ΔE_p, and calculated k_s (using Laviron's method) for each CV time point shown in Figure 2.7.

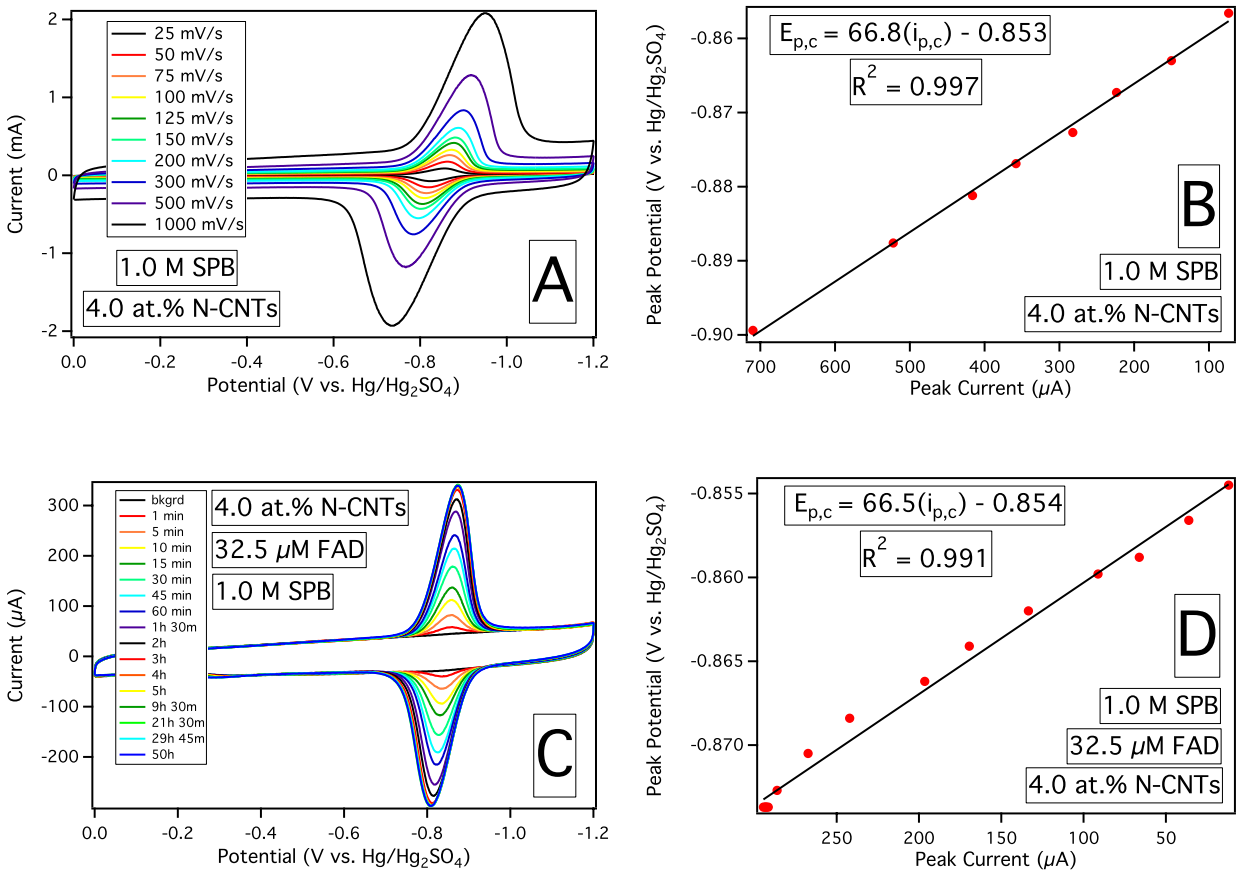

Figure 2.8. CVs of FAD on 4.0 at.% N-CNTs at increasing scan rates (A, 25 – 1000 mV/s) and during adsorption at a constant scan rate (C, 100 mV/s). The $E_{p,c}$ vs. $i_{p,c}$ plots (B and D) present the measured resistance as a function of scan rate (B) or amount adsorbed (D).

Table 2.2. Adsorption Time, Peak-to-Peak Cathodic and Anodic Potential Splitting (ΔE_p), and Electron Transfer Rate Constant (k_s) for FAD adsorbing onto 4.0 at.% N-CNTs in 0.1 M (pH 7.0) or 1.0 M SPB (pH 6.75).

Adsorption Time (0.1M)	ΔE_p (mV)	k_s (s^{-1})	Adsorption Time (1.0M)	ΔE_p (mV)	k_s (s^{-1})
1 min	27.8	2.19	1 min	18.1	3.70
5 min	26.7	2.31	5 min	13.9	5.03
10 min	32.1	1.82	10 min	11.8	6.06
15 min	39.5	1.38	15 min	17.1	3.96
30 min	47.0	1.08	30 min	14.9	4.64
45 min	51.3	0.95	45 min	18.2	3.68
60 min	58.7	0.77	60 min	20.3	3.23
1h 30m	70.5	0.57	1h 30m	20.3	3.23
2h	76.9	0.49	2h	22.4	2.87
3h	87.6	0.38	3h	23.5	2.70
4h	95.0	0.32	4h 15m	26.7	2.31
5h	105.8	0.50*	8h 45m	37.3	1.49
9h 20m	122.8	0.36*	18h	47.0	1.08
21h	123.9	0.35*	26h 15m	51.3	0.95
25h	126.0	0.33*	42h 30m	54.5	0.86
33h 30m	128.2	0.32*	50h 30m	53.4	0.89
43h 30m	127.1	0.33*			

* According to Laviron's method, when the peak-to-peak splitting becomes larger than 200mV/n (in this case since, n = 2, so 100 mV) another equation is used to calculate k_s

CVs of FAD display a peak splitting (ΔE_p) which is independent of scan rate or amount adsorbed. This ΔE_p is approximately 10 mV, which may be explained by a N-shaped free energy curve.[120] In this case, FAD is expected to undergo a structural change, where the oxidized form is planar and the reduced form resembles a butterfly conformation.[82] This structural change is most likely the reason for a persistent ΔE_p, even though it should ideally be zero at slow scan rates.

The $E_{p,c}$ vs. $i_{p,c}$ plots at varying scan rates are dependent on the ratio of adsorbed FAD current to the background capacitive current. Table 2.3 displays the measured resistances as a function of the ratio of the FAD current to the background current on 4.0 atom % N-CNTs in 0.1 SPB pH 7.0. Unusually high resistances are measured when the capacitive current is dominanting the overall current, but as more FAD is adsorbed, the slope eventually matches the slope of $E_{p,c}$ vs. $i_{p,c}$ plots where FAD is increasingly adsorbed at a constant scan rate. Resistances converge to 56.6 ± 13.5 Ω for 1.0 M SPB pH 6.75, and 266 ± 52 Ω for 0.1 M SPB pH 7.0. Interestingly, the measured resistance provides an excellent estimate of the uncompensated resistance R_u, which can be matched up to the universal working curve presented by Feldberg.[119] Feldberg's working curve models the ideal behavior of a surface-bound redox system with finite R_u. Since our data aligns with Feldberg's working curve when our measured resistances are used in place of R_u, we can reasonably assume that our measured resistances are a good estimate of R_u. Furthermore, it should also be noted that in 1.0 M SPB pH 6.75 and at high scan rates (500-40,000 mV/s), FAD adsorbed onto a roughened GC surface or an edge-plane pyrolytic graphite electrode (PINE AFE2M050GE) display peak shifts whose $E_{p,c}$ vs. $i_{p,c}$ slopes of 62.7 ± 12.3 Ω correlate well with those measured on CNT/N-CNT electrodes. This indicates that the measured resistance from the $E_{p,c}$ vs. $i_{p,c}$ plots most likely represent

Table 2.3. Measured resistances from $E_{p,c}$ vs. $i_{p,c}$ plots at varying scan rates of FAD adsorbed onto 4.0 at.% N-CNTs in 0.1 M SPB pH 7.0.

FAD Peak Current (μA)	Amount Adsorbed (pmol)	Background current (μA)	Ratio (FAD/Background)	Measured Resistance (Ω)
6.6	25	37.7	0.18	2337
19.8	78	36.8	0.54	842
33.0	131	33.0	1.00	562
136.1	679	37.8	3.60	388
232.9	1347	38.0	6.13	264

solution resistance, since neither film resistance (the CNT/N-CNT film was removed) nor the electron transfer resistance (the peak-to-peak splitting should have remained constant at a constant scan rate during adsorption) is playing a major role in the measured resistance. The calculated k_s for FAD on GC was measured as high as 30.7 s^{-1} (Laviron's method), suggesting that this value may still be slower than the actual rate constant.

2.3.4 GOx Activity and Bioelectrocatalysis

In the presence of GOx and oxygen, glucose is oxidized by GOx into D-Glucono-1,5-Lactone while oxygen is reduced by GOx to H_2O_2. The product D-Glucono-1,5-Lactone is subsequently hydrolyzed in aqueous solutions into D-gluconic acid. Both reactions are shown below (eq. 2.3 and 2.4):

$$\beta\text{-D-Glucose} + O_2 \rightarrow \text{D-Glucono-1,5-Lactone} + H_2O_2 \qquad (2.3)$$

$$\text{D-Glucono-1,5-Lactone} + H_2O \leftrightarrow \text{D-Gluconic Acid} \qquad (2.4)$$

The cofactor, FAD, is the redox reaction center of GOx, where two protons and two electrons are transferred from glucose. Under normal physiological conditions, oxygen would be reduced by aquiring the two protons and two electrons from $FADH_2$, re-oxidizing the active center, thereby allowing GOx to turnover another glucose molecule. In the absence of O_2 or another appropriate electron mediator, only the electrode would be able oxidize $FADH_2$ to FAD, subsequently producing an anodic current at the electrode surface. The electrode turnover scheme, known as bioelectrocatalysis, is shown below (eq. 2.5 and 2.6):

$$GOx(FAD) + \beta\text{-D-Glucose} \rightarrow GOx(FADH_2) + \text{D-Glucono-1,5-Lactone} \qquad (2.5)$$

$$GOx(FADH_2) \rightarrow GOx(FAD) + 2H^+ + 2e^- \text{ (anodic current at the electrode)} \quad (2.6)$$

The main test for DET between enzyme active FAD and CNTs is the appearance of anodic current when glucose is added in an oxygen-free (and mediator-free) environment. The adsorbed GOx was tested for bioelectrocatalysis by rotating disk chronoamperometry where in an Ar saturated buffer (continuously bubbled Ar), the potential was held at specific points that would sufficiently oxidize $FADH_2$ back to FAD, shown in Figure 2.9C-F. Figure 2.9A and 2.9B also displays CVs of GOx and FAD adsorbed onto CNT and 7.4 at.% N-CNT electrodes. The dotted blue lines indicate the open circuit potential (-0.37 V for CNTs and -0.18 V for 7.4 at.% N-CNTs) and the formal potential (-0.86 V for CNTs and -0.85 V for 7.4 at.% N-CNTs) for adsorbed FAD/GOx. CNT and 7.4 at.% N-CNT electrodes with adsorbed FAD were used as a non-glucose active background. Rotating disk chronoamperograms held at the open circuit potential display lower noise and less background drift than those held at the formal potential; however, anodic current is not observed at either electrode, at either potential held. Besides a small mixing artifact when glucose is added at 300 s, there is virtually no change in the chronoamperograms. Figure 2.10 displays the exact same experiments, but using a glucose solution that was not Ar purged. Oxygen reduction plays a major role, even in minute amounts, as seen by the large reduction currents when glucose is injected into the solution at the formal potential (Figure 2.10E and F). The oxygen reduction reaction (ORR) occurs at nondoped CNTs and 7.4 at.% N-CNTs at -0.81 V and -0.30 V, respectively.[121] Since the formal potential of FAD on nondoped CNTs and 7.4 at.% N-CNTs occurs more negative of the ORR, it is clear why such a pronounced oxygen

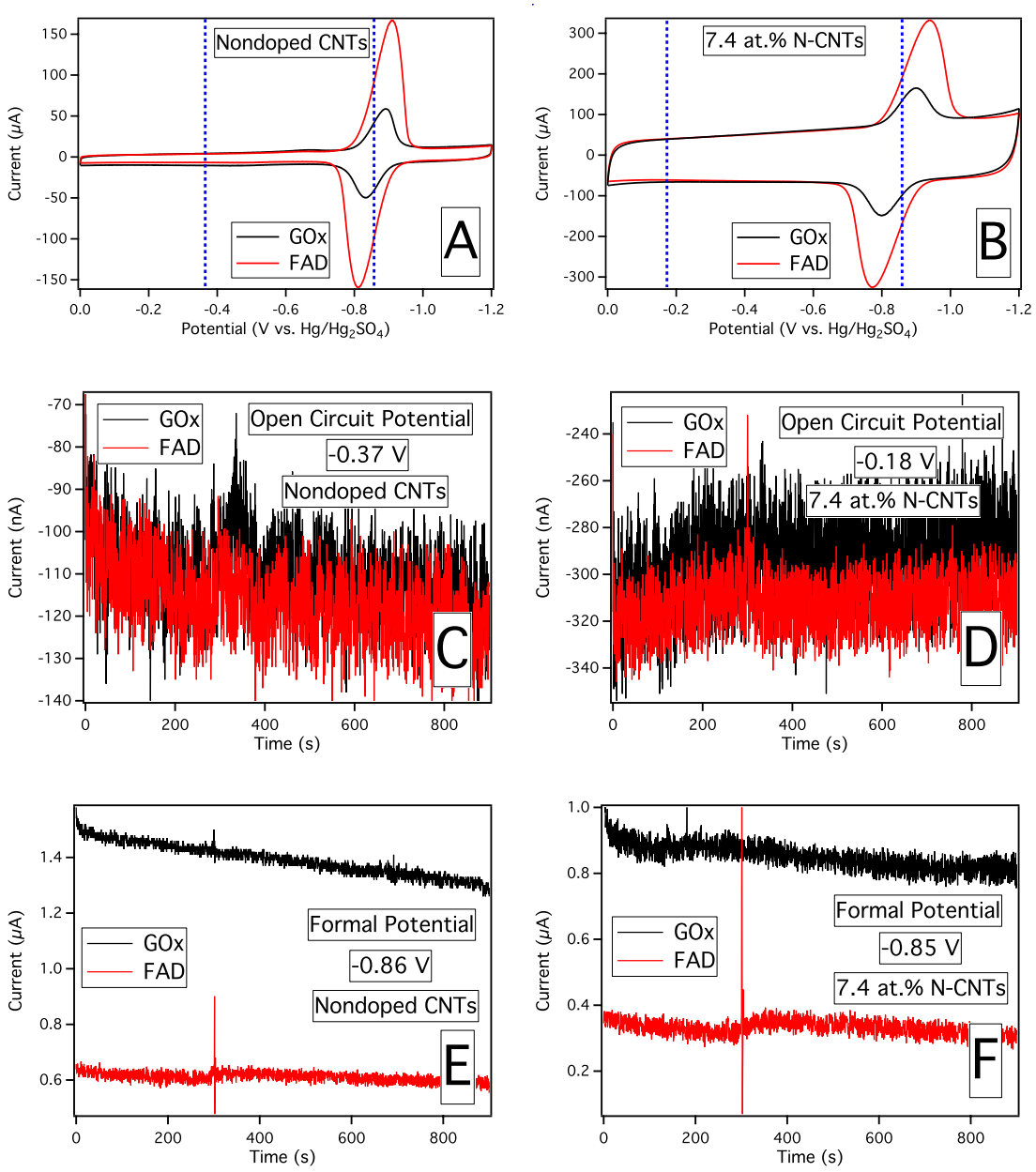

Figure 2.9. CVs of FAD and GOx adsorbed onto (A) nondoped CNT and (B) 7.4 at.% N-CNT modified electrodes (scan rate 100 mV/s 0.1 M SPB pH 7.0). Rotating disk chronoamperograms (1000 rpm) of FAD and GOx adsorbed onto nondoped CNT and 7.4 at.% N-CNT electrodes, where 10 mM of Ar purged glucose is injected into the solution at 300 s (Ar is continuously bubbled in the 0.1 M SPB) while the potential is held at the open circuit potential (C and D) or the formal potential (E and F).

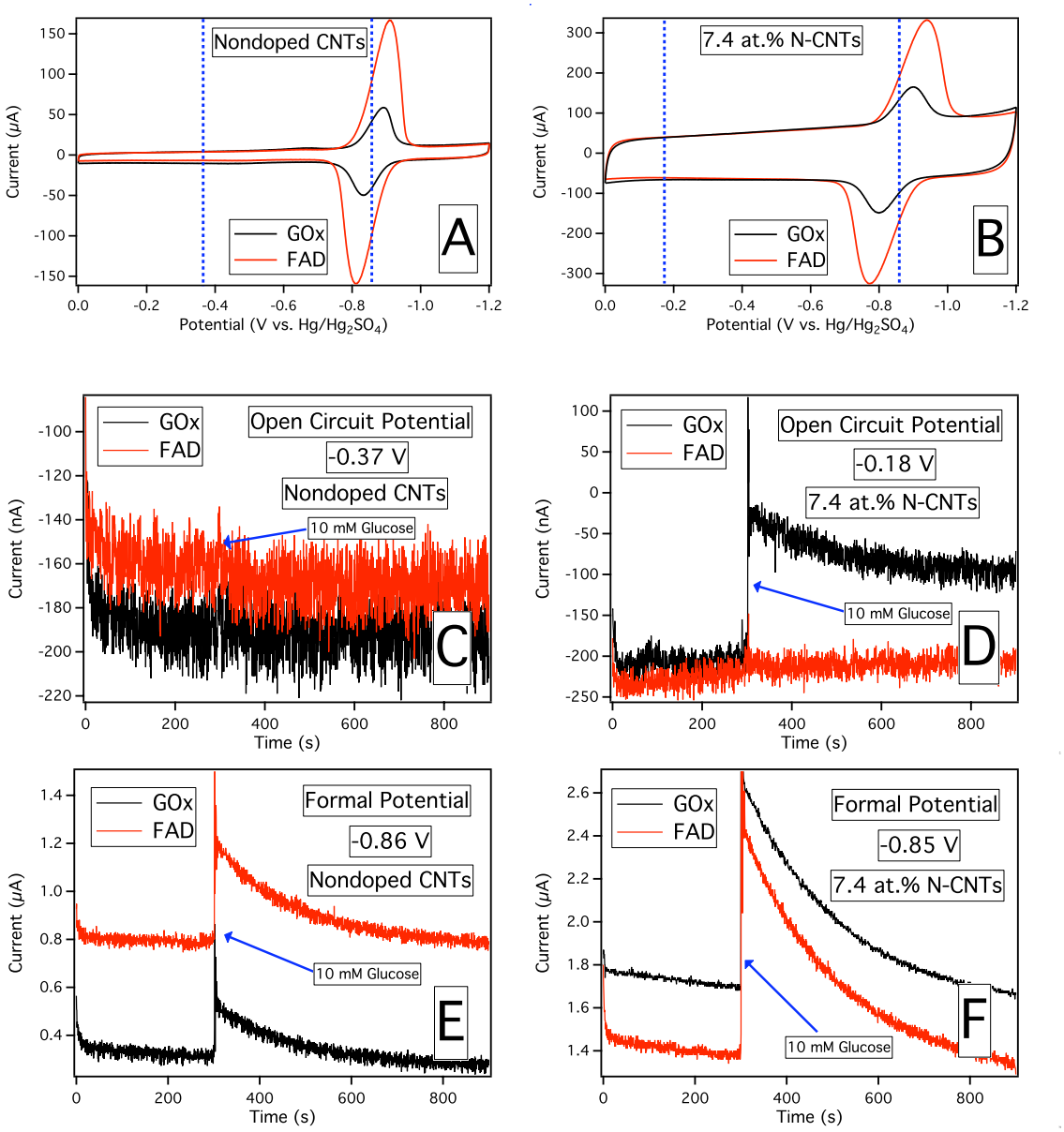

Figure 2.10. CVs of FAD and GOx adsorbed onto (A) nondoped CNT and (B) 7.4 at.% N-CNT modified electrodes (scan rate 100 mV/s 0.1 M SPB pH 7.0). Rotating disk chronoamperograms (1000 rpm) of FAD and GOx adsorbed onto nondoped CNT and 7.4 at.% N-CNT electrodes, where 10 mM of air saturated glucose (1 ml of 1 M glucose into 99 ml of 0.1 M SPB) is injected into the solution at 300 s (Ar is continuously bubbled in the 0.1 M SPB) while the potential is held at the open circuit potential (C and D) or the formal potential (E and F).

reduction current is observed. At nondoped CNTs, the ORR potential is far enough away from the open circuit potential that no change is observed when glucose is added (Figure 2.10C); however, at 7.4 atom % N-CNTs, the open circuit potential is near the onset of the ORR (Figure 2.10D). In addition, the ORR occurs via a different pathway on N-CNTs[60,61], so the small amount of injected oxygen that is enzymatically transformed into H_2O_2 subsequently disproportionates into more oxygen at N-CNTs, increasing the reductive component of the background current.[62,121]

Figure 2.11 shows CVs of nondoped CNT and 7.4 at.% N-CNT electrodes with adsorbed GOx as Ar purged glucose is added to the solution (2.11A and B). If DET occurs, the glucose should spontaneously reduce FAD, causing the reduction peak to decrease. No change is observed in the CVs as the glucose concentration is increased (2.11A and B), except for a slow desorption of GOx from the nondoped CNTs during the timeframe of the measurement. Even though no change is observed, GOx is still active, and can be verified if an electron mediator is present, or if the natural electron mediator oxygen is present. Figure 2.11 also displays CVs of GOx adsorbed onto nondoped CNT and 7.4 at.% N-CNTs when an electron mediator, 1,4-hydroquinone/1,4-benzoquinone (H_2Q/Q), is added to the SPB solution (2.11E and F). When the H_2Q/Q redox couple is present, an increase in the anodic wave for the H_2Q/Q couple appears when glucose is added to the solution. This anodic wave is the result of the enzymatic turnover of glucose, whereby the reduced $FADH_2$ is re-oxidized by Q to FAD, and Q is reduced to H_2Q. The cathodic wave of the quinone couple goes down, while the anodic peak is increased concurrently with the glucose concentration, indicative of the enzyme turnover rate. Note that the FAD peak (potential or current) does not change, thus giving more evidence that DET is not occurring between GOx and CNTs. Wang and Yao have also

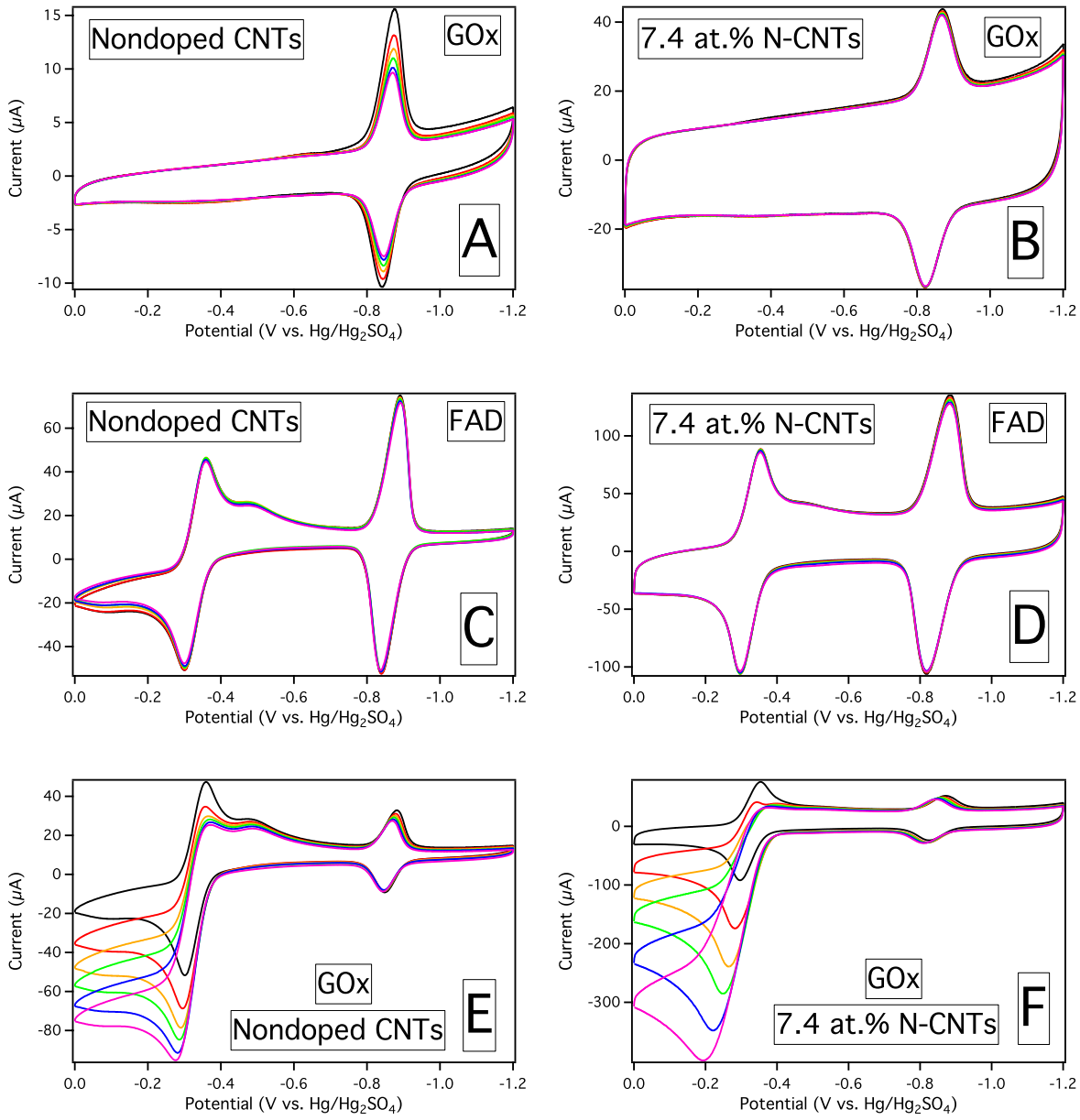

Figure 2.11. CVs of GOx adsorbed onto nondoped CNTs and 7.4 at.% N-CNTs with increasing concentrations of Ar purged glucose (black = 0 mM, red = 10 mM, orange = 20 mM, green = 30 mM, blue = 50 mM, purple = 75 mM) in the absence (A and B), and presence (E and F) of 0.5 mM 1,4-hydroquinone and 0.5 mM 1,4-benzoquinone. FAD is used instead of GOx in C and D as a non-glucose active control (also in the presence of the redox mediator). Scan rate is 25 mV/s for all the CVs presented, 0.1 SPB pH 7.0.

shown that the widely reported DET between GOx and CNTs is without value in certain mediator-free applications.[122] Figure 2.11C and D display FAD adsorbed onto nondoped CNTs and 7.4 at.% N-CNTs, which do not show enzymatic activity as a function of the glucose concentration in the presence of H_2Q/Q.

A second more interesting way of verifying the activity of adsorbed GOx on the surface of the N-CNTs is by using the natural electron mediator oxygen. The ORR at N-CNTs occurs via a peroxide pathway, whereby H_2O_2 created from oxygen reduction will rapidly disproportionate on the N-CNT surface to create a local increase in oxygen.[60,61] This unique pathway allows for detection of glucose (through enzymatically generated H_2O_2) at close to the open circuit potential of the electrode, minimizing electroactive interferents and background processes. We have previously demonstrated that this electrochemical detection scheme can be applied to GOx[62] or other enzymes, such as lactate oxidase[121], which also produce H_2O_2 as a byproduct. We note that in our paper describing the detection of L-lactate via lactate oxidase and N-CNTs[121], we mistakenly assigned the observed FAD signal (FAD is also the active center of lactate oxidase) to DET. The aforementioned analysis has shown that the observed FAD signal was not DET, but simply electroactive FAD derived from inactive enzyme. Figure 2.12 shows rotating disk chronoamperometric data of a 7.4 at.% N-CNT electrode with GOx adsorbed on the surface in an oxygen saturated or an argon saturated 0.1M SPB pH 7.0. When aliquots of 0.5 mM glucose are injected into the solution, a clear reduction current response is observed, directly proportional to the glucose concentration in the oxygen saturated solution, while no response is observed in the argon saturated solution. This glucose biosensor, without optimization, displays a sensitivity of 0.011 A M^{-1} cm^{-2} (based upon the geometric area of the GC electrode), a detection limit of 24 μM, and a linear

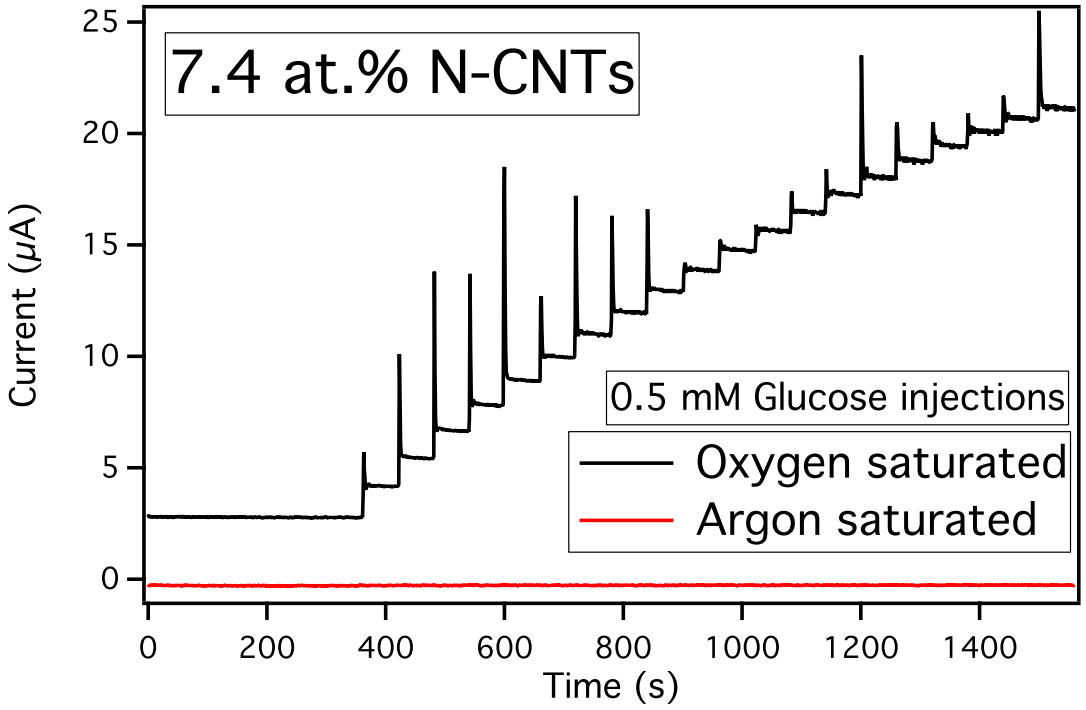

Figure 2.12. Rotating disk chronoamperogram of GOx adsorbed onto 7.4 at.% N-CNTs as 0.5 mM injections of glucose are added to a oxygen saturated solution or an argon saturated solution (Ar or O_2 constantly bubbled, 0.1 M SPB pH 7.0, rotating rate 1000 rpm).

range of 6.5 mM (based on $R^2 > 0.995$) at -0.23 V vs. Hg/Hg_2SO_4 after GOx was allowed to adsorb onto the 7.4 at.% N-CNTs at room temperature for 42 hours.

2.4 CONCLUSION

FAD and GOx were spontaneously adsorbed onto CNTs and N-CNTs without covalent attachment, oxidizing agents, surfactants, or binders. The subsequent unimpeded phyisisorbed interactions were investigated by cyclic voltammetry and chronoamperomtery, which showed a dependence of the amount adsorbed on the exposure time to the adsorbing species, the concentration of adsorbate, and the ionic strength of the adsorbate solution. CNT and N-CNT electrodes with adsorbed GOx were examined for DET, but anodic current associated with the oxidation of glucose was not observed when glucose was added to an oxygen-free solution. Adsorbed GOx is active, however, as a clear anodic current increase was observed if an appropriate electron mediator was present, or the natural electron mediator oxygen was employed. Since the surface confined redox reaction is identical for adsorbed FAD and GOx, the observed FAD peak from adsorbed GOx is a result of FAD which is not enzymatically active. The well-defined FAD redox peaks were used to determine the heterogeneous electron transfer rate constant (k_s) between FAD and CNTs/N-CNTs using Laviron's method. The measured value of 7.6 s^{-1} was determined to be under ohmic control, thereby suggesting that the actual k_s is much faster.

CHAPTER 3

Electrochemical Behavior of Flavin Adenine Dinucleotide Adsorbed onto Carbon Nanotube and Nitrogen-Doped Carbon Nanotube Electrodes*

3.1 INTRODUCTION

Carbon nanotubes (CNTs) are only one of the many conductive carbon materials available for electrochemical applications[123], but provide attractive features over traditional carbon electrodes such as increased surface area, high mechanical strength, improved electronic conductivity, and enhanced electrocatalysis.[124,125] Their use as an electrode material for chemical sensing is ubiquitous[86,124,126], and are often coupled with enzymes for biosensor and biofuel cell applications.[35,40,85,89,95,127,128] Flavoenzymes are one of the most common enzymes employed (e.g. glucose oxidase), identified by their use of the enzymatic cofactor flavine adenine dinucleotide (FAD). FAD is electroactive[129], and generally displays a two-electron two-proton redox reaction shown in equation 1 (eq 3.1) below:

$$FAD + 2H^+ + 2e^- \leftrightarrow FADH_2 \qquad (3.1)$$

Although FAD has been studied on electrode materials such as Hg[82,101,102,112], Au[106,130], Ti[107], TiO_2[108], TiO_2 nanoparticles[131], Ni oxide[132], Zr oxide[133], $SiO_2/ZrO_2/C$ ceramic electrode[134], Co oxide[135], conducting polymers[136–138], poly(FAD) films[139,140], glassy carbon[103–105,141,142], and graphite[109,110] its electrochemical behavior on CNTs has only been minimally investigated. The vast majority of studies involving FAD and CNTs have

*Portions of this chapter were published in Goran, J. M.; Stevenson, K. J. *Langmuir* **2013**, *29*, 13605-13613. (Stevenson supervised this work)

been focused on glucose oxidase (GOx) and an apparent direct electron transfer (DET) between GOx and CNTs.[36,37,40,42,43,93,95,99,143] Thus, subsequent electrochemical characterizations of FAD on CNTs are limited to conditions appropriate for enzymatic activity, and ignore inherent electrochemical benefits of FAD as a surface sensitive redox probe. This retricts pH depedence studies to a narrow range of about pH 4-8[36,37,93,99,143,144], neglecting to observe a pK_a shift that commonly occurs when a solution species is immobilised on an electrode surface.[145,146] Furthermore, FAD is particularly useful when addressing drop cast CNT mesh electrodes, which are difficult to characterize by conventional techniques. Previous studies in our group have shown that DET is not observed when GOx spontaneously adsorbs onto CNTs from solution.[147] FAD was shown to spontaneously adsorb onto CNTs and nitrogen-doped CNTs (N-CNTs), subsequently dislaying Langmuir adsorption characteristics. N-CNTs have been noted as being more biocompatible[148], hydrophilic[57], and electrocatalytic to biologically relevant molecules such as NADH and H_2O_2, in comparison to nondoped CNTs.[53,54,60,61,121,149] Herein, we present a detailed look at the electrochemical behavior of FAD adsorbed onto CNT and N-CNT electrodes, which exhibit strikingly different electrochemical behavior during FAD desorption/transformation. In order to properly assess FAD adsorption, binders, surfactants, dispersion agents, and oxidative acids (sulfuric, nitric) are not used as these change both the type and density of surface sites on CNT and N-CNT electrodes available for adsorption of FAD.

3.2 EXPERIMENTAL

3.2.1 Chemicals

Sodium phosphate dibasic (Na_2HPO_4), sodium phosphate monobasic (NaH_2PO_4), potassium nitrate (KNO_3), sodium hydroxide (NaOH), *o*-phosphoric acid (85%), pH

calibration buffers (4.00, 7.00, 10.00), and pyridine were purchased from Fisher (all ACS Grade). Flavin adenine dinucleotide disodium salt hydrate (≥95%, stored at - 20°C when not in use) and *m*-xylene (anhydrous) were purchased from Sigma-Aldrich. Bis(cyclopentadienyl)iron (ferrocene, 99%) was obtained from Alfa Aesar. Hexaammineruthenium (III) chloride (99%) was purchased from Strem Chemicals. Calibration buffers at pH 1.68 and 12.46 were obtained from Oakton.

3.2.2 CNT/N-CNT Synthesis

CNTs and N-CNTs were synthesized in a quartz tube via a chemical vapor deposition (CVD) process. The CVD process used a customized LabVIEW program which coordinated two identical tube furnances (Carbolite Model HST 12/35/200/2416CG), two gas mass flow controllers (MKS type 1179A), and an automated syringe pump (New Era Pump Systems NE-1000) simultaneously. Briefly, a 20 mg mL^{-1} solution of ferrocene dissolved in either m-xylene (CNTs) of pyridine (N-CNTs) was injected into the quartz tube (0.1 ml min^{-1}) via a glass syringe (Hamilton 81320) loaded into the automated syringe pump. The first tube furnace (were the ferrocene solution entered into the quartz tube) was set at a temperature to cause the liquid ferrocene solution to vaporize (130°C for pyridine and 150°C for m-xylene). Argon gas from first gas mass flow controller was used to carry the vaporized precursor solution along the quartz tube into the second tube furnace which was set at a temperature to initiate growth of the multiwlled CNT/N-CNTs along inner wall of the quartz tube (700°C for CNTs, 800°C for N-CNTs). The second mass flow controller coinjected either H_2 (75 sccm for CNTs) or NH_3 (0 sccm for 4.0 at.% N-CNTs and 43 sccm for 7.4 at.% N-CNTs) during nanotube formation at a total gas flow rate of 575 sccm (including Ar).

3.2.3 Electrochemistry and Electrode Preparation

Electrochemical measurements were performed using an Autolab PGSTAT30 potentiostat (GPES software version 4.9) in a five-neck glass cell (125ml) with a Hg/Hg_2SO_4 reference electrode (CH Instruments, +0.64 V vs SHE; +0.44 V vs Ag/AgCl; +0.40 V vs SCE) and a coiled Au counter electrode. CNT and N-CNT electrodes were prepared by drop casting 24 μg (six 10 μl aliquots of a 0.4 mg ml^{-1} solution for CNTs or one 12 μl aliquot of a 2 mg ml^{-1} solution for N-CNTs) onto a 0.5 cm diameter rotating disk electrode (Pine Instruments AFE2M050) which were polished with a 0.05 μm alumina slurry on microcloth (Buehler) and breifly sonicated in 18 MΩ cm water to remove adsorbed alumina. Electron micrographs of the "as grown" CNT/N-CNTs and prepared electrodes were obtained using a FEI Quanta 650 FEG with secondary electrons (electron energy of 30 keV). CNT/N-CNT solutions were prepared in absolute ethanol and sonicated for two hours prior to use. Electrodes were "wet" in a mixture of ethanol and sodium phophate buffer to ensure complete surface contact with the electrolyte solution. Preceding FAD adsorption, CNT/N-CNT electrodes were cycled between 0 and -1.2 V to passivate electroactive iron remaining from CVD synthesis.[55] FAD was allowed to adsorb at open circuit and rinsed briefly with SPB prior to electrochemical measurements (in an FAD free solution) to ensure only adsorbed FAD remained. Since FAD can phototlytically react, adsorption of FAD was carried out in the absence of light; however, FAD loaded electrodes were exposed to ambient light during electrochemical measurements (~3 min). The same adsorption procedure was used for all the flavins (FAD, FMN, RF) included in this study. CVs are displayed with negative anodic current and positive cathodic current.

3.3 Results and Discussion

3.3.1 CNT/N-CNT Electrode Characterization

Figure 3.1 presents electron micrographs of the "as grown" CNT/N-CNTs (Figure 1A, 1B, 1C) and their morphology after sonication and solution drop casting on a 0.5 cm diameter electrode (Figure 1D, 1E, 1F). It is clear from the micrographs that the morphology of the nondoped CNTs and 4.0 at.% N-CNTs remains nearly identical, but the heavily bundled 7.4 at.% N-CNTs still remain slightly bundled after sonication. Regardless, all three electrodes consist of a three-dimensional mesh of nanotubes.

Table 1 shows the results of using the Cottrell equation to determine the electroactive surface area (ESA) of the CNT/N-CNT mesh electrodes via chronocoulometry (integral of the Cottrell equation) with hexaammineruthernium ($Ru(NH_3)_6^{3+}$), a traditional way of measuring the ESA. Although this technique works with well-defined electrode surfaces, the ESA is underestimated when applied to the CNT/N-CNT mesh electrodes. The one-electron reduction of $Ru(NH_3)_6^{3+}$ to $Ru(NH_3)_6^{2+}$ relies on the steady-state diffusion of the oxidized species to the electroactive redox sites. In the case of a three-dimensional mesh, the diffusion controlled current is merely $Ru(NH_3)_6^{3+}$ being reduced at the mesh surface, and not actually penetrating into mesh pores, displayed in the table as an ESA nearly identical to the background glassy carbon (GC).[150] A common way of measuring the surface area of porous materials is by nitrogen adsorption, a technique developed and named after Brunauer, Emmett, and Teller (BET).[151] BET is an overestimate of the ESA since it uses nonelectroactive nitrogen as a probe molecule, but provides a more accurate measurement of the total available surface area. BET measurements on the CNTs/N-CNTs were made in a prior report.[152]

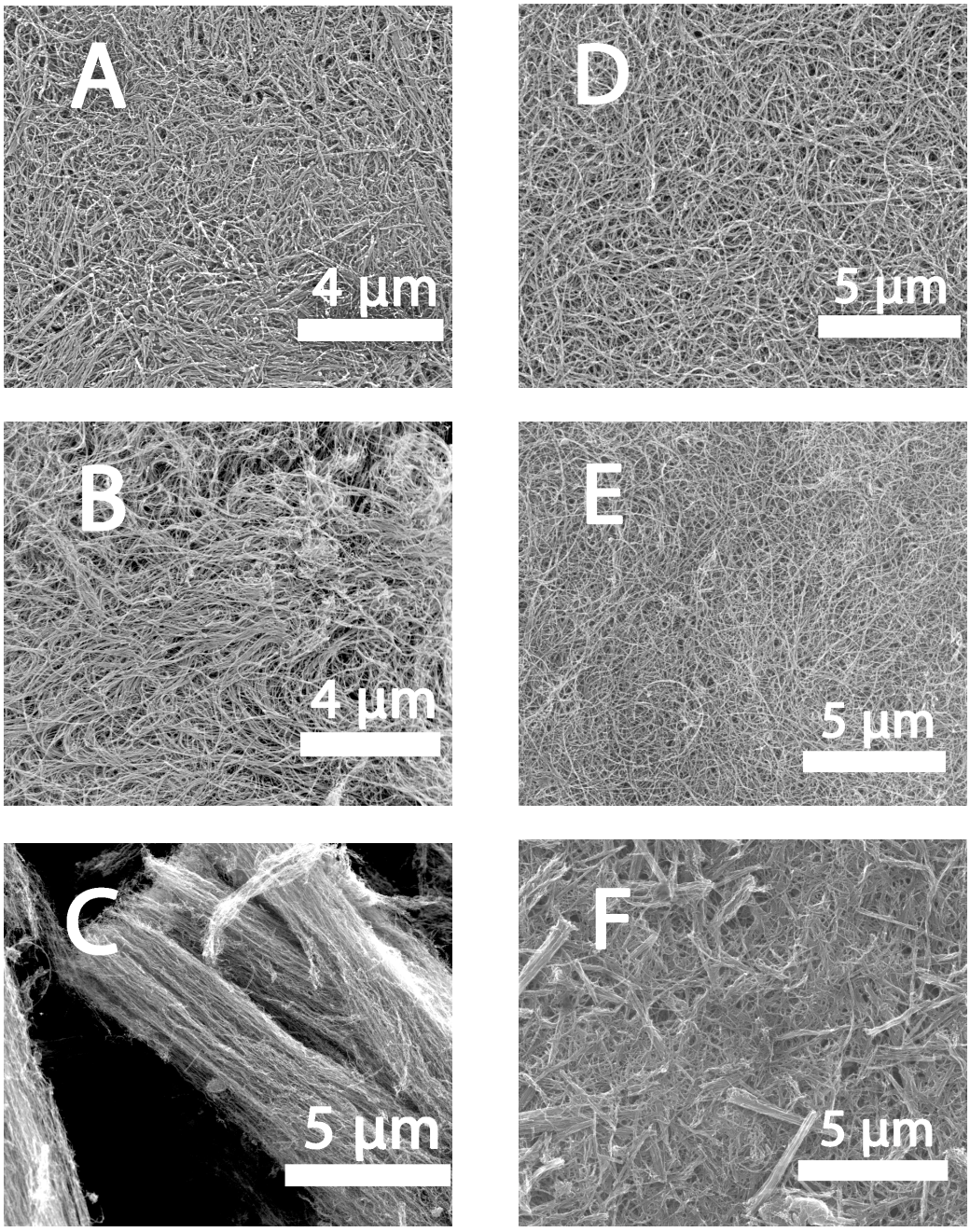

Figure 3.1. Scanning electron micrographs of the "as grown" nanotubes (A, B, C; nondoped CNTs, 4.0 at.% N-CNTs, and 7.4 at.% N-CNTs, respectively) and the resulting morphology after soncation and solution drop casting (D, E, F; nondoped CNTs, 4.0 at.% N-CNTs, and 7.4 at.% N-CNTs, respectively)

Table 3.1. Surface Area Measurements of CNT/N-CNT Electrodes

Type	Chronocoulometry (cm^2)	BET (cm^2)	FAD Adsorption (cm^2)
Glassy Carbon	0.32 ± 0.01	NM	NM
Nondoped CNTs	0.33 ± 0.01	30	12 ± 1
4.0 at.% N-CNTs	0.35 ± 0.01	31	24 ± 1
7.4 at.% N-CNTs	0.39 ± 0.01	54	27 ± 2

Chonocoulometry was peformed in 1M KNO_3, Geometric Area is 0.196 cm^2, NM = Not Measured
CNT/N-CNT Electrodes are Mass Normalized (24 μg)

Identical to the chronocoulometry measurements, an increase in the BET surface area is observed concurrent with increased nitrogen content. The BET surface area, however, is approximately 100 times larger than the ESA measured by chronocoulometry. The chemically reversible, surface confined redox reaction of FAD can provide an alternate and more accurate approach to measuring the ESA. Assuming a parallel orientation of the isoalloxazine moiety on the electrode surface to maximize π-π stacking[153], and a coordinating surface area of 1.0 nm^2 per FAD molecule[104,109,112], the Langmuir model of FAD adsorption can be used to estimate the number of molecules at a complete monolayer, and subsequently, the ESA. Evidence that adsorption of FAD onto CNT/N-CNT electrodes is indicative of the Langmuir model is provided herein and also provided in a prior report.[147] The calculated ESA from adsorbed FAD under the assumption of Langmuir adsorption behavior provides results that are reasonable, lying between that of the underestimated chronocoulometry or overestimated BET measurements (Table 1).

3.3.2 Spontaneous FAD Adsorption onto CNT/N-CNT Electrodes

Figure 3.2 displays cyclic voltammograms (CVs) of FAD spontaneously adsorbing onto CNT/N-CNT electrodes from a 6.5 μM FAD solution in 1.0 M sodium phosphate buffer (SPB) at pH = 6.75 over one hour. The $E_{1/2}$ of the FAD surface reaction occurs at -0.84 V on N-CNTs and -0.85 V on nondoped CNTs. The background capacitance increases with nitrogen content, indicating increased ESA as a function of incorporated nitrogen as observed in Table 3.1. This increase in capacitance was previously studied, and is attributed to the increased disorder caused by nitrogen incorporation into the carbon lattice, as measured by Raman spectroscopy.[59] This disorder is often described as an increase in edge plane character, since CNTs are commonly compared to the basal plane (tube sidewalls) and edge plane (tube ends) of highly ordered

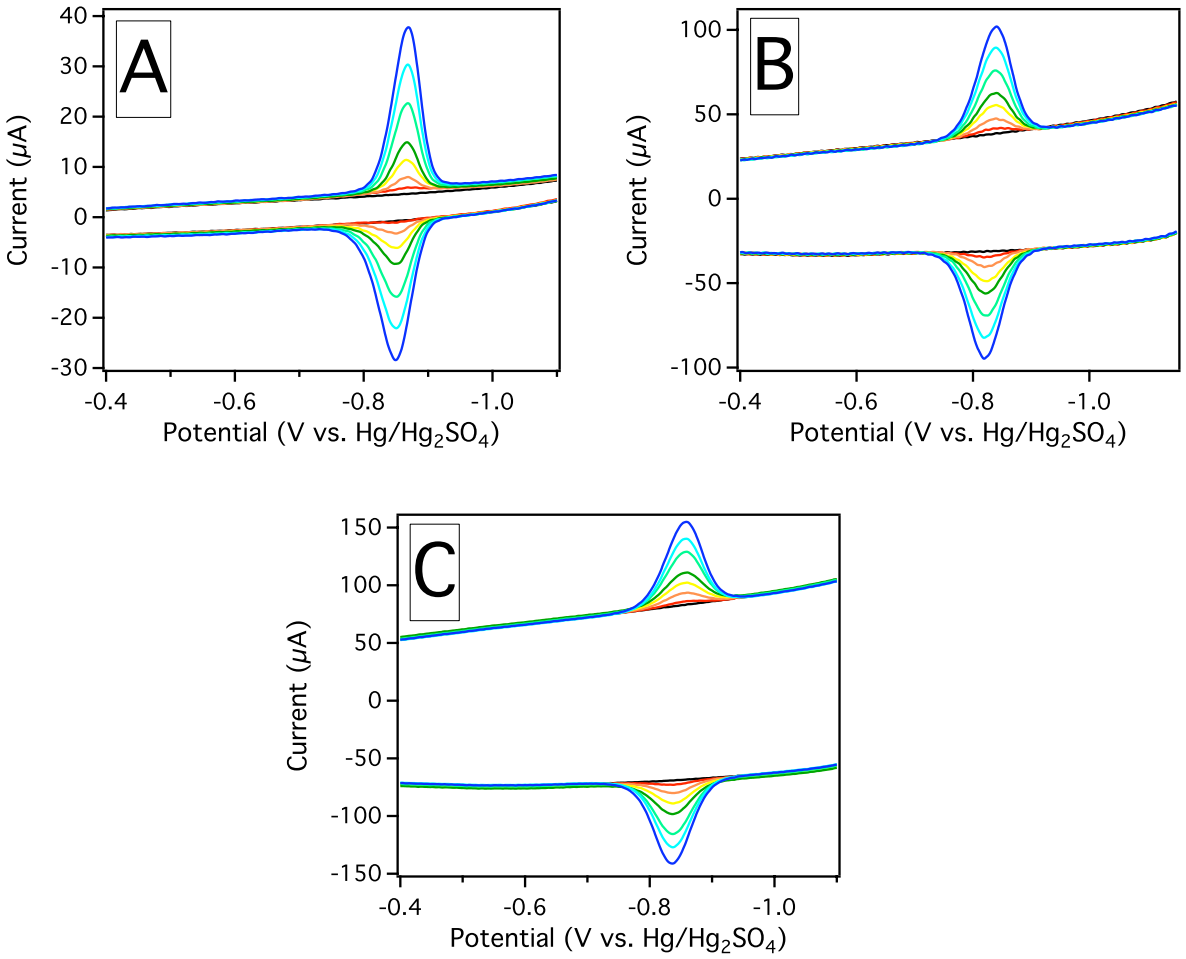

Figure 3.2. CVs of 6.5 μM FAD in 1.0 M SPB (pH = 6.75) spontaneously adsorbing onto (A) nondoped CNTs (B) 4.0 at.% N-CNTs and (C) 7.4 at.% N-CNTs over one hour (scan rate at 100 mV/s; black = background, red = 1 min, orange = 5 min, yellow = 10 min, green = 15 min, aqua = 30 min, light blue = 45 min, blue = 60 min).

pyrolytic graphite (HOPG).[48,154] The surface microstructure of HOPG plays a large role in the apparent capacitance, displaying significantly different capacitance values of about 1.5-3 μF cm^{-2} for basal plane or >50 μF cm^{-2} for edge plane microstructures.[51,155] A quick estimate of the background capacitance observed in 1.0 M SPB (pH = 6.75) can be calculated from the BET surface area and apparent capacitance (determined from the total charge in the potential window -0.25 to -1.00 V at a scan rate of 100 mV/s) at 2 μF cm^{-2}, 21 μF cm^{-2}, and 26 μF cm^{-2} for nondoped CNTs, 4.0 at.% N-CNTs, and 7.4 at.% N-CNTs, respectively. These capacitance values give a general indication of ESA, but as already mentioned, the BET surface area includes both electroactive and inactive areas. Additionally, adsorption sites for FAD may not directly correlate with background capacitance, especially since FAD is expected to adsorb with the isoalloxazine moiety in a parallel orientation to the nanotube sidewall (basal plane), which exibits a low capacitance due to microstructure. Intergration of the cathodic or anodic peak from adsorbed FAD provides a means of determining the total amount of FAD adsorbed, calculated from equation (eq 3.2) below:

$$\text{Total amount adsorbed (mol)} = Q/(nF) \qquad (3.2)$$

where Q is the charge obtained by integration of the cathodic or anodic surface wave, n is the number of electrons transferred in the redox reaction (n = 2), and F is Faraday's constant (96485 C mol^{-1}). The rate at which FAD initially adsorbs onto the CNT/N-CNT electrodes (during the first 15 minutes) in the 1.0 M SPB solution (pH = 6.75) is shown in Table 3.2. As already reported, the rate of adsorption is slower in 1.0 M SPB as compared to 0.1 M SPB; however, the amount adsorbed at equilibrium is higher than that obtained in 0.1 M SPB, most likely due to hydrophobic interactions.[147]

Table 3.2. Initial Adsorption Rate of FAD onto CNT and N-CNTs electrodes (6.5 μM FAD in 1.0 M SPB pH = 6.75)

Type	Adsorption Rate (pmol/min)
Nondoped CNTs	2.5 ± 1.0
4.0 at.% N-CNTs	5.2 ± 0.6
7.4 at.% N-CNTs	6.6 ± 0.7

CNT/N-CNT Electrodes are Mass Normalized (24 μg)

The initial adsorption rate increases with concentration of FAD, as does the coordinating amount adsorbed at equilibrium. Figure 3.3 presents the amount of FAD adsorbed as a function of time after a 7.4 at.% N-CNT electrode was placed in a 6.5 μM FAD solution (1.0 M SPB pH = 6.75) and subsequently placed in increasing concentrations of FAD.

The amount adsorbed (or the equilibrium position) at each FAD concentration is clearly differentiated from one another and very stable, since measurements are collected over hundreds of hours. This adsorption behavior is indicative of a Langmuir isotherm model, which can be used to obtain the amount adsorbed at full coverage (one monolayer), the equilibrium constant of the adsorption and desorption processes (K), and the Gibbs free energy of adsorption ($\Delta G°$). Langmuir behavior for FAD adsorption is in agreement with other reports in the literature, such as FAD adsorption onto TiO_2[108], glassy carbon[103], and Ru-modified glassy carbon[142]. The general expression for the Langmuir adsorption model is shown below (eq 3.3):

$$\Gamma = \Gamma_{max} (Kc/(1 + Kc)) \qquad (3.3)$$

where Γ is the surface coverage of adsorbed FAD (mol cm^{-2}), Γ_{max} is the maximum amount of FAD that can be adsorbed on the electrode surface as a single monolayer (mol cm^{-2}), K is the equilibrium constant for the adsorption and desorption processes (M^{-1}), and c is the concentration of FAD in solution (M). If the surface area is not known, Γ and Γ_{max} can be expressed as the amount adsorbed and the maximum amount adsorbed (mol), respectively. Figure 3.4 presents CVs of the equilibrium amount of FAD adsorbed onto CNT/N-CNT electrodes from eight different FAD concentrations ranging from 6.5 μM to 8.14 mM (1.0 M SPB pH = 6.75). Figure 3.5 presents a plot of Γ vs. c (where Γ is

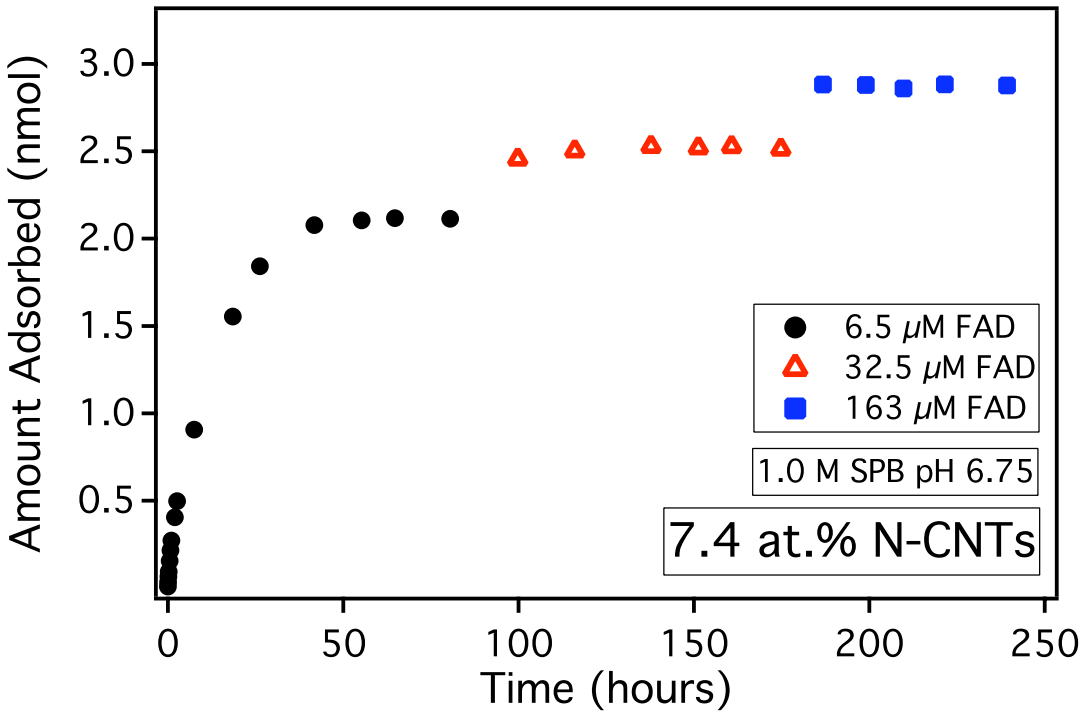

Figure 3.3. The amount of FAD adsorbed onto the surface of 7.4 at.% N-CNT electrode as a function of the time in a 6.5 μM FAD solution, and then placed in two higher concentrations of FAD (32.5 μM and 163 μM; 1.0 M SPB pH = 6.75)

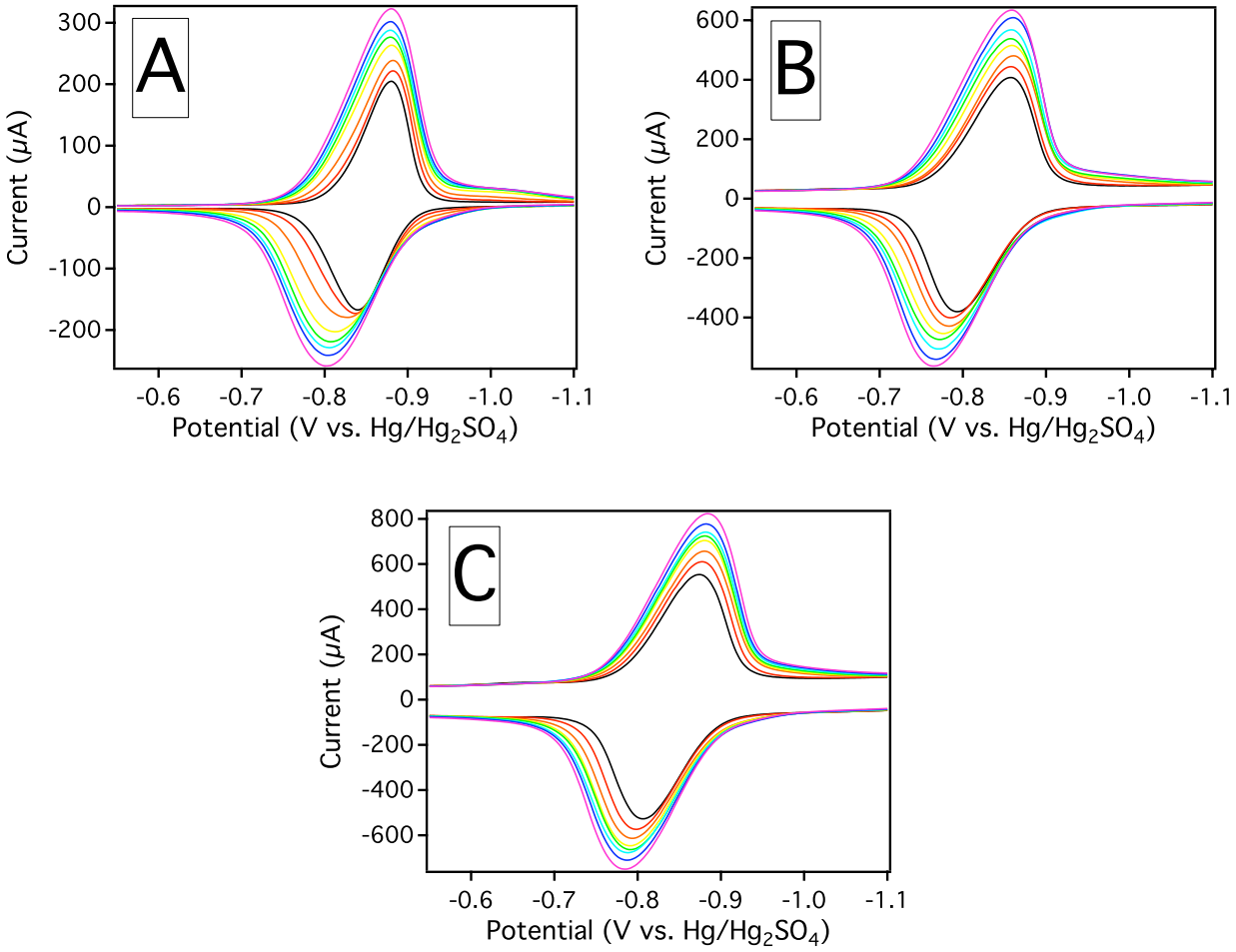

Figure 3.4. CVs of the surface adsorbed FAD on (A) nondoped CNTs (B) 4.0 at.% N-CNTs and (C) 7.4 at.% N-CNTs after being placed in increasing concentrations of FAD (1.0 M SPB pH = 6.75; scan rate 100 mV/s; black = 6.5 μM; red = 32.5 μM; orange = 163 μM; yellow = 814 μM; aqua = 1.36 mM; light blue = 2.03 mM; blue = 4.07 mM; purple = 8.14 mM)

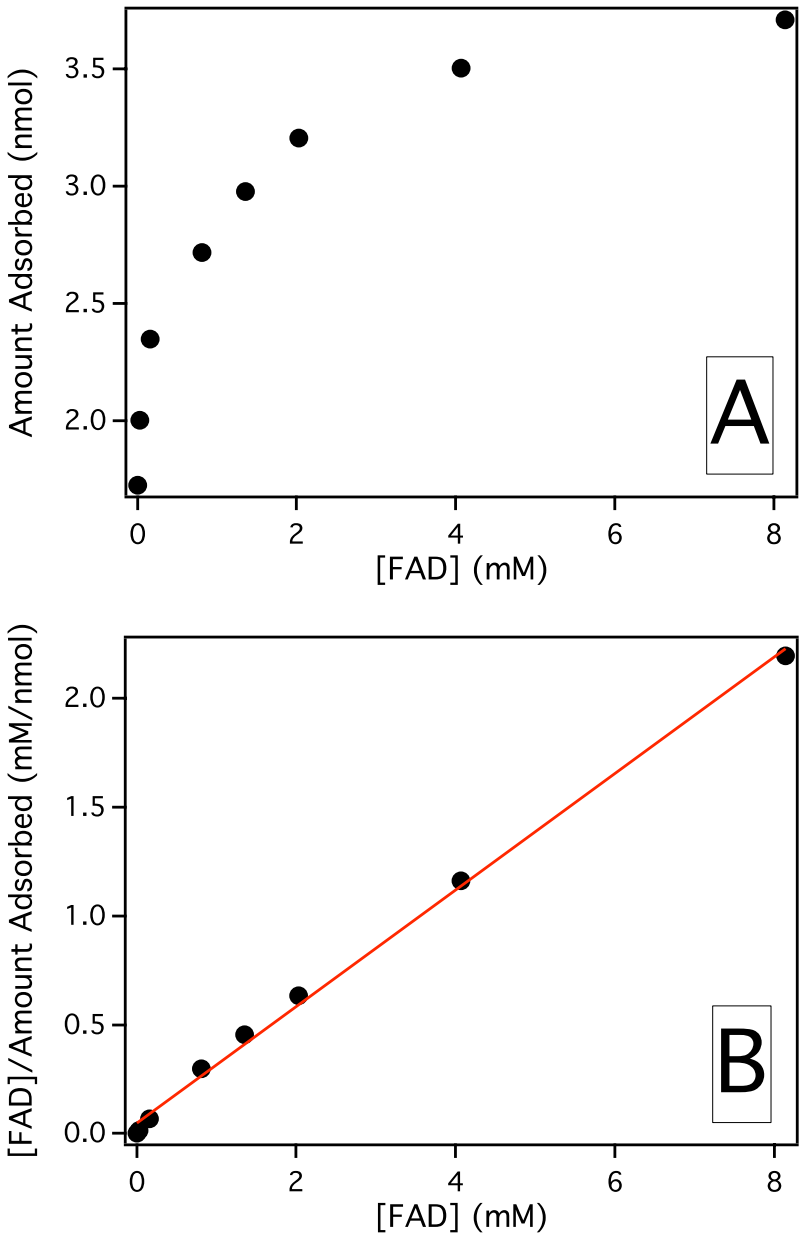

Figure 3.5. A plot of the equilibrium amount adsorbed as a function of FAD concentration on a 4.0 at.% N-CNT electrode (A) and, the Langmuir linearized form of that plot (B)

calculated from integration of the cathodic peak), and a Langmuir linearized form of that plot (c/Γ vs. c) for a 4.0 at.% N-CNT electrode. The Langmuir linearization of eq. 3.2 is expressed below (eq. 3.4):

$$c/\Gamma = c/\Gamma_{max} + 1/(K\Gamma_{max}) \quad (3.4)$$

where the slope is equal to $1/\Gamma_{max}$ and the y-intercept is $1/(K\Gamma_{max})$. All three types of CNT electrodes had R^2 values of ≥ 0.996 for the Langmuir linearized plots. The equilibrium constant (K) is related to the Gibbs free energy of adsorption (ΔG°) by the following formula (eq. 3.5):

$$\Delta G° = - RTln(K) \quad (3.5)$$

where R is the gas constant (8.314 J mol^{-1} K^{-1}), T is the temperature (298 K), and K is the calculated equilibrium constant (M^{-1}). Table 3.3 presents the equilibrium constant and the Gibbs free energy of adsorption for FAD on all three types of CNT electrodes. The calculated values do not show a significant difference between CNT types, and are quite similar to the value reported for FAD adsortion on Au.[130]

3.3.3 FAD Desorption from CNT/N-CNT Electrodes

FAD is known to photolytically react[112], subsequently becoming lumichrome (LC). LC, also known as 7,8-dimethylalloxazine, spontaneously adsorbs onto N-CNTs displaying a chemically reversible surface confined redox reaction with $E_{1/2}$ at -0.93 V (1.0 M SPB pH = 6.75), about 90 mV more negative than the main FAD surface reaction. Figure 3.6C displays LC adsorbing onto a 4.0 at.% N-CNT electrode over one hour. There is a small surface reaction with $E_{1/2}$ at -0.78 V observed to increase over the first 20 hours of adsorption. Beyond 20 hours, the peak decreases and completely disappears

Table 3.3. The Equilibrium Constant (K) and Gibbs Free Energy of Adsorption (ΔG°) for FAD Adsorption onto CNTs and N-CNTs

Type	K (M^{-1})	ΔG° (kJ mol^{-1})
Nondoped CNTs	5200 ± 600	-21.2 ± 0.3
4.0 at.% N-CNTs	4900 ± 800	-21.0 ± 0.4
7.4 at.% N-CNTs	5700 ± 1000	-21.4 ± 0.4

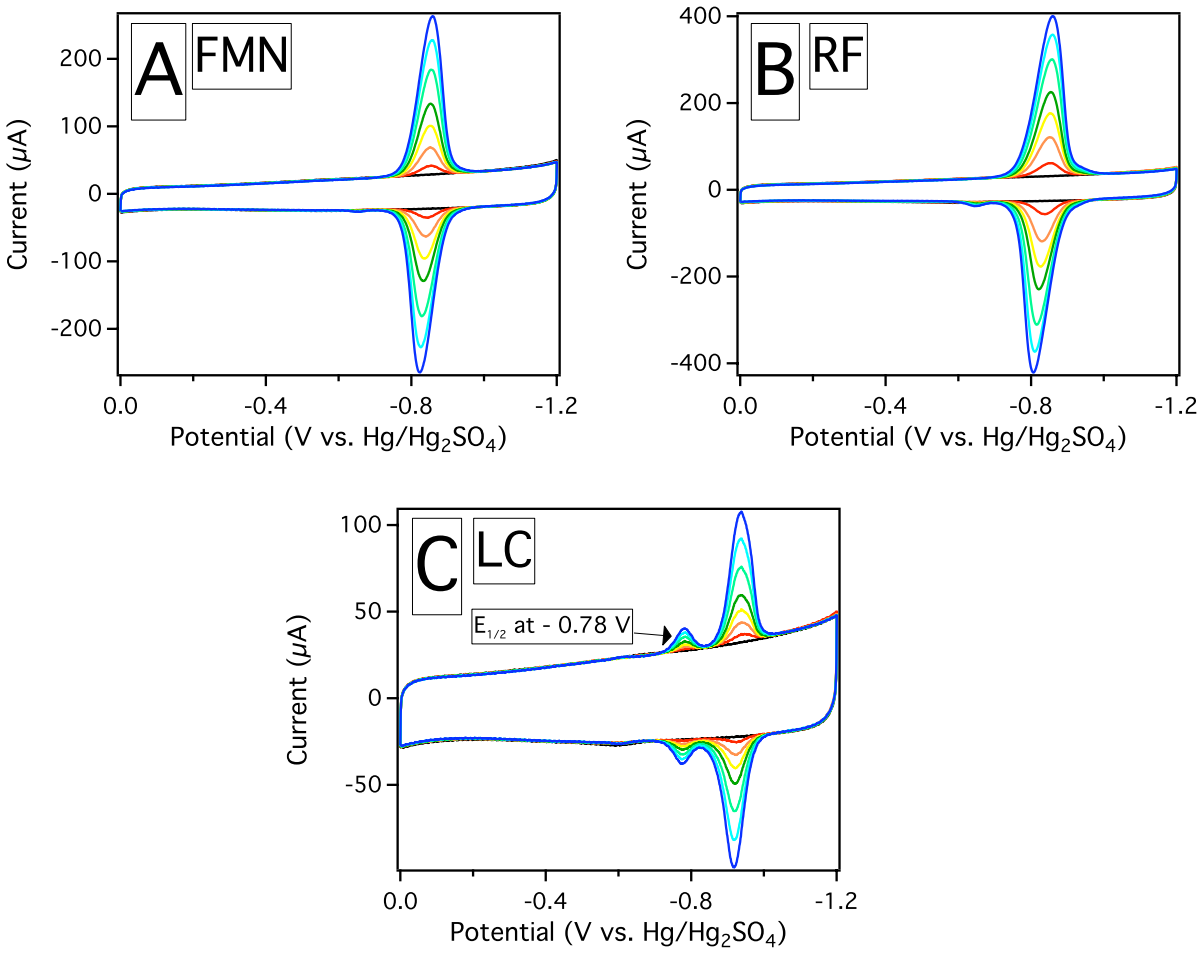

Figure 3.6. CVs of (A) Flavin Mononucleotide (FMN), (B) Riboflavin (RF), and (C) Lumichrome (LC) adsorbing onto a 4.0 at.% N-CNT electrode over one hour (FMN concentration is 32.5 μM, RF and LC are saturated solutions; 1.0 M SPB pH = 6.75; scan rate at 100 mV/s; black = background, red = 1 min, orange = 5 min, yellow = 10 min, green = 15 min, aqua = 30 min, light blue = 45 min, blue = 60 min)

after 50 hours, leaving only the main LC surface redox reaction. Flavin mononucleotide (FMN), FAD, and riboflavin (RF) all share the redox active 7,8,10-trimethylisoalloxazine moiety, also known as lumiflavin, which displays the surface confined reaction with $E_{1/2}$ at -0.84 V (1.0 M SPB pH = 6.75) on N-CNTs. Figure 3.6A and 3.6B present FMN and RF, respectively, spontaneously adsorbing onto a 4.0 at.% N-CNT electrode over one hour.

If an electrode with adsorbed FAD is placed in back into a blank SPB solution (without FAD), FAD will slowly desorb from the surface; however, on N-CNTs, a second chemically reversible surface confined redox reaction will form, which is not observed at nondoped CNTs. Figure 3.7 shows CVs before and after FAD was allowed to desorb from a nondoped CNT, a 4.0 at.% N-CNT, and a 7.4 at.% N-CNT electrode for 314 hours. The new peak on N-CNTs is observed with $E_{1/2}$ at -0.65 V. There is almost no change in the main FAD surface wave at nondoped CNTs before and after desorption. The new reversible surface wave at N-CNTs is clearly derived from FAD, since the main wave is considerably less with respect to the original. Birss *et al*. have observed the appearance of a redox peak about 150 mV positive of the main wave from adsorbed flavins on Hg, but only when photolysis was carried out in the presence of oxygen.[112] In our case, analysis was carried out in an Ar saturated solution, and light was excluded during desorption. Furthermore, any inter or intramolecular reaction of FAD on the surface should have been observed at nondoped CNTs, indicating that the surface nitrogen in N-CNTs plays a critical role in the development of the new redox reaction. If N-CNT electrodes with desorbed FAD (displaying the new redox reaction) are placed back into a solution of FAD, the new peak with $E_{1/2}$ at -0.65 V will disappear concurrently with an increase in the main FAD wave. This indicates that the adsorbed

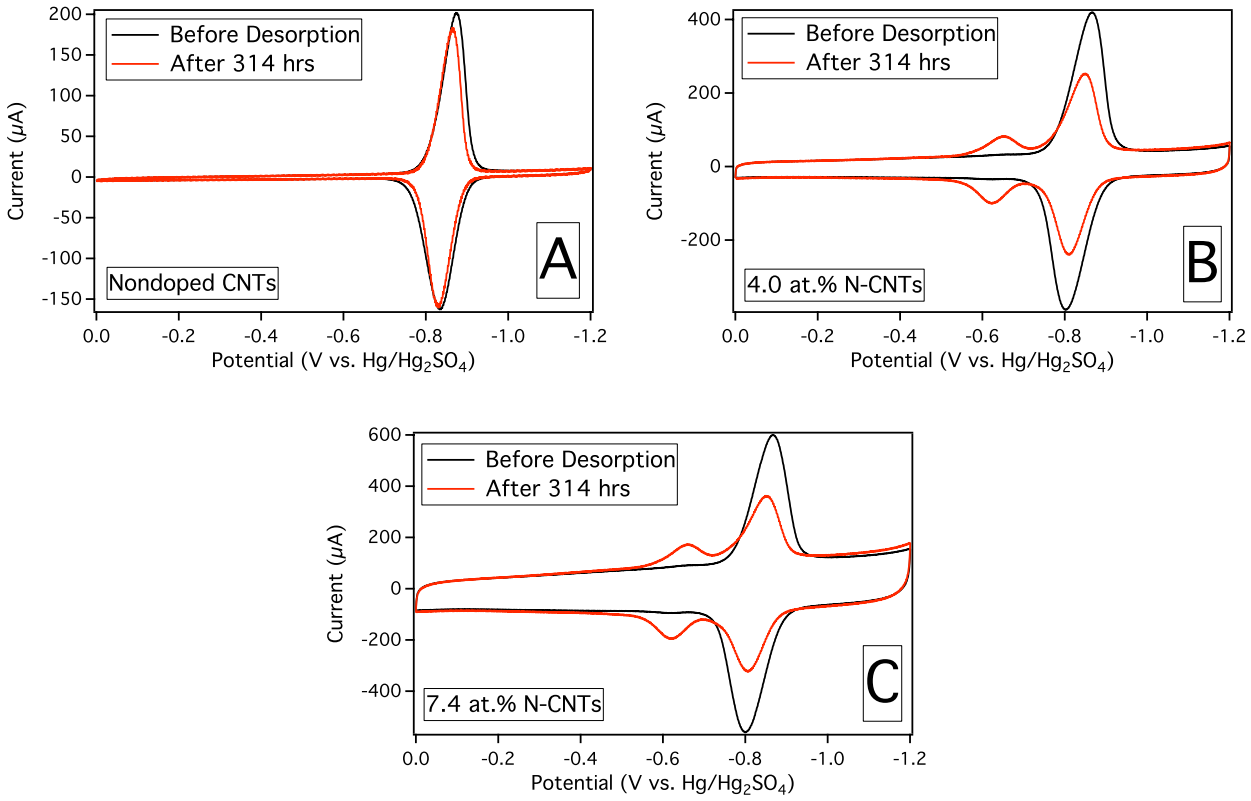

Figure 3.7. CVs of FAD adsorbed onto a (A) nondoped CNT (B) 4.0 at.% N-CNT and (C) 7.4 at.% N-CNT electrode before and after 314 hours of desorption in 1.0 M SPB (pH = 6.75, scan rate 100 mV/s)

FAD surface species, with multiple surface redox reactions, will be readily relaced by fresh FAD from solution. Figure 3.8 shows the peak with $E_{1/2}$ at -0.65 V disappearing as fresh FAD from solution adsorbs on the surface and replaces the transformed FAD.

If FAD is allowed to desorb over longer periods of time on N-CNTs, a third surface confined redox reaction will appear with $E_{1/2}$ at -0.76 V. Figure 3.9A displays FAD desorbing from a 4.0 at.% N-CNT electrode over 1320 hours (a CV was taken about every 24 hours). Figure 3.9B presents a CV of the same electrode after 1000 hours of desorption, clearly showing the three surface confined redox reactions. All three reactions are also observed if flavin derivatives such as FMN or RF are allowed to desorb from N-CNT electrodes. Figure 3.10 presents a CV of FMN and RF that have been allowed to desorb from a 4.0 at.% N-CNT electrode for 257 hours. Both flavin derivatives display three redox reactions, albeit, a small surface wave for the $E_{1/2}$ at -0.76 V. Identical to the redox reaction with $E_{1/2}$ at -0.65 V, the reaction with $E_{1/2}$ at -0.76 V is a transformation of the main FAD surface wave. Since FMN and RF both display the FAD redox transformation, the ribitol group on 7,8-dimethylisoalloxazine could possibly play a role in the appearance of the new surface redox reactions. Adsorption of 7,8,10-trimethylisoalloxazine (lumiflavin) would rule out this possibility since the ribitol group is replaced with a methyl group, otherwise the transformation of the main FAD surface wave is a unique interaction between 7,8,10-trimethylisoalloxazine and N-CNTs.

3.3.4 Determination of the pK_a of FAD on the surface of CNTs and N-CNTs

The chemically reversible, surface confined redox reaction of FAD involves two-protons and two-electrons as displayed in eq 3.1. Accoring to the Nernst equation, any electrochemical reaction that involves an equal number of protons and electrons will shift as a function of pH at a rate of 59 mV per pH unit (negative shift as pH increases) shown

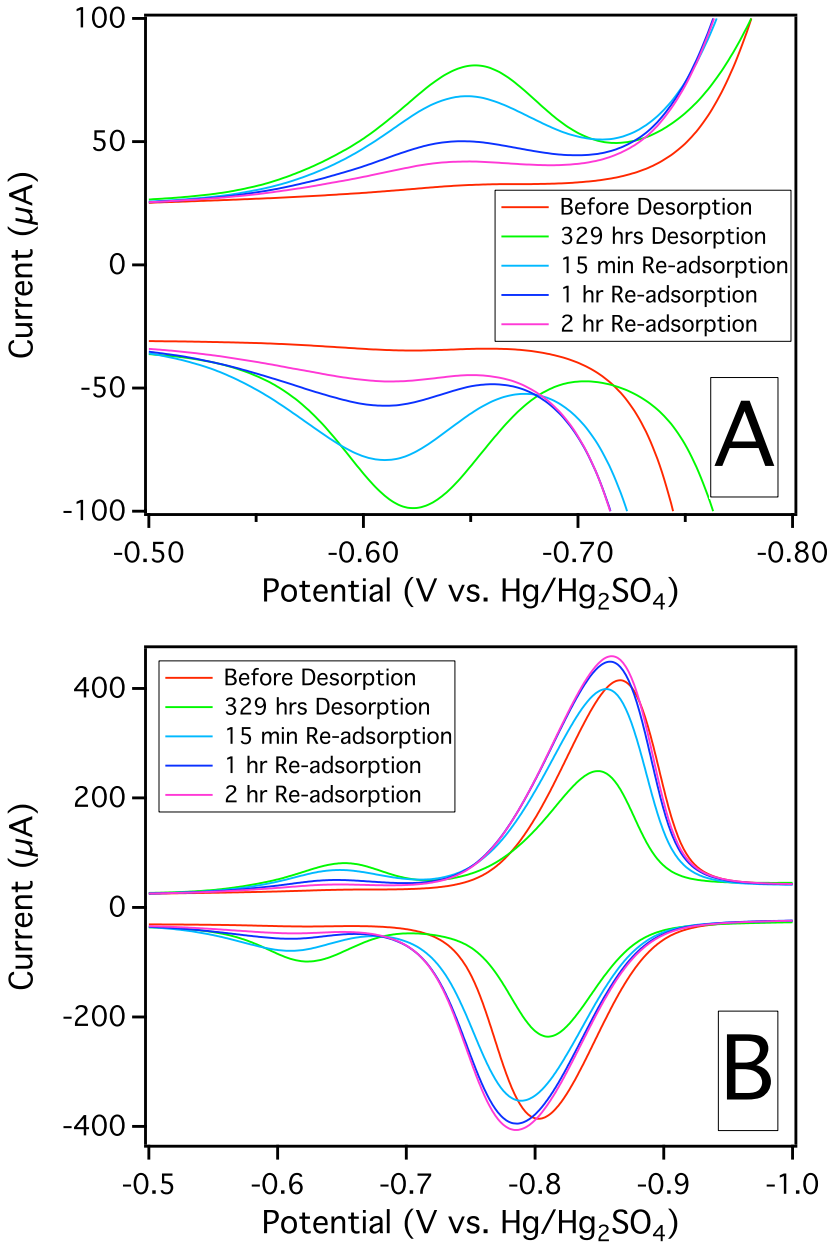

Figure 3.8. CVs showing the (A) disappearance of the redox reaction with $E_{1/2}$ at - 0.65 V after the being placed into a fresh FAD solution (163 μM) and (B) the concurrent increase in the main FAD surface redox reaction at $E_{1/2}$ at - 0.84 V (1.0 M SPB pH = 6.75)

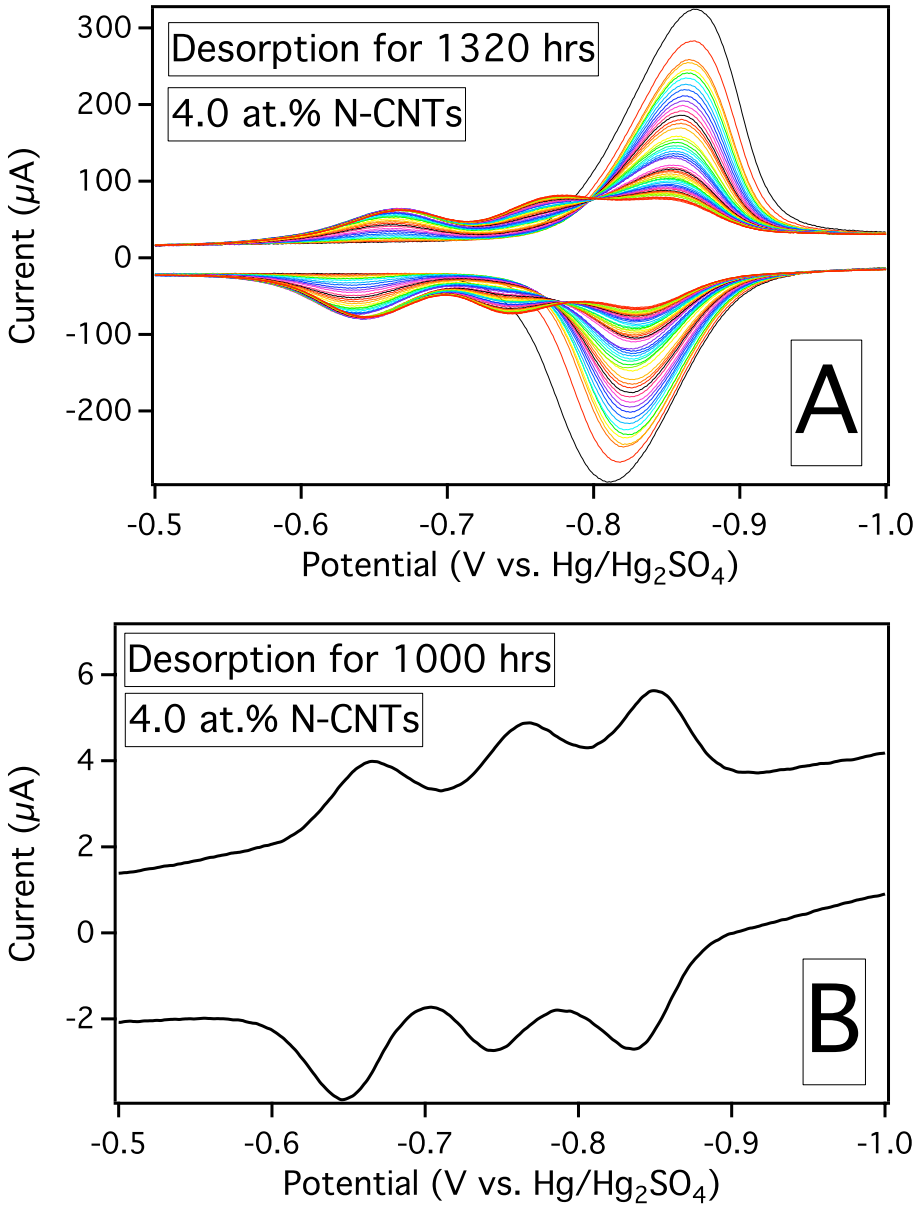

Figure 3.9. (A) CVs of FAD desorbing from a 4.0 at.% N-CNT electrode over 1320 hours (scan rate 100 mV/s; CV taken about every 24 hours) and (B) a CV after desorption for 1000 hours at 10 mV/s showing the appearance of two new surface confined redox peaks (1.0 M SPB pH = 6.75)

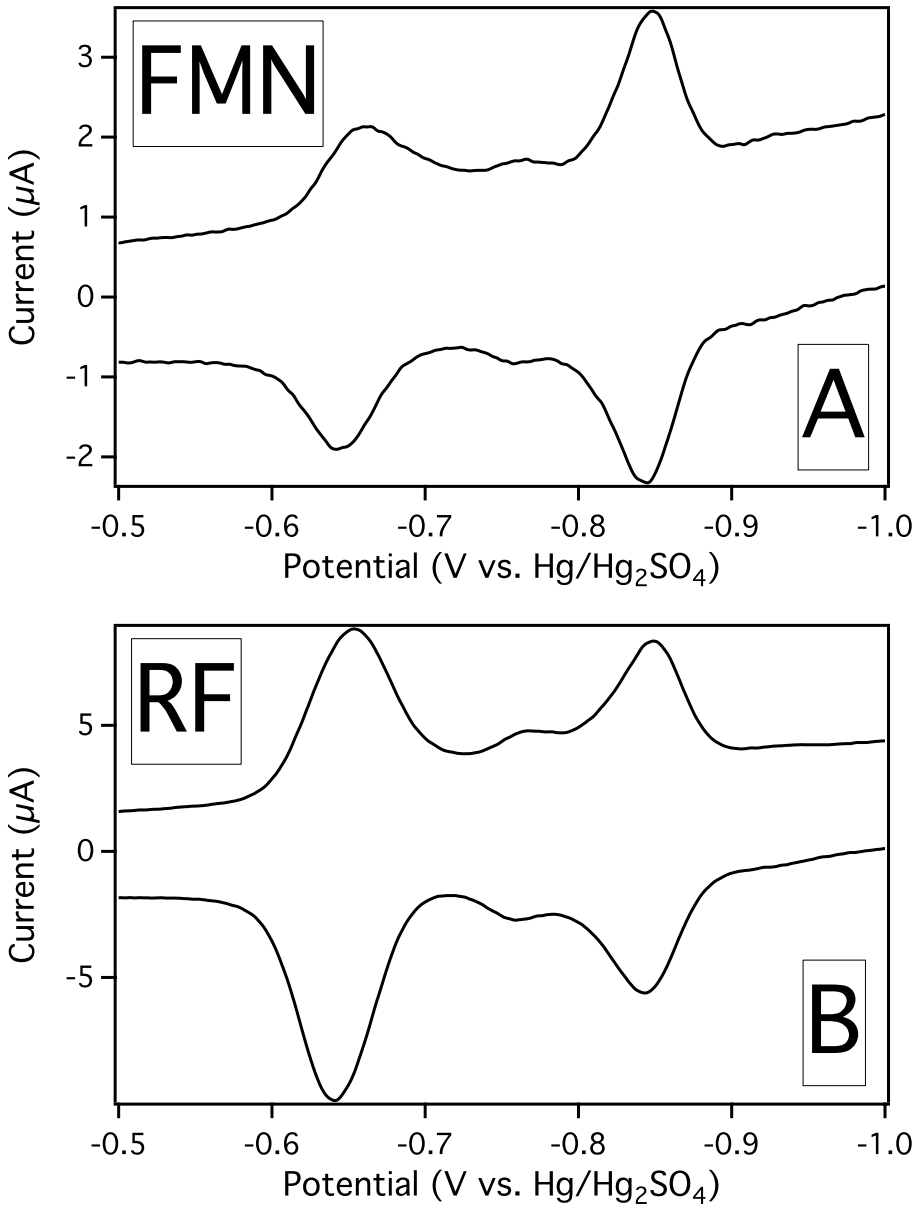

Figure 3.10. CVs of (A) Flavin mononucleotide (FMN) and (B) riboflavin (RF) after being allowed to desorb from a 4.0 at.% N-CNT electrode for 257 hours (scan rate 10mV/s, 1.0 M SPB pH = 6.75)

below for a surface bound redox reaction (eq. 3.6):

$$E_{1/2} = E° + (RT/nF)\ln(\Gamma_{Ox}[H^+]^2/\Gamma_{Red}) \quad (3.6)$$

$$\Gamma_{Ox} = \Gamma_{Red} \quad (3.7)$$

$$E_{1/2} = E° - (0.059/n)\log([H^+]^2) \quad (3.8)$$

where $E_{1/2}$ is the half-way point between the cathodic and anodic peak potentials (or formal potential at a given pH), E° is the standard potential at pH 0, R is the gas constant (8.314 J K^{-1} mol^{-1}), T is the temperature (298 K), n is the number of electrons transferred in the redox reaction (n = 2), F is Faraday's constant (98645 C mol^{-1}), $[H^+]$ is the proton concentration in solution, and Γ_{Ox} and Γ_{Red} are the surface concentrations of FAD and $FADH_2$, respectively, in mol cm^{-2}. Since the surface concentrations of FAD and $FADH_2$ are identical (shown in eq. 3.7, as measured by integration of the cathodic and anodic peaks in a CV), eq. 3.6 becomes eq. 3.8, where the only remaining variables are n and $[H^+]$. Figure 3.11 presents CVs of a 4.0 at.% N-CNT electrode with adsorbed FAD scanned in 0.1 M SPB solutions of increasing pH, and the resulting $E_{1/2}$ vs. pH plot. The observed redox reaction of FAD shifts negative with increasing pH. The slope of the $E_{1/2}$ vs. pH plot displays a shift of 58 mV/pH, as expected based on the Nerstian relationship shown in eq. 3.8; however, the slope changes to 31 mV/pH between pH values of 9.66 to 13. This sudden shift indicates that the redox reaction in high pH solutions is not a two-electron two-proton transfer, but rather, a two-electron one-proton transfer, thereby identifying the pK_a of FAD on the electrode surface (eq 8). Figure 3.12 presents CVs of FAD adsorbed onto nondoped CNTs, 4.0 at.% N-CNTs, and 7.4 at.% N-CNTs and scanned in 0.1 M SPB solutions of increasing pH. The E°, calculated from the

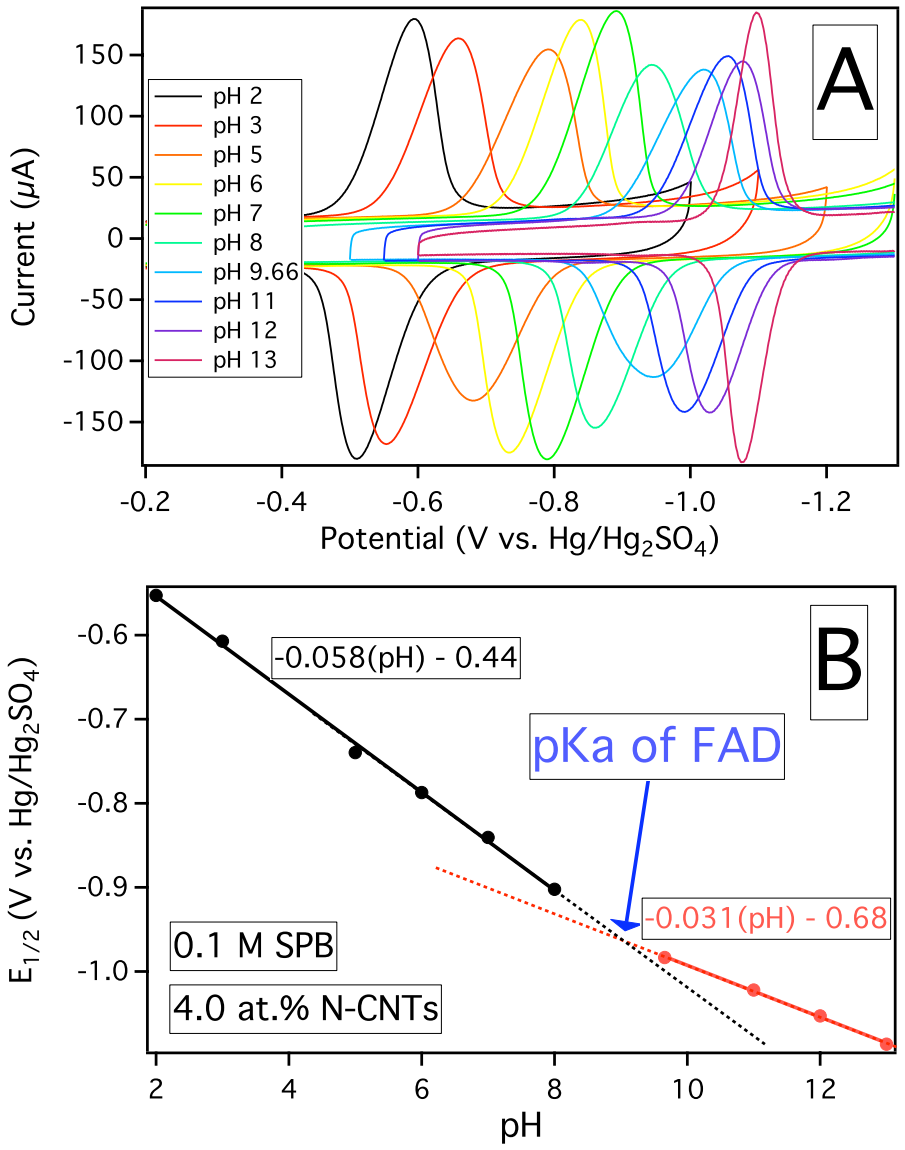

Figure 3.11. (A) CVs of FAD adsorbed onto a 4.0 at.% N-CNT electrode and cycled in 0.1 M SPB solutions of increasing pH values (2, 3, 5, 6, 7, 8, 9.66, 11, 12, and 13) and (B) the resulting plot of $E_{1/2}$ as a function of *p*H

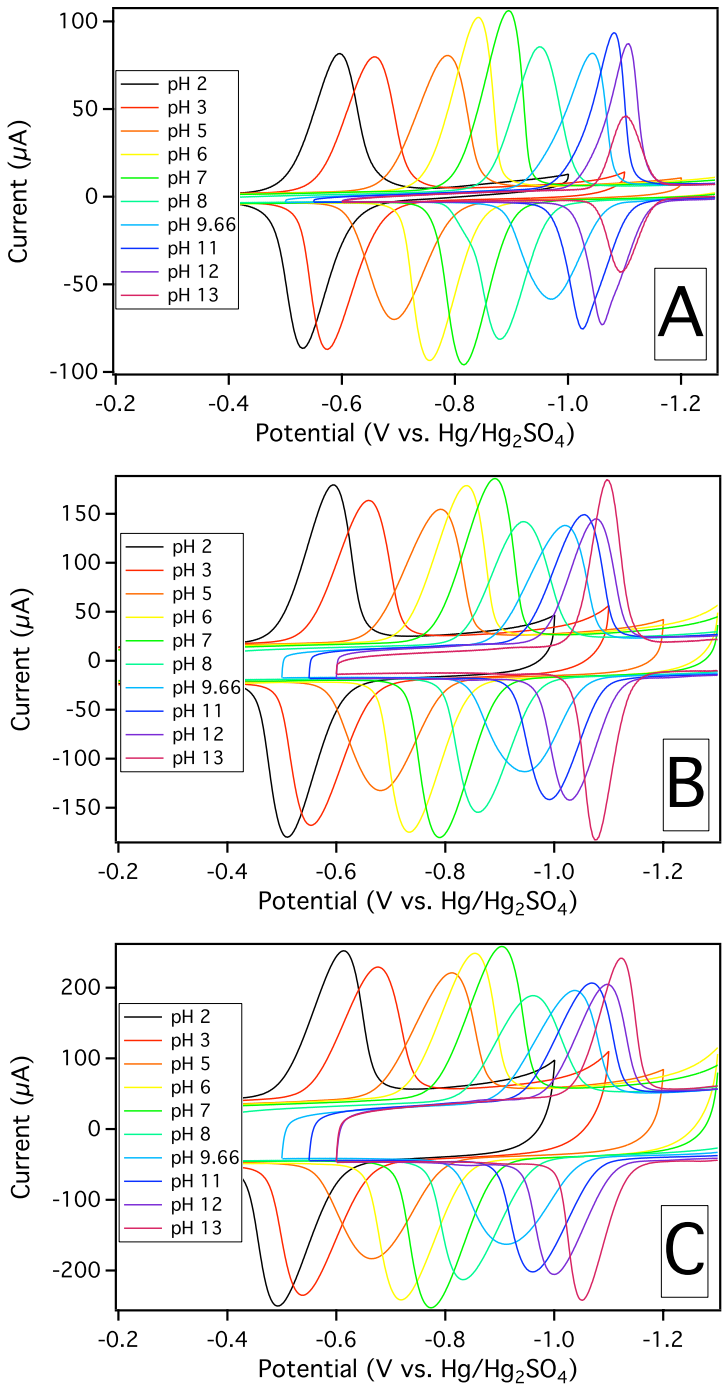

Figure 3.12. CVs of FAD adsorbed onto Nondoped CNTs, 4.0 atom % N-CNTs, and 7.4 at.% N-CNTs and scanned in 0.1 M SPB solutions of increasing pH values (2, 3, 5, 6, 7, 8, 9.66, 11, 12, and 13; scan rate 50 mV/s)

y-intercept at low *p*H values, is -0.44 V for N-CNTs and -0.45 V for nondoped CNTs. This 10 mV more positive shift at N-CNTs was previously observed[147] and is attributed to the incorporated nitrogen, which presumably decreases hydrophobicity, and increases the edge plane sites for facile electron transfer at N-CNTs.[57]

Table 3.4 displays the calculated pK_a of the surface bound FAD on nondoped CNTs, 4.0 at.% N-CNTs, and 7.4 at.% N-CNTs which show a trend towards lower pK_a values with increasing nitrogen content of the CNT electrode. The pK_a of free $FADH_2$ has been reported to be between 6.4 and 6.8.[129,156,157] Upon adsorption on graphite, the pK_a was found to be higher then 8.0 where it was suggested that adsorption might be strong enough to shift the pK_a.[109] Riboflavin adsorbed onto pyrolytic graphite has also exhibited a pK_a shift to 8.5.[158] The observed shift in pK_a resulting from surface immobilization is mainly due to a change in the coordinating solvent environment.[145,146] The pK_a trend of FAD adsorbed onto CNTs and N-CNTs points to the decreased hydropobicity of the N-CNT surface, compared to the more hydrophobic nondoped CNT surface.[145]

The $E_{1/2}$ as a function of pH was examined for flavin mononucleotide (FMN), riboflavin (RF), and LC adsorbed onto 4.0 at.% N-CNT electrodes, along with FAD that had been allowed to desorb from a 4.0 at.% N-CNT electrode for 1320 hours. Figure 3.13 presents CVs in increasing pH solutions of FMN, RF, and LC adsorbed onto 4.0 at.% N-CNT electrodes. Adsorbed FMN and RF display a pK_a at 8.0 and 8.1, respectively. LC did not display a clear pK_a; however, the cathodic peak did partially resolve into two waves in the 0.1 M SPB solution (as opposed to the 1.0 M SPB solution, see Figure 3.6C). At pH values 11 to 13, both the cathodic and anodic surface waves for adsorbed LC display two peaks, most likely due to a partial resolution of the two

Table 3.4. pK_a of FAD Adsorbed onto CNT and N-CNT electrodes

Type	pK_a of FAD
Nondoped CNTs	10.3 ± 0.1
4.0 at.% N-CNTs	8.9 ± 0.2
7.4 at.% N-CNTs	8.6 ± 0.2

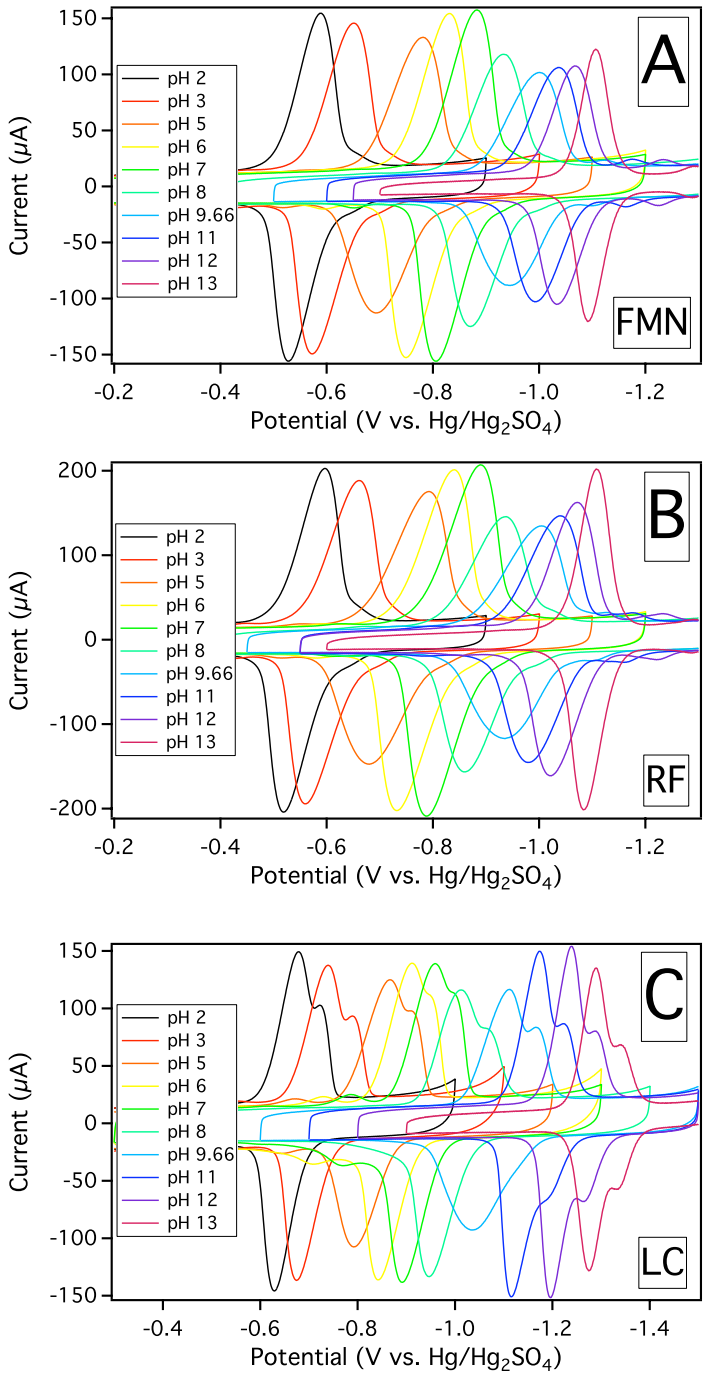

Figure 3.13. CVs of (A) FMN, (B) Riboflavin, and (C) Lumichrome adsorbed onto 4.0 at.% N-CNTs and scanned in 0.1 M SPB solutions of increasing pH values (2, 3, 5, 6, 7, 8, 9.66, 11, 12, and 13; scan rate 50 mV/s)

overlapping one-electron transfer reactions. Figure 3.15 presents the cathodic half of CVs where FAD was allowed to desorb from a 4.0 at.% N-CNT for 1320 hours, and then cycled in 0.1 M SPB solutions of increasing pH values. After 1320 hours of desorption, the remaining FAD was transformed into three surface confined redox reactions (Figure 3.9A). The middle peak (with $E_{1/2}$ at -0.76 V in 1.0 M SPB pH = 6.75) dislayed a $E_{1/2}$ shift of 72 mV/pH between pH values of 5 to 8, but changed to 33 mV/pH between 9.66 to 12. The middle peak merges with the main FAD surface wave at pH 13, and in the low *p*H range starting at 3, merges with the most positive surface reaction (with $E_{1/2}$ at -0.65 V 1.0 M SPB pH = 6.75). A pK_a was determined from the change in slope ($E_{1/2}$ vs. pH) for the main FAD peak and the middle peak at 8.9 and 8.8, respectively. The most positive surface reaction did not display a clear change in the $E_{1/2}$ as a function of pH, showing a 51 mV/pH shift from 2 to 8 and a 49 mV/pH shift from 9.66 to 13.

3.4 CONCLUSION

FAD was allowed to spontaneously interact (adsorb or desorb) at CNT and N-CNT electrodes. The adsorption of FAD onto CNT/N-CNTs displayed Langmuir behavior, which provided a model to determine the electroactive surface area, the equilibrium constant of the adsorption and desorption processes (K), and the Gibbs free energy of adsorption ($\Delta G°$). The change in $E_{1/2}$ as a function of pH for adsorbed FAD provided a means to measure the pK_a of the surface confined species, which showed a decreasing pK_a with increasing nitrogen content. Desorption of FAD from N-CNTs transformed the main surface redox reaction with $E_{1/2}$ at -0.84 V into two more chemically reversible, surface confined redox reactions with $E_{1/2}$ at -0.65 V and -0.76 V (1.0 M SPB pH = 6.75). The additional surface redox reactions were not observed at nondoped CNT electrodes.

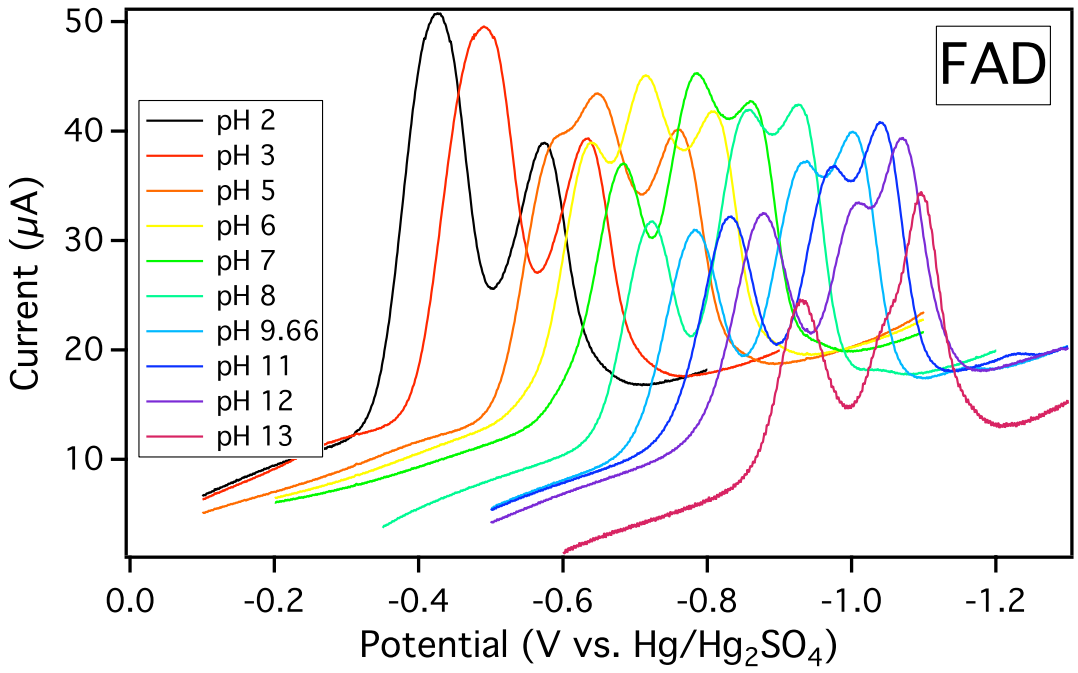

Figure 3.14. The cathodic surface redox reaction of adsorbed FAD as a function of pH after being allowed to desorb for 1320 hours (0.1 M SPB pH values at 2, 3, 5, 6, 7, 8, 9.66, 11, 12, and 13; scan rate 50 mV/s)

CHAPTER 4

Electrochemical Oxidation of Dihydronicotinamide Adenine Dinucleotide at Nitrogen-Doped Carbon Nanotube Electrodes*

4.1 INTRODUCTION

Dihydronicotinamide adenine dinucleotide (NADH) is a cofactor for hundreds of dehydrogenase enzymes[159] commonly used for the design of electrochemical biosensors[159–162] and biofuel cells[127,128,163]. In order to continue the advance of dehydrogenase based biosensors and biofuel cells, there is a clear need to develop electrodes that can efficiently oxidize NADH to NAD^+, the necessary form of NADH that allows turnover of the enzymatic substrate. Oxidation of NADH at conventional electrode surfaces generally requires a large overpotential, which in-turn introduces a high background current and unwanted side reactions from electroactive interferents. This large overpotential also lowers the overall power density of a NADH-based biofuel cell. In order to mitigate these deleterious effects, redox-active mediators are often introduced to lower the overpotential while efficiently shuttling electrons between NADH and the electrode surface.[159,160,164,165] Although effective in specified systems, redox mediators add another level of difficulty to the transport of electrons, and often must be immobilized or confined to ensure consistent results. An ideal electrode would inherently lower the oxidation overpotential, without additional mediation, referred to as an electrocatalyst. Although the differences between an electrocatalyst and a mediator are often not well defined, here we refer to mediators as any molecule that is not inherently part of the electrode material, and aids in the transfer of electrons from NADH

*Portions of this chapter were published in Goran, J. M.; Favela, C. A.; Stevenson, K. J. *Anal. Chem.* **2013**, *85*, 9135-9141. (Favela performed experiments, Stevenson supervised this work)

to the electrode material. This includes covalently bound mediators found in chemically modified electrodes, physically adsorbed mediators, immobilized mediators (such as mediators within a hydrogel or polymer matrix), freely diffusing mediators, or even surface functionalities (which can be considered both mediators or inherently part of the electrode material) which were created on the electrode material post synthesis. Carbon nanotubes (CNTs), a unique carbon allotrope, were shown to exhibit electrocatalytic characteristics by dramatically lowering the NADH oxidation potential in comparison to glassy carbon by Wang and co-workers.[44–46] Carbon electrodes such as glassy carbon (GC) or highly ordered pyrolytic graphite (HOPG) are favored for bioanalytical applications since biomolecules such as enzymes have a higher tendency to denature at traditional noble metal electrode surfaces. The unique form of carbon found in CNTs significantly lowered the activation energy necessary to oxidize NADH, while also displaying higher resistance to surface fouling, known to occur during NADH oxidation.[166] Since that seminal discovery, a number of other studies related to the use of CNTs as an advanced electrode material for NADH oxidation have been performed. These include ordered CNTs[167], the use of dispersing agents such as hyaluronic acid[168], chitosan[169], mediators including Meldola's blue[170], Variamine blue[171], TCBQ[172], toluidine blue,[173] toluidine blue O/chitosan matrix[174], poly(toluidine blue O)[175], poly(methylene green)/ carboxylated CNT composite[176], SWCNT "Bucky Paper"/poly(methylene green)[177], azure C/chitosan[178], azine/hydrogel[179], CNT/PDDA-poly(azure B) composite[180], CNT/DHB/nafion hybrid films[181], polyluminol/CNTs[182], 1,10-phenanthroline-5,6-dione[183], silica-azure C nanoparticles/CNTs/chitosan film[184], conducting polymers such as Poly-(3-methylthiophene)[185], PEDOP/MWCNT-Pd nanoparticles[186], PANI/PABS/SWCNTs,[187] dopamine/PEI/CNT composite[188], PDDA/PSS-[MWCNTs-

NH_3^+-graphene-$COO^-]_5$,[189] carbodiimde coupled MWCNTs[190], and oxidative pretreatment of CNTs by microwave treatment in nitric acid[191]. In the vein of ideal NADH electrodes, heteroatom-doped CNTs have been shown to decrease the NADH oxidation potential without additional mediation. Boron-doped CNTs (B-CNTs), a p-type dopant in carbon, significantly enhanced the oxidation of NADH compared to nondoped CNTs.[192] Nitrogen-doped CNTs (N-CNTs), a n-type dopant in carbon, are cited as being both more biocompatible[148] and better electrocatalysts for important biomolecules such as H_2O_2.[53,54,121] Herein, we present an electrochemical investigation of NADH oxidation at N-CNTs, showing how incorporated nitrogen can further lower the overpotential and increase the sensitivity of CNTs to NADH as compared to glassy carbon (GC), edge plane pyrolytic graphite (EPPG), or nondoped CNTs. CNTs and N-CNTs were investigated without the use of binders, solubilizing/dispersing agents, or oxidative acid pretreatment as these have been shown to affect electrochemical performance.[191,193,194] The natural degradation of NADH in phosphate buffer and the effects of electrode fouling are also investigated, since degradation and electrode fouling are often difficult to distinguish between and must be taken into account for accurate analytical measurements. The use of N-CNTs as a platform for dehydrogenase-based biosensing are demonstrated by allowing glucose dehydrogenase to spontaneously adsorb onto N-CNTs, subsequently creating a sensitive glucose biosensor.

4.2 EXPERIMENTAL

4.2.1 Enzyme and Chemicals

β-Nicotinamide adenine dinucleotide disodium salt hydrate, β-nicotinamide adenine dinucleotide dipotassium salt, α-D-glucose, *m*-xylene (anhydrous), and glucose dehydrogenase (from *Pseudomonas sp.*, E.C. 1.1.1.47, lyophilized powder ≥200 U/mg)

were obtained from Sigma-Aldrich. Sodium phosphate monobasic (monohydrate), sodium phosphate dibasic (anhydrous), pyridine, and sodium hydroxide were purchased from Fisher. Bis(cyclopentadienyl)iron (ferrocene) was obtained from Alfa Aesar.

4.2.2 CNT/N-CNT Synthesis

CNTs and N-CNTs were synthesized by a chemical vapor deposition (CVD) process using ferrocene as a nucleation catalyst for CNT/N-CNT growth. A ferrocene solution of 20 mg mL^{-1} was prepared using *m*-xylene (CNTs) or pyridine (N-CNTs) and then pumped into a quartz tube at 0.1 mL min^{-1} through a glass syringe (Hamilton 8132) by an automated syringe pump (New Era Pump Systems NE-1000). The quartz tube was laid across two identical tube furnaces (Carbolite model HST 12/35/200/2416CG) which were set at different temperatures. The first furnace (where the ferrocene solution is injected into the quartz tube) was set at a temperature to ensure the solvent entered into the gas phase (150 °C for *m*-xylene and 130 °C for pyridine). Argon gas was used to direct the vaporized precursor along the quartz tube into the second furnace, which was set at a temperature to initiate CNT/N-CNT growth along the inner diameter of the tube wall (700 °C for *m*-xylene and 800 °C for pyridine). Ammonia gas was introduced during N-CNT synthesis to increase the incorporated nitrogen content above the level set by the pyridine precursor (4.0 at.% N-CNTs). Incorporated nitrogen as a function of the ammonia flow rate was characterized in a prior report.[52] A total gas flow rate of 575 sccm was maintained during synthesis including H_2 gas for nondoped CNTs or NH_3 for N-CNTs above 4.0 at.% N-CNTs.

4.2.3 Electrochemistry and Electrode Preparation

Cyclic voltammograms (CVs) and chronoamperograms are plotted with a negative anodic current (pointing down) and a positive cathodic current (pointing up). Pine rotating disk electrodes (RDE, 5 mm diameter, AFE2M050) were polished using a 0.05 μm alumina slurry on a microfiber (Buehler) cloth, sonicated in nanopure (18 MΩ cm) water, and then rinsed with absolute ethanol. A mass normalized 24 μg of CNT/N-CNTs were drop cast on polished RDEs from a 2 mg mL^{-1} solution of N-CNTs, or a 0.4 mg mL^{-1} solution of CNTs in absolute ethanol, and allowed to air dry. CNT/N-CNT solutions were sonicated for 2 hours prior to use, to ensure a homogenous solution. Once dried, the CNT/N-CNT electrodes were wet with a mixture of ethanol and 0.10 M sodium phosphate buffer (SPB) at a pH of 7.0. CNT/N-CNT electrodes were cycled between (0 and -1.2 V vs Hg/Hg_2SO_4) in order to passivate residual electroactive iron remaining from synthesis.[55]. Electrochemical measurements were carried out with a Hg/Hg_2SO_4 reference electrode (CH Instruments, +0.64 V vs SHE; +0.44 V vs Ag/AgCl; +0.40 V vs SCE) and a coiled Au counter electrode using an Autolab PGSTAT30 potentiostat (GPES software version 4.9). NADH concentrations were calculated by mass, assuming one water molecule was associated with the disodium salt hydrate, and that the NADH (either disodium salt hydrate or anhydrous dipotassium salt) was 100% pure. Error associated from the purity assumption would only cause the electrochemical sensitivity measurements to be underestimated.

4.3 Results and Discussion

4.3.1 Electrocatalytic Oxidation of NADH at CNT/N-CNT Electrodes

Figure 4.1 displays cyclic voltammograms (CVs) of glassy carbon (GC), edge plane pyrolytic graphite (EPPG), nondoped CNT, 4.0 at.% N-CNT, and 7.4 at.%

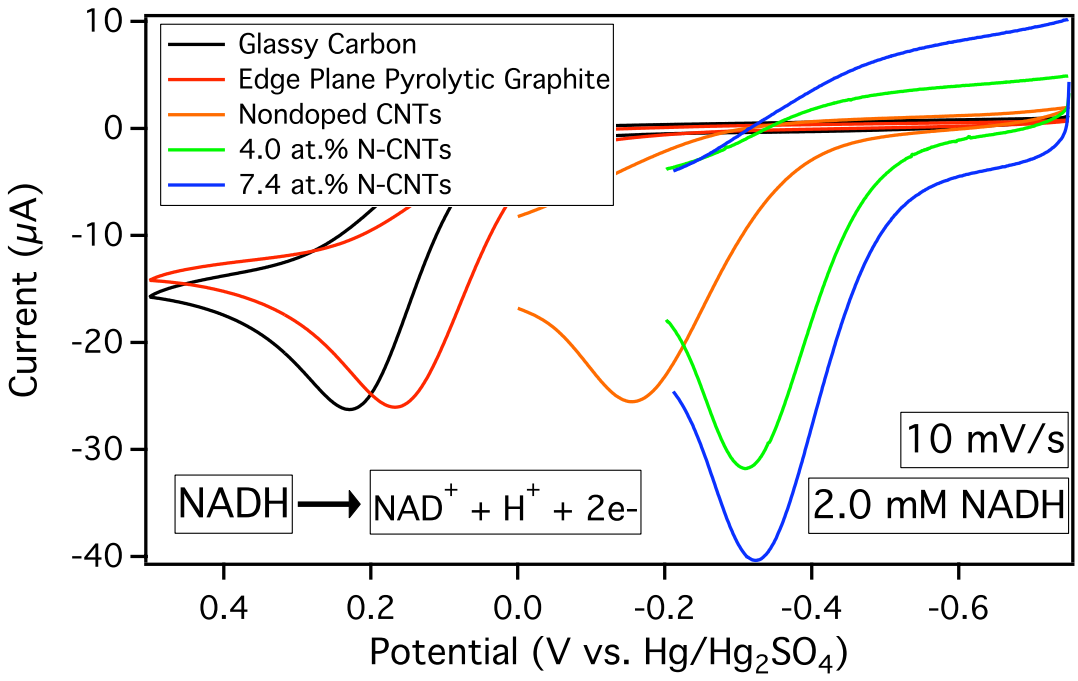

Figure 4.1. Oxidation of 2.0 mM NADH at glassy carbon, edge plane pyrolytic graphite, nondoped CNT, 4.0 at.% N-CNT, and 7.4 at.% N-CNT electrodes at a scan rate of 10 mV/s in 0.1 M SPB (pH 7.0).

N-CNT electrodes in 0.1 M sodium phosphate buffer (SPB) at a pH of 7.0 in the presence of 2.0 mM NADH. The oxidation peak potential of NADH (E_p) dramatically decreases from traditional carbon electrodes such as GC and EPPG to the CNT electrodes, with an additional decrease when nitrogen is introduced into the CNT lattice. It is often cited that the increased edge plane character of CNT imparts electrocatalytic activity for NADH oxidation.[195,196]

Incorporation of nitrogen into CNTs has been shown to increase the edge plane character of CNTs,[52,57,59] thereby increasing their electrocatalytic activity towards NADH oxidation. Nitrogen-doping, however, is distinctly different than a simple increase in the edge plane density of an all carbon lattice, elegantly visualized as a single nitrogen dopant in nitrogen-doped graphene.[197] For N-CNTs, both the type and density of reactive surface sites (which now may involve nitrogen) and the electronic properties of the electrode material (such as the density of states and charge carrier density) are altered due to the n-type dopant, both of which affect the overall electrode kinetics.[59,123,198] Furthermore, the sidewalls of CNTs have been clearly shown to be active sites for electron transfer, thereby suggesting that edge plane character is not solely indicative of observed electrochemical behavior.[199] We aim to investigate a simple preparation of these carbon surfaces, alumina polish for GC/EPPG electrode surfaces and drop casting of CNT/N-CNT electrodes, to accurately determine a base level of NADH reactivity, without additional surface treatments, binders, dispersing agents, or NADH mediators. The results in Figure 4.1 suggests that N-CNTs both increase the oxidation current, probably due to the increased surface area of N-CNTs[59], and decrease the potential at which NADH oxidation occurs. Table 4.1 presents the peak potential (E_p) for NADH oxidation at each of the electrodes shown in Figure 4.1. Figure 4.2 displays each

Table 4.1. Oxidation peak potentials (E_p) of 2mM NADH in 0.1 M SPB (pH 7.0) at 10 mV/s

Type	E_p (V vs. Hg/Hg_2SO_4)	# of Trials	ΔE_p from GC (mV)
GC	+ 0.22 ± 0.05	51	0
EPPG	+ 0.17 ± 0.04	31	50
Nondoped CNTs	- 0.15 ± 0.04	48	370
4.0 at.% N-CNTs	- 0.30 ± 0.02	24	520
7.4 at.% N-CNTs	- 0.32 ± 0.01	26	540

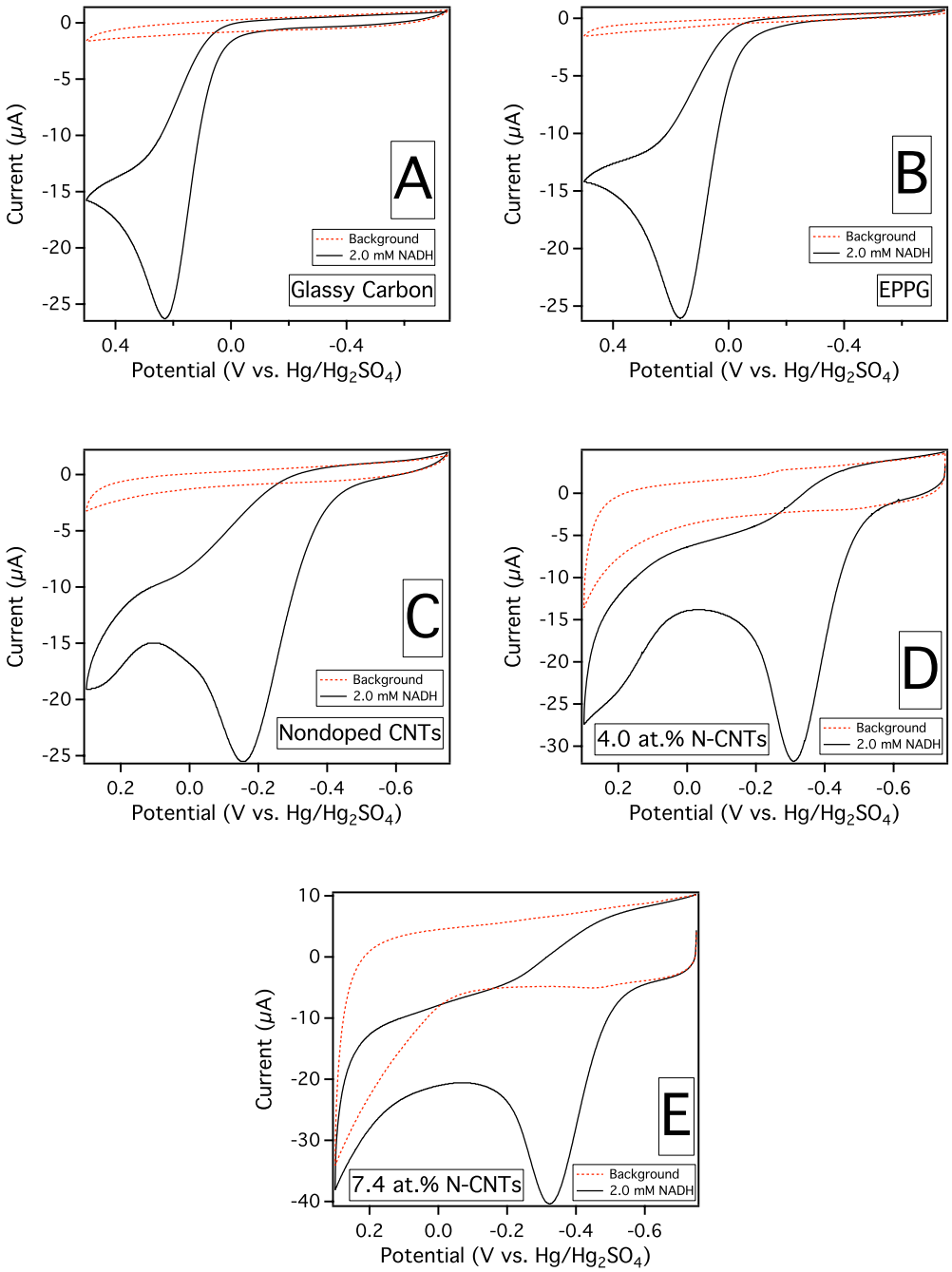

Figure 4.2. CVs of Glassy Carbon (A), Edge Plane Pyroltic Graphite (EPPG; B), Nondoped CNT (C), 4.0 at.% N-CNT (D), and 7.4 at.% N-CNT (E) electrodes in the presence and absence of 2.0 mM NADH (0.1 M SPB pH 7.0, scan rate at 10 mV/s)

oxidation peak (from Figure 4.1) with its respective background. Nondoped CNTs lower the oxidation potential by 370 mV from GC, while N-CNTs further lower the potential by 170 mV compared to nondoped CNTs. There is only a modest decrease in the E_p (20 mV) between 4.0 at.% N-CNTs and 7.4 at.% N-CNTs. Overall, there is a 540 mV decrease in the E_p from GC to our 7.4 atom % N-CNT electrodes. It should be pointed out that the standard deviation for E_p is smaller at N-CNTs compared to GC, EPPG, or nondoped CNTs.

The E_p is often used as a figure of merit for NADH electrocatalysts; however, E_p is highly dependent on experimental conditions. Early work done by Moiroux and Elving[200–202] and Blaedel and Jenkins[203] indicated that variables such as scan rate, concentration of NADH, supporting electrolyte, and pretreatment as well as prior conditioning of the electrode surface play an important role in the observed potential of NADH oxidation. Analysis of NADH oxidation is further confounded by electrode fouling, NADH degradation, and other factors such as uncompensated resistance, making E_p an inconsistent metric for comparison between electrocatalysts. In general, a less positive E_p is observed at slower scan rates and lower concentrations of NADH. Figure 4.3 displays CVs of 4.0 at.% N-CNTs in the presence of 0.5, 1.0, 2.0, 4.0, and 8.0 mM NADH at both 50 and 100 mV/s. Table 4.2 identifies the shift in E_p as a function of NADH concentration from Figure 4.3. The oxidation peak shifts positive concurrent with both increasing concentrations of NADH and scan rate. Figure 4.4 and Table 4.3 the shift in E_p as a function of scan rate from 10 mV/s to 200 mV/s in a constant concentration of 2.0 mM NADH (also at a 4.0 at.% N-CNT electrode). The observed E_p shifts under these measurements conditions, which are relatively standard conditions, can vary up to

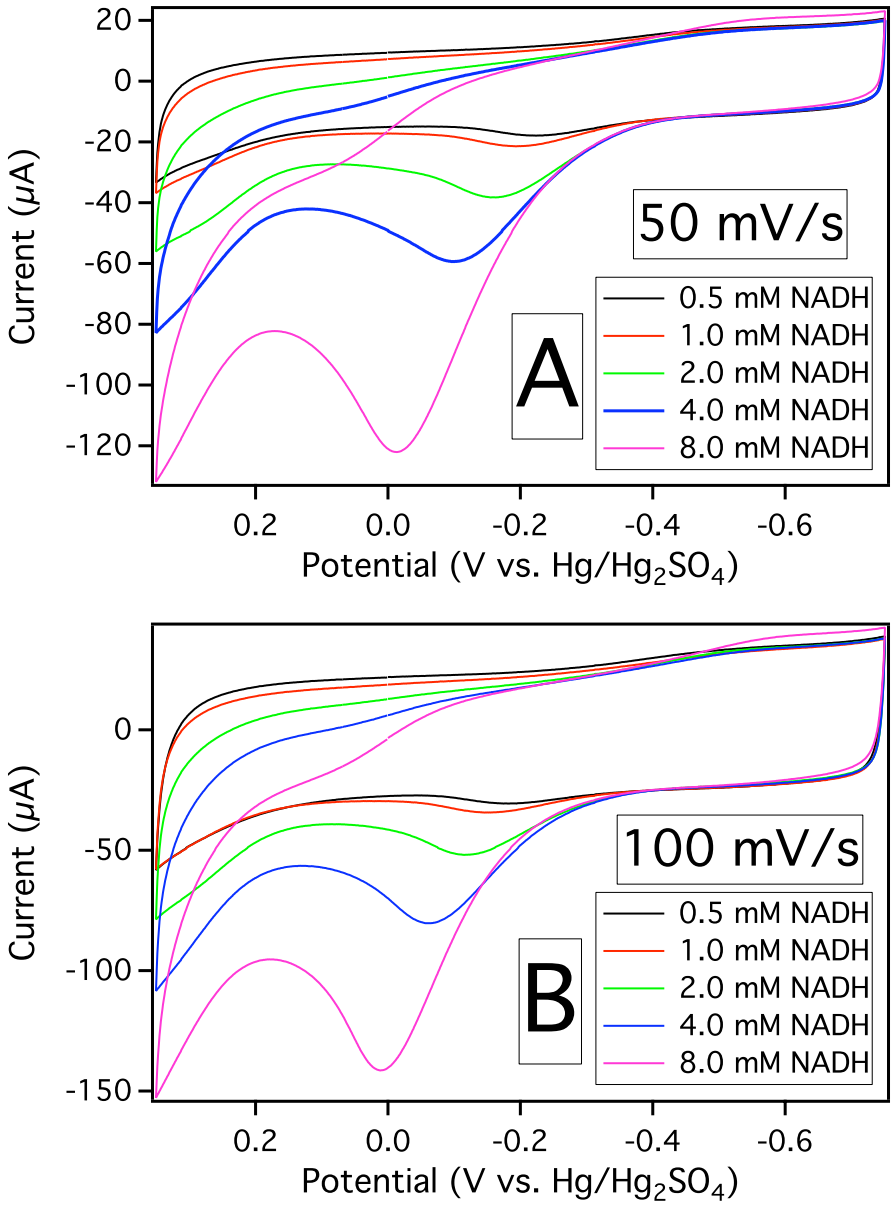

Figure 4.3. CVs of 4.0 at.% N-CNTs in the presence of increasing concentrations of NADH (0.5, 1.0, 2.0, 4.0, and 8.0 mM) at 50 (A) and 100 mV/s (B) (0.1 M SPB pH 7.0, 5th cycle is shown for each concentration)

Table 4.2. E_p measured at increasing concentrations of NADH at 50 and 100 mV/s at 4.0 at.% N-CNTs (from Figure 4.3)

NADH Concentration (mM)	Oxidation Peak at 50 mV/s (V vs. Hg/Hg_2SO_4)	Oxidation Peak at 100 mV/s (V vs. Hg/Hg_2SO_4)
0.5	-0.221	-0.183
1.0	-0.192	-0.150
2.0	-0.160	-0.116
4.0	-0.099	-0.062
8.0	-0.013	+0.011

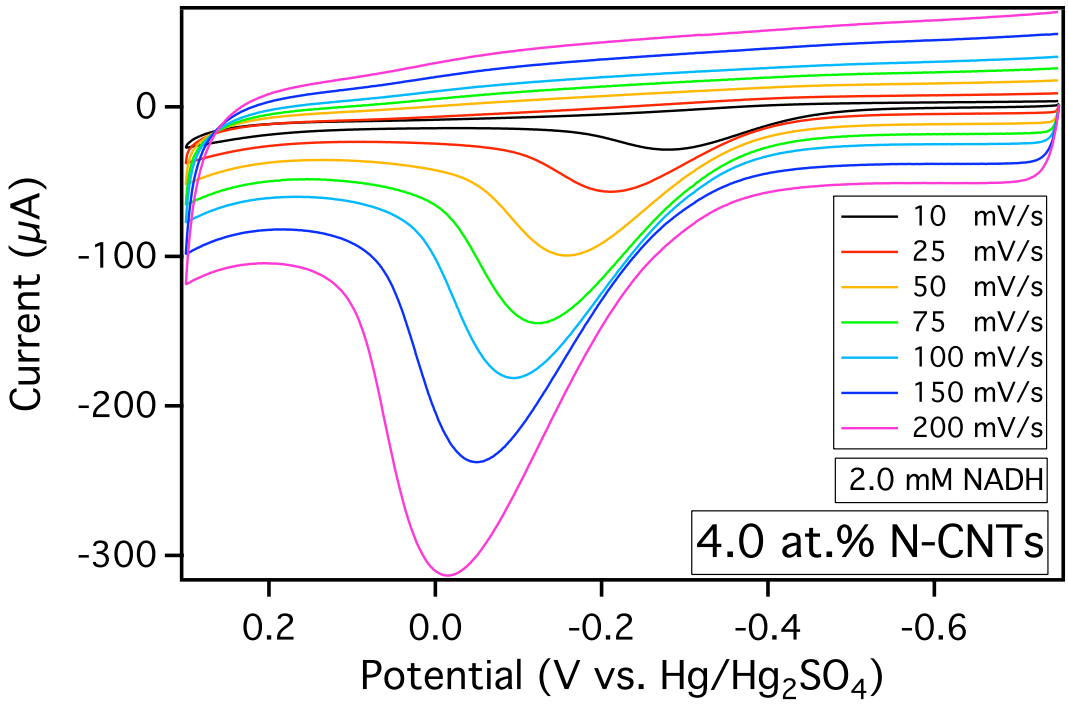

Figure 4.4. CVs of a 4.0 at.% N-CNT electrode in the presence of 2.0 mM NADH at 10, 25, 50, 75, 100, 150, and 200 mV/s (0.1 M SPB pH 7.0, 1st cycle is shown for each scan rate)

Table 4.3. E_p measured at increasing scan rates at a 4.0 at.% N-CNT electrode in the presence of 2.0 mM NADH (from Figure 4.4)

Scan Rate (mV/s)	E_p (V vs. Hg/Hg_2SO_4)
10	-0.280
25	-0.211
50	-0.158
75	-0.123
100	-0.094
150	-0.050
200	-0.015

200 - 300 mV. With such a wide range of E_p values based on standard operating conditions, it is clear why E_p becomes an inconsistent metric between NADH electrocatalysts. Quantitative assessment of NADH oxidation can also be characterized by measuring the sensitivity of an electrode to NADH, poised at a constant potential,as discussed below in the NADH sensitivity section. In order to attempt a comparison of NADH oxidation electrode materials, Table 4.4 presents CNT based NADH oxidation electrodes found in the literature.

It has been reported in the literature that nondoped CNTs will sometimes display two NADH oxidation peaks.[46,195] This phenomenon has been ascribed to NADH oxidation at the background electrode, on which the CNTs are applied.[195] This additional E_p, however, is often between that reported for CNTs or the E_p of NADH at the background electrode. Although not consistently, we observe two NADH oxidation peaks at CNTs in addition to a wave associated with the background electrode, shown in Figure 4.5A. We also observe two oxidation peaks if CNTs are drop cast on GC or Au background electrodes, shown in Figure 4.5B.

4.3.2 NADH Sensitivity

The sensitivity of each electrode material to NADH was determined by rotating disk amperometry, where the concentration of NADH was increased while the electrode was poised at a constant potential (i.e. the steady-state current at each concentration was recorded relative to the background). The potential at which the electrode was poised plays a major role in determining the sensitivity to NADH. Figure 4.6 and Table 4.5 presents the sensitivity of a 7.4 at.% N-CNT electrode to 5 μM aliquots of NADH as a function of potential. The results point out that although the sensitivity of the linear

Table 4.4. Comparison of NADH oxidation potentials and NADH sensitivities at CNT-based electrodes from the literature

CNT Type	Acid Oxidation of CNT	Main Modifications/Mediators	Concentration of NADH (mM)	Scan Rate (mV/s)	E_p (V vs. Hg/Hg_2SO_4)	Sensitivity ($A\ M^{-1}\ cm^{-2}$) Poised Potential(V vs. Hg/Hg_2SO_4)	Reference
N-CNTs	no	Nitrogen doped	2	10	- 0.320	0.31 (- 0.320 V)	This work
MWCNTs	yes	None	5	50	- 0.110	NR	10
MWCNTs	no	Poly-(3-methylthiophene)	1	25	- 0.001	0.042 (- 0.140 V)	32
SWCNTs	no	Hyaluronic acid	1	50	- 0.026	0.00713 (- 0.050 V) FIA	15
SWCNTs	yes	Meldola's blue	5	50	- 0.540	0.0074 (- 0.540 V)	17
B-CNTs	yes	Boron doped	1	50	- 0.100	0.00225 *A/M (- 0.100 V)	39
CNTs	no	Ordered/aligned CNTs	2	10	- 0.400	NR	14
MWCNTs	no	Azure C/Chitosan	1	50	- 0.520	0.146 (- 0.540 V)	25
MWCNTs	yes	PDDA-poly(Azure B) composite	1	10	- 0.340	0.004 (- 0.340 V)	27
MWCNTs	yes	Poly(toluidine blue O)	1	50	- 0.400	NR	22
MWCNTs	no	TCBQ	4	NR	- 0.310	0.842 (- 0.290)	19
MWCNTs	yes	PEDOP and Pd nanoparticles	4	100	- 0.040	0.18 (- 0.020 V)	33
MWCNTs	no	Chitosan	0.1	50	- 0.100	0.13 (- 0.040 V)	16
MWCNTs	yes	Acid Microwaved CNTs	1	5	- 0.480	0.012 (- 0.490 V)	38
MWCNTs	no	Dopamine polyethylenimine	2	10	- 0.480	0.269 (- 0.465 V)	35
MWCNTs	yes	Carbodiimide coupled CNTs	1	50	- 0.220	0.2238 (- 0.250 V)	37
MWCNTs	yes	DHB and Nafion binder	2	10	- 0.490	0.02368 (- 0.490 V)	28
MWCNTs	yes	Toluidine blue	5	50	- 0.419	0.122 (- 0.640 V)	20
MWCNTs	yes	PDDA/PSS-[MWCNTs-NH_3^+-graphene-COO^-]$_5$	5	50	- 0.330	0.055 (- 0.330 V)	36
MWCNTs	yes	Polyluminol	0.5	NR	- 0.290	0.184 (- 0.340 V)	29
MWCNTs	yes	1,10-phenanthroline-5,6-dione	1	50	~ - 0.400	0.124 (- 0.400 V)	30
MWCNTs	no	Silica-azure C nanoparticles/ chitosan	1	50	~ - 0.390	0.238 (-0.040 V)	31

Geometric Area of Electrode was used in sensitivity calculations
NR = Not Reported
FIA = Flow Injection Analysis
*A/M = Electrode Area was not given
~ = E_p estimated from reference figure

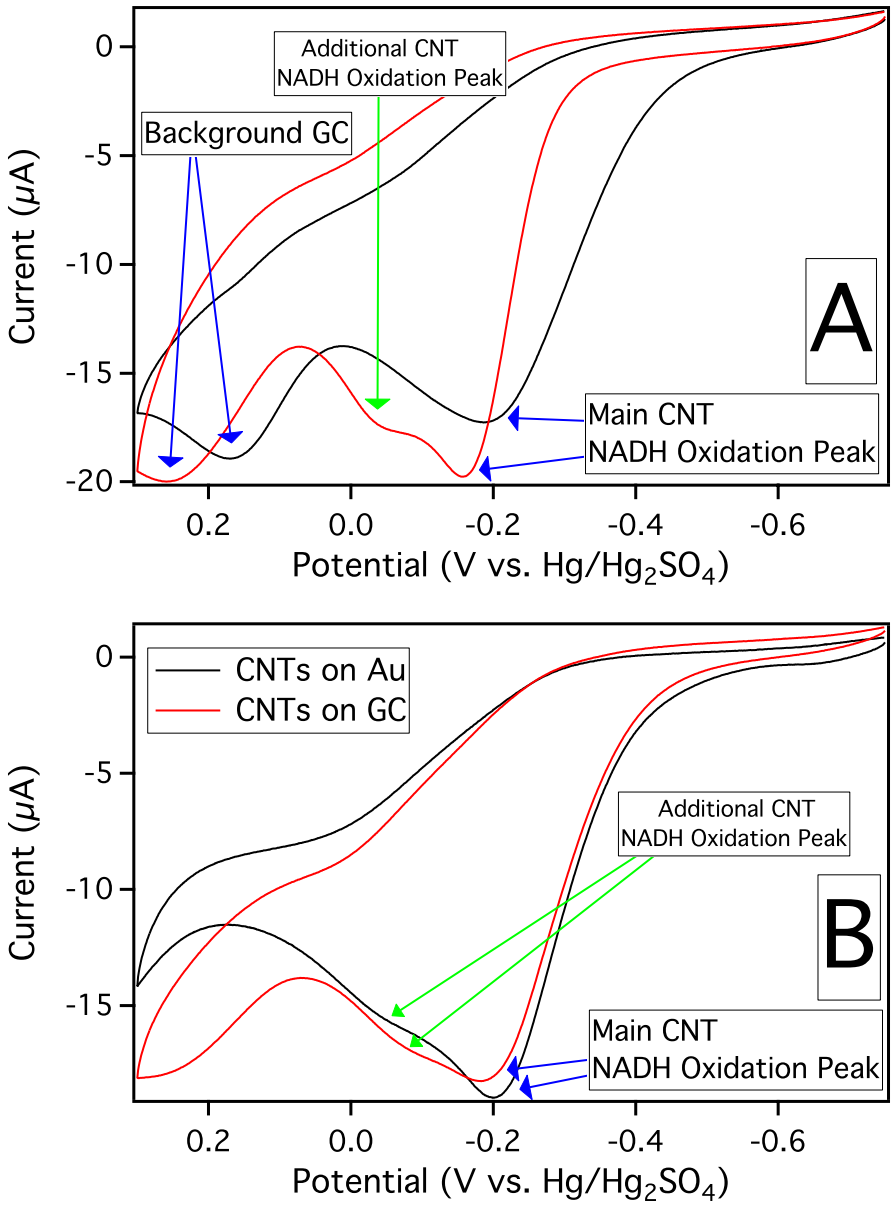

Figure 4.5. CVs of nondoped CNTs on a (A) GC background electrode or (B) Au and GC background electrodes in the presence of 2.0 mM NADH (0.1 M SPB pH 7.0, scan rate 10 mV/s) displaying the NADH oxidation peaks associated with nondoped CNTs or the background electrodes

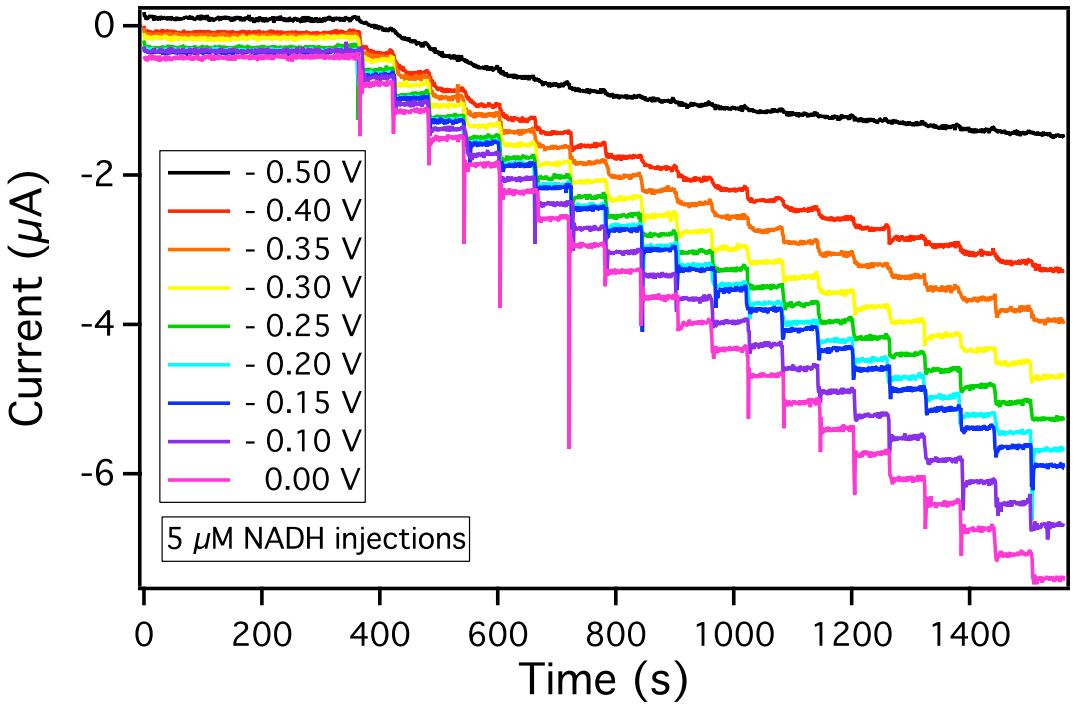

Figure 4.6. Chronoamperograms of a 7.4 at.% N-CNT rotating disk electrode poised at increasingly positive potentials to 5 μM injections of NADH (0.1 M SPB pH 7.0, 1000 rpm)

Table 4.5. Figures of merit for each poised potential (from Figure 4.6)

Sensitivity ($A\ M^{-1}\ cm^{-2}$)	Limit of Linear Range (μM)	Limit of Detection (μM)	Sensitivity to 50 μM NADH ($A\ M^{-1}\ cm^{-2}$)	Poised Potential (V vs. Hg/Hg_2SO_4)
0.10	5	2.58	0.12	- 0.50
0.25	20	1.25	0.20	- 0.40
0.25	35	0.97	0.23	- 0.35
0.25	60	1.14	0.27	- 0.30
0.25	> 100	1.38	0.28	- 0.25
0.27	> 100	1.27	0.29	- 0.20
0.28	> 100	1.39	0.30	- 0.15
0.32	> 100	0.94	0.34	- 0.10
0.36	> 100	1.12	0.36	0.00

range stays fairly constant, the linear range is clearly extended at higher potentials. A better way to characterize the increased performance at higher potentials (since the constantly changing linear ranges have similar sensitivities) is to compare the electrode sensitivity at a constant NADH concentration (in this case 50 μM, or the average response of the first 10 aliquots). Table 4.6 displays the sensitivity (based on the linear range) of each type of electrode material to NADH, along with the linear range, limit of detection, sensitivity to 50 μM NADH, and poised potential, which was chosen to be the E_p from Figure 4.1. It appears that the GC and EPPG electrodes have the highest sensitivity to NADH, however, the poised potential is significantly higher than the CNT/N-CNT electrodes. If the 7.4 at.% N-CNTs are poised at the same potential as GC, the sensitivity is slightly higher than that of GC, but more importantly, the linear range is significantly extended. Furthermore, if the GC electrode is poised at the potential for CNTs or either type of N-CNTs, the observed oxidation current is insignificant, as seen in Figure 4.7, which displays representative chronoamperograms for each electrode material, and the coordinating background (GC) current for comparison.

4.3.3 Electrochemical Fouling

It is well know that oxidation of NADH fouls the electroactive surface of the working electrode.[159,160,166] Fouling is most commonly ascribed to the adsorption of the oxidation product NAD^+ (a self-inhibitory oxidation reaction)[195,204] and the formation of dimers, created by radical intermediates.[205] The initial electron transfer from NADH creates a cation radical which subsequently deprotonates forming a neutral radical which can dimerize. There are claims that CNTs mitigate fouling when compared to GC.[46] Given that the incorporated nitrogen in N-CNTs causes significant differences in their physical properties as compared to nondoped CNTs (such as a more positive surface

Table 4.6. Sensitivity to NADH measured by rotating disk amperometry

Type	Sensitivity ($A\ M^{-1}\ cm^{-2}$)	Limit of Linear Range (μM)	Limit of Detection (μM)	Poised Potential (V vs. Hg/Hg_2SO_4)
GC	0.37 ± 0.03	410 ± 80	0.4 ± 0.2	0.22
EPPG	0.35 ± 0.04	270 ± 100	0.5 ± 0.2	0.17
Nondoped CNTs	0.21 ± 0.06	40 ± 20	0.6 ± 0.2	- 0.15
4.0 at.% N-CNTs	0.27 ± 0.04	40 ± 10	0.8 ± 0.2	- 0.30
7.4 at.% N-CNTs	0.30 ± 0.04	70 ± 10	1.1 ± 0.3	- 0.32
7.4 at.% N-CNTs	0.38 ± 0.02	> 600	1.0 ± 0.3	0.22

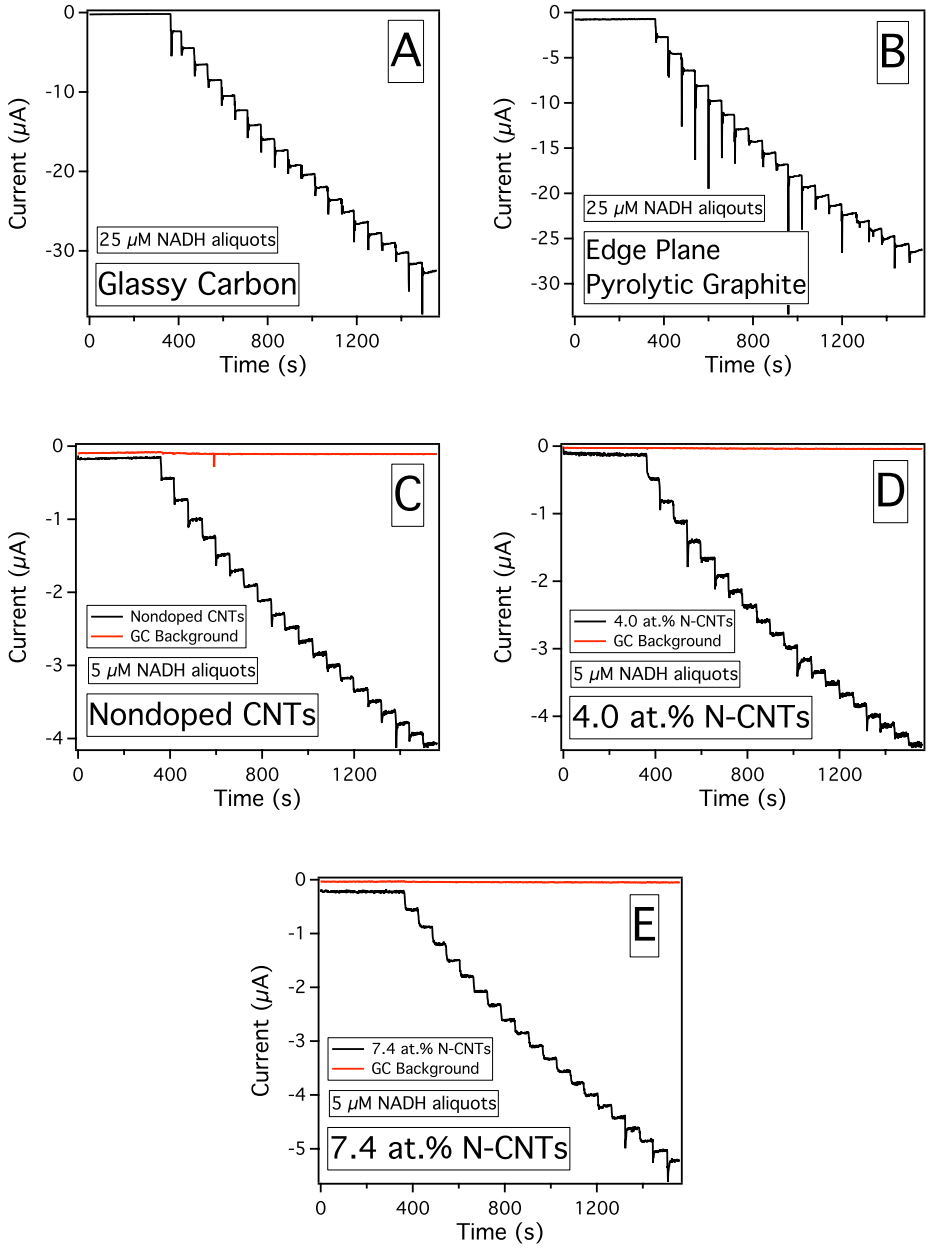

Figure 4.7. Representative chronoamperograms of a (A) GC electrode (poised at 0.22 V); a (B) EPPG electrode (poised at 0.17 V); a (C) nondoped CNT electrode (poised at -0.15 V); a (D) 4.0 at.% N-CNT electrode (poised at -0.30 V); and a (E) 7.4 at.% N-CNT electrode (poised at -0.32 V) while 5 μM aliquots of NADH are introduced into the solution (0.1 M SPB pH 7.0, rotation rate 1000 rpm)

charge at pH 7.0)[52,57,59], we investigated electrode fouling from NADH oxidation on N-CNT electrodes compared to nondoped CNT, EPPG, and GC electrodes. Figure 4.8 presents CVs of the five electrode materials cycled in 2.0 mM NADH for 10 cycles at 10 mV/s. Figure 4.9 displays CVs of the five electrode materials more extensively fouled by cycling at 500 mV/s for 1000 cycles (checked periodically at 10 mV/s). As one would expect, fouling is visualized in the CVs as an increasing overpotential (peak shifts more positive) and a decrease in the peak current as the surface sites become inhibited. Interestingly, nondoped CNTs will often display an increasing peak current, although the overpotential is still increased (Figure 4.8C and 4.9C). Fouling is electroactivated and not spontaneous, as freshly made N-CNT electrodes cycled once in 2.0 mM NADH at 10 mV/s, allowed to sit for the timeframe of eight cycles and subsequently cycled once more, display E_p shifts identical to the second cycle of continuously cycled electrodes. Table 4.7 presents the E_p shift for each type of electrode material for both the 10 cycles at 10 mV/s and the 1000 cycles at 500 mV/s (which were measured periodically at 10 mV/s). The shift after 10 cycles seems to suggest that the traditional carbon electrodes are more resistant to fouling. After 1000 cycles, the shift is fairly random across the 5 electrode types, making any assessment of fouling based on the E_p shift difficult; however, the sensitivity of each type of electrode to NADH was also measured after the extensive fouling. Sensitivity analysis indicates that the CNT/N-CNT electrodes are more resistant to fouling as compared to the traditional carbon electrodes. N-CNTs do not show any significant advantage to nondoped CNTs with respect to NADH fouling.

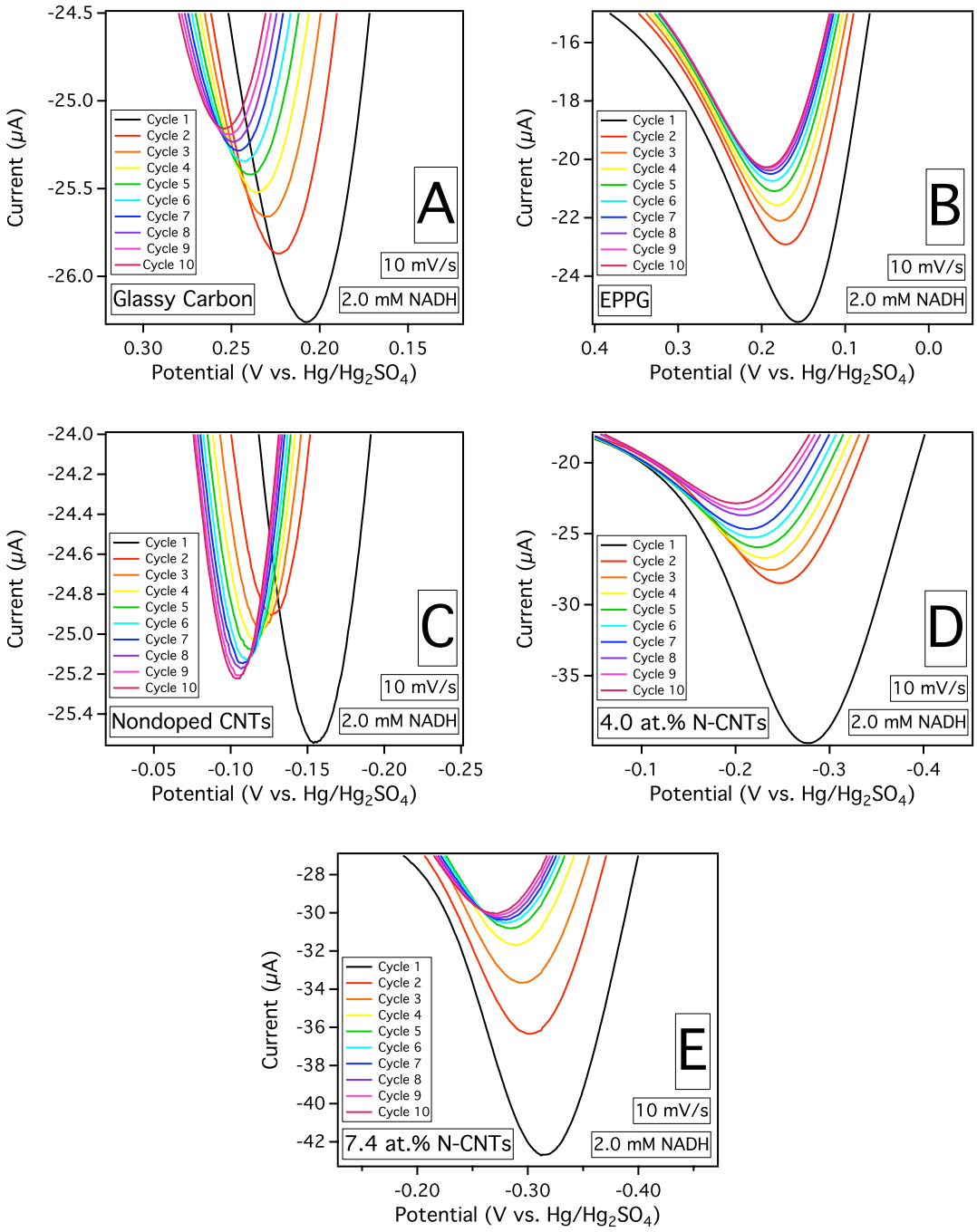

Figure 4.8. Representative CVs of a (A) GC electrode; a (B) EPPG electrode; a (C) nondoped CNT electrode; a (D) 4.0 at.% N-CNT electrode; and a (E) 7.4 at.% N-CNT electrode cycled 10 times at 10 mV/s in 2.0 mM NADH (0.1 M SPB pH 7.0)

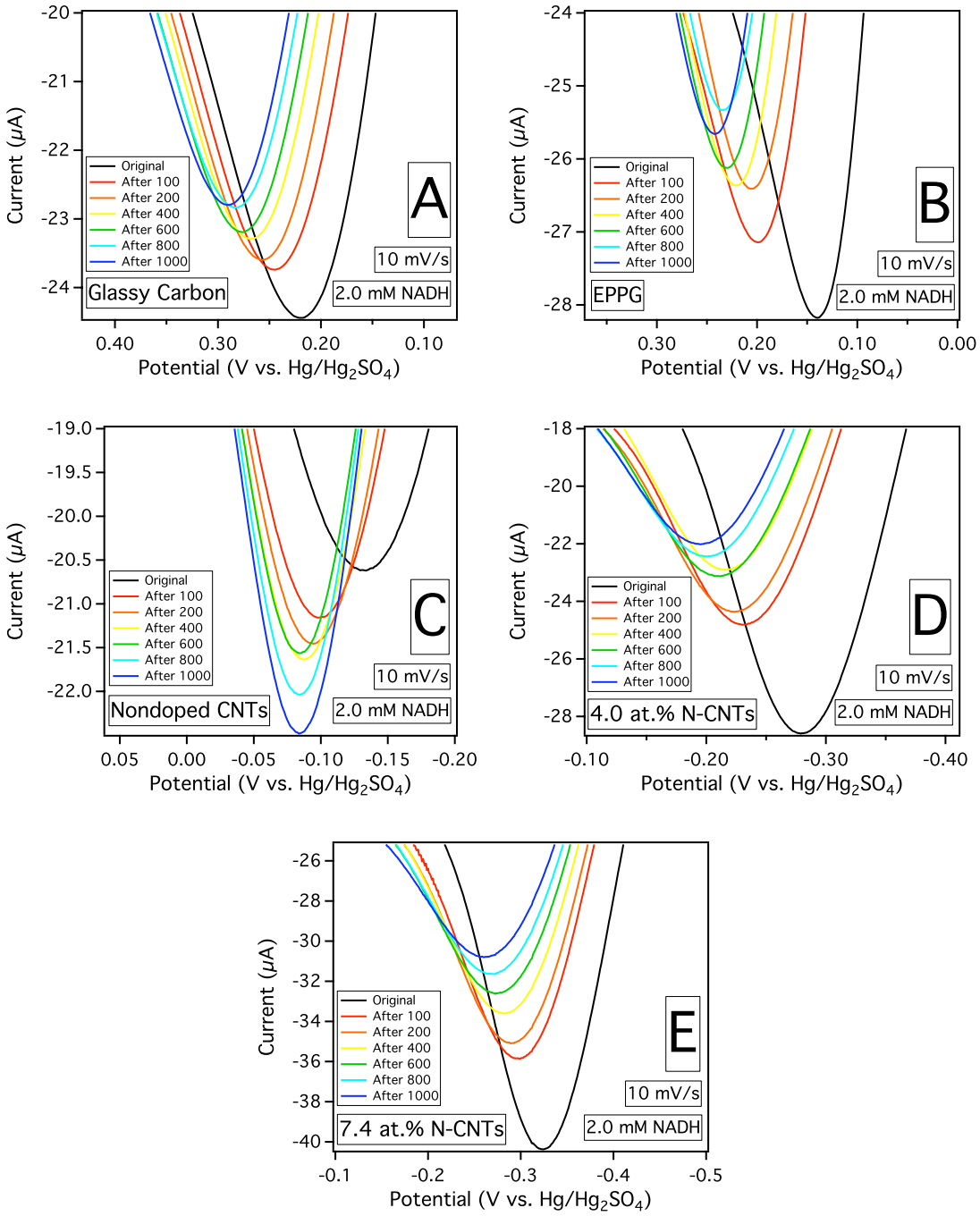

Figure 4.9. Representative CVs of a (A) GC electrode; a (B) EPPG electrode; a (C) nondoped CNT electrode; a (D) 4.0 at.% N-CNT electrode; and a (E) 7.4 at.% N-CNT electrode cycled 1000 times at 500 mV/s in 2.0 mM NADH (checked periodically at 10 mV/s, 0.1 M SPB pH 7.0)

Table 4.7. E_p shift for NADH oxidation in 2.0 mM NADH and sensitivity to NADH after extensive fouling (0.1 M SPB pH 7.0)

Type	10 cycles at 10 mV/s (mV)	1000 cycles at 500 mV/s (mV)	Sensitivity Remaining (after 1000 cycles)
GC	40 ± 10	80 ± 30	21 %
EPPG	30 ± 10	70 ± 40	37 %
Nondoped CNTs	40 ± 10	40 ± 10	81 %
4.0 at.% N-CNTs	70 ± 10	100 ± 40	70 %
7.4 at.% N-CNTs	60 ± 10	70 ± 10	76 %

4.3.4 NADH Degradation

An important aspect of measuring NADH oxidation is the degradation of NADH in solution, especially phosphate buffer.[176,206] NADH displays an absorbance at 340 nm due to the pyridine ring of nicotinamide. This absorbance can be monitored over time as NADH degrades in solution displayed in the equation below as the percent degradation (eq. 4.1):

$$\% \text{ Degradation } = 100 - ((A_t/A_{(t=0)}) \times 100) \qquad (4.1)$$

where A_t is the absorbance at time t, t is the time elapsed since NADH was placed in solution, and $A_{(t=0)}$ is the initial absorbance (at t = 0). This procedure provides a reasonable estimate of NADH degradation; however, since the decrease in absorbance at 340 nm is indicative of the disruption of the nicotinamide pyridine ring, the electroactivity should be correlated. As previously mentioned, electrode fouling confounds these measurements, but pre-fouled electrodes can correlate degradation and electroactivity with minimal fouling interference. Figure 4.10 shows chronoamperograms of a pre-fouled 7.4 at.% N-CNT electrode where either fresh or degraded NADH is injected into solution. The fresh NADH, used both before and after the degraded NADH is injected, overlay quite well, allowing the sensitivity loss due to degradation to be accurately measured. NADH degradation as measured by UV-vis displayed a linear degradation rate of 2.2 ± 0.1 % per hour, over eight hours of measurements. This value remained true after NADH was used immediately after purchase or continuously used over 3 months, being stored at - 20°C when not in use. Figure 4.11A displays the change in absorbance at 340 nm over eight hours. The degradation rate was non-linear over a longer timeframe, as this rate should have no absorbance after 45.5 hours. Figure 4.11B displays the normalized absorbance

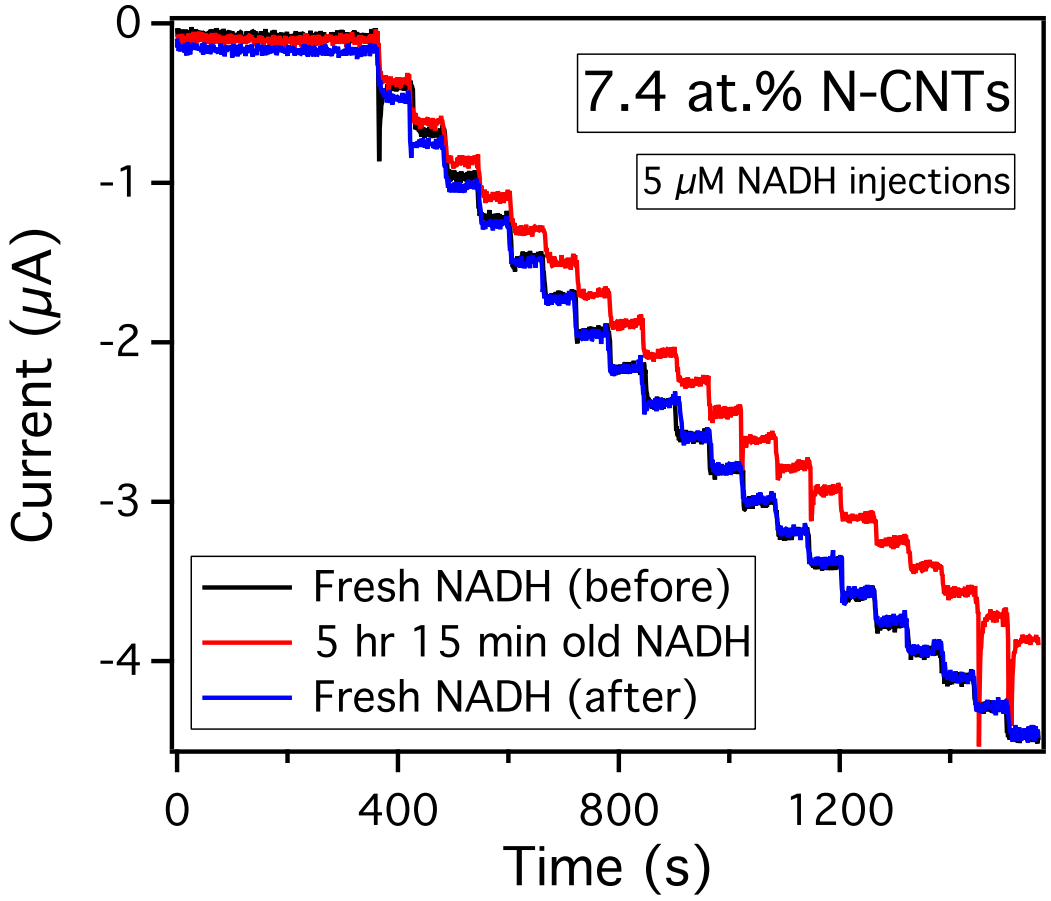

Figure 4.10. Chronoamperograms of a pre-fouled 7.4 at.% N-CNT rotating disk electrode to 5 μM injections of fresh NADH or NADH that was allowed to degrade for 5 hours and 15 minutes (1000 rpm, 0.1 M SPB pH 7.0)

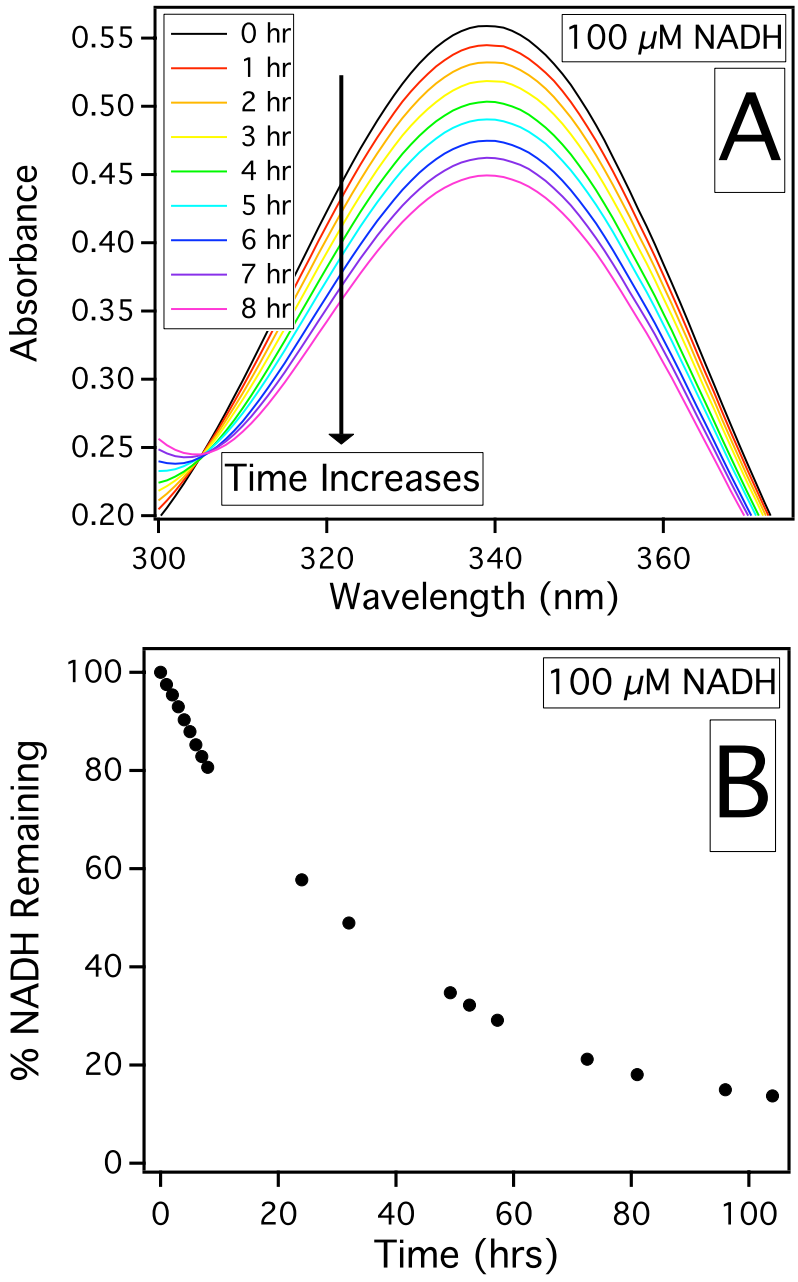

Figure 4.11. UV-Vis spectra displaying the decrease in the absorbance of the nicotinamide peak centered at 340 nm over 8 hours (A) or the normalized absorbance over 104 hours (B) in 0.1 M SPB (pH 7.0).

(normalized to the initial absorbance) as measured over 104 hours. The electroactivity scales reasonable well with the decrease in the absorbance, with the normalized electroactivity (normalized to a fresh NADH sample) generally being slightly higher than the normalized absorbance at any given timepoint. At approximately 50 hours, the UV-vis absorbance is 34 % of the initial absorbance while the electroactivity is 40% that of a fresh NADH solution. At approximately 100 hours the UV-vis absorbance is at 14 %while the electroactivity is at 17 %. The sensitivity loss of 7.4 at.% N-CNTs to NADH due to degradation in the linear regime (the first 8 hours) was found to decrease at 0.006 ± 0.001 A M^{-1} cm^{-2} hr^{-1}.

4.3.5 Demonstration of NADH Biosensing using Glucose Dehydrogenase

Dehydrogenase enzymes will convert NAD^+ to NADH in the presence of an appropriate substrate. Since N-CNTs can effectively detect NADH by oxidation at a low potential, N-CNTs were coupled with glucose dehydrogenase (GDH) to demonstrate their utility as a functional biosensing material. N-CNTs were previously shown to display spontaneous adsorption of biologically active enzyme[147], thus, we choose to allow GDH to adsorb onto the N-CNT surface from a 20 μM GDH solution (0.1 M SPB pH 7.0). Figure 4.12 presents the sensitivity of GDH loaded 7.4 at.% N-CNT electrodes to 50 μM injections of glucose as a function of adsorption time. Table 4.8 displays the biosensing figures of merit for each adsorption timepoint in Figure 4.12. The sensitivity to glucose increases concurrently with adsorption time until 20 min, where the sensitivity begins to decrease with increased GDH loading. This observation suggests that there is a balance between available surface sites where NADH oxidation occurs, and the surface coverage of GDH (which blocks reactive sites). The glucose biosensor displayed a linear range up to 440 ± 50 μM, a limit of detection at 6 ± 1 μM, and a sensitivity of 0.032 ±

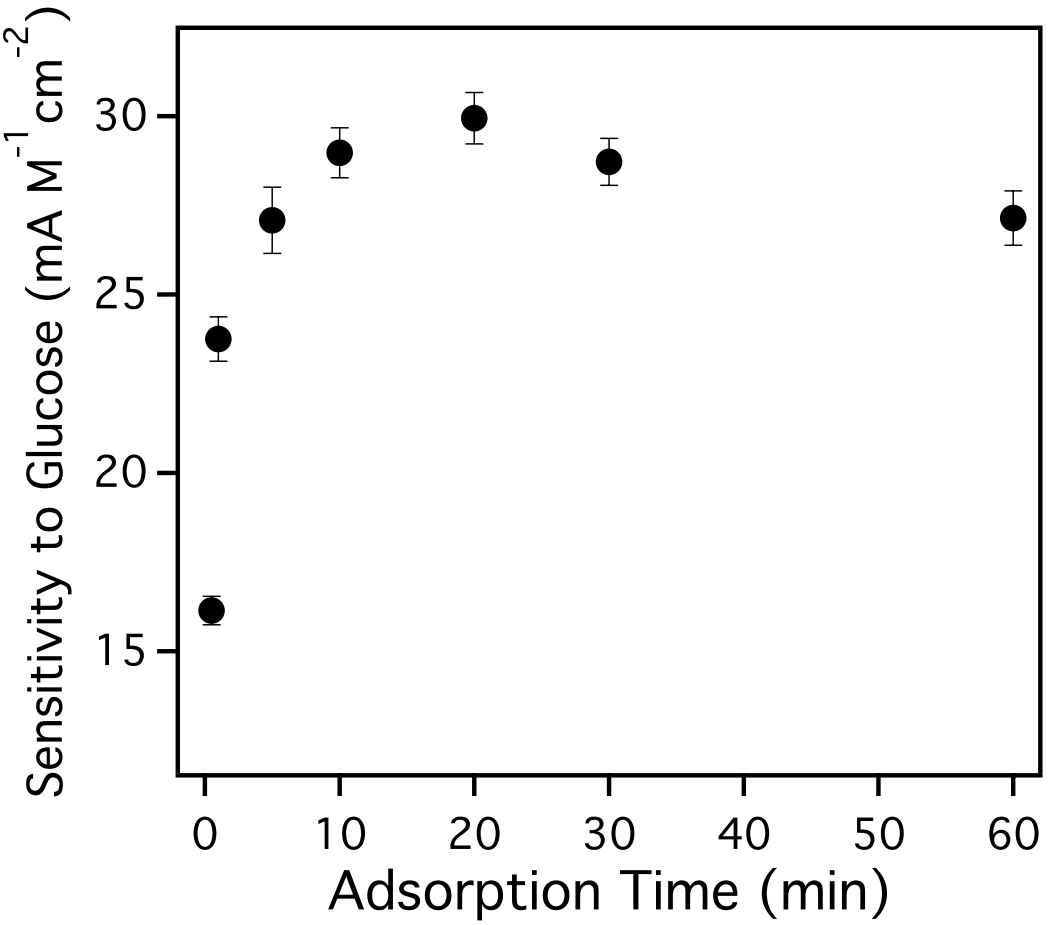

Figure 4.12. The sensitivity of a GDH loaded 7.4 at.% N-CNT electrode to glucose as a function of adsorption time in a 20 μM GDH solution (0.1 M SPB pH 7.0).

Table 4.8. Figures of merit for the glucose biosensor as a function of adsorption time in a 20 μM GDH solution (0.1 M SPB pH 7.0)

Adsorption Time (20 μM GDH)	Sensitivity (A M^{-1} cm^{-2})	Limit of Linear Range (μM)	Limit of Detection (μM)	Sensitivity to 500 μM Glucose (A M^{-1} cm^{-2})
30 sec.	0.017	450	15.94	0.016
1 min	0.029	200	6.56	0.024
5 min	0.031	300	6.16	0.027
10 min	0.030	450	7.00	0.029
20 min	0.031	450	6.31	0.030
30 min	0.029	500	8.75	0.029
60 min	0.030	350	8.09	0.027

0.003 A M^{-1} cm^{-2} (based on the linear range) in a 0.1 M SPB solution with 2.0 mM NAD^+. Figure 4.13A presents a representative chronoamperogram of a 7.4 at.% N-CNT electrode with adsorbed GDH (20 min) as 50 μM glucose injections are introduced. Figure 4.13B displays the corresponding anodic current response (absolute value) as a function of glucose concentration. Compared to the sensitivity of 7.4 at.% N-CNTs to direct injections of NADH (Table 4.6), the sensitivity of the glucose biosensor to glucose is only 11%. Although the available surface sites for NADH oxidation are expected to decrease as GDH is adsorbed onto the surface, and the local formation of NADH is determined by the orientation of the adsorbed GDH, there appears to be room for improvement. Nonetheless, the N-CNT electrodes offer a simple platform to create a multitude of biosensors from the spontaneous adsorption of enzymes.

Enzyme kinetics were measured for the adsorbed GDH electrodes where at -0.32 V (vs. Hg/Hg_2SO_4) the glucose concentration was increased until saturation. The apparent Michaelis constant (K_M^{app}) and the maximum velocity (V_{max}) were determined from Lineweaver-Burk plots. Values of 2.9 ± 0.2 mM for K_M^{app} and 106 ± 6 pmol/s for V_{max} were obtained. Since the sensitivity of NADH is strongly dependent on potential, we issue a word of caution when measuring enzyme kinetics. The strong potential dependency indicates that the electrooxidation of NADH is probably a kinetically limited reaction, since the enzymatic reaction should be spontaneous and independent of electrode potential. When enzyme kinetics were measured at 0.17 V, the same amount of glucose did not saturate the electrode, and the K_M^{app} and V_{max} were 9.9 mM and 398

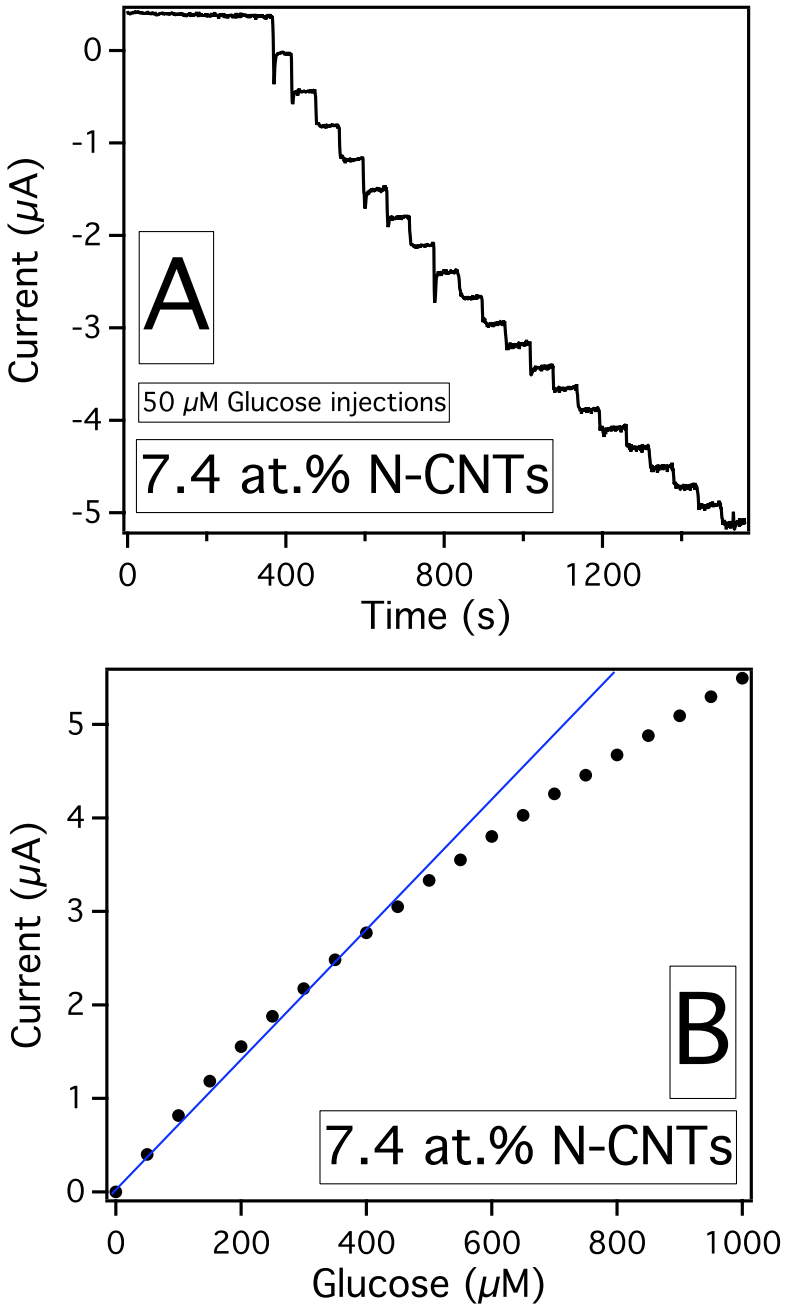

Figure 4.13. Chronoamperogram of a GDH loaded (20 min in a 20 μM GDH solution) 7.4 at.% N-CNT rotating disk electrode (1000 rpm) to 50 μM injections of glucose (A) and the corresponding anodic current response as a function of glucose concentration (B, line indicates linear range).

pmol/s, respectively. Since these values are over 3 times that measured at -0.32 V (and well beyond the standard deviation at that potential) we can confidently assume that the measured kinetic parameters are arising from the electrochemical reaction, rather than the spontaneous enzymatic reaction.

4.4 CONCLUSION

N-CNTs were shown to be electrocatalytic towards the oxidation of NADH as compared to nondoped CNTs or traditional carbon electrodes. The sensitivity of 7.4 at.% N-CNTs to NADH (poised at a low applied potential of -0.32 V vs. Hg/Hg_2SO_4) rivals that of the best CNT-based electrodes, even when mediators are included. Fouling of the electrode surface from NADH oxidation was characterized by E_p and the resulting electrode sensitivity loss. Although the shifting E_p made comparison between electrode types difficult, CNT/N-CNT electrodes displayed a higher resistance to fouling based upon the sensitivity loss after extensive fouling. The degradation of NADH in 0.10 M SPB was characterized by absorbance at 340 nm and correlated with the loss of NADH electroactivity. The enhanced electroactivity toward NADH and spontaneous adsorption of dehydrogenase enzyme provides a simple platform for dehydrogenase-based biosensing using N-CNTs, as demonstrated using glucose dehydrogenase as a model enzyme. Chapter 5 will investigate the reaction kinetics of NADH oxidation at N-CNTs.

CHAPTER 5

Investigating the Electrocatalytic Oxidation of Dihydronicotinamide Adenine Dinucleotide at Nitrogen-Doped Carbon Nanotube Electrodes: Implications to Electrochemically Measuring Dehydrogenase Enzyme Kinetics*

5.1 INTRODUCTION

Carbon nanomaterials such as carbon nanotubes (CNTs) and graphene are increasingly being coupled with enzymes to create bioelectrodes[207] for biosensing[84,85,208,209] and biofuel cell[127,128,210] applications. Enzymes incorporated into an electrode impart a biorecognition element that is selective to a specific substrate or fuel in the case of biofuel cell electrodes. NAD^+-dependent dehydrogenase enzymes are one of the more commonly applied enzymes, requiring the cofactor nicotinamide adenine dinucleotide (NAD^+) in conjunction with an appropriate substrate to cause enzymatic turnover. The general enzymatic reaction for a NAD^+-dependent dehydrogenase is shown below:

$$\text{Substrate} + NAD^+ \rightarrow \text{Product} + NADH \text{ (in the presence of enzyme)} \quad (5.1)$$

The reduced cofactor, dihydronicotinamide adenine dinucleotide (NADH), can be reoxidized at an electrode surface via a 2-electron one-proton oxidation shown below:

$$NADH \rightarrow NAD^+ + 2e^- + H^+ \quad (5.2)$$

The formal potential of the $NADH/NAD^+$ couple is low, at - 0.96 V vs. Hg/Hg_2SO_4

*Portions of this chapter were taken from a manuscript submitted to *ACS. Catal.* (2014) by Goran, J. M.; Favela, C. A.; Stevenson, K. J. (Favela performed experiments, Stevenson supervised this work)

(-0.52 vs. Ag/AgCl; -0.56 vs. SCE; -0.32 vs. NHE)[160] and requires a large overpotential in order to be observed at conventional electrodes such as Pt or carbon. In order to lower the overpotential, mediators or catalysts are employed.[164,211] CNTs have been shown to be electrocatalytic towards NADH oxidation by substantially lowering the overpotential compared to conventional glassy carbon.[44–47,167,190,191,194] Often, CNTs are coupled with mediators to further lower the oxidation overpotential[170–173,212] Mediators are polymerized on the CNT surface, or dispersed within a polymer, biopolymer, or hydrogel matrix to effectively couple the individual components and create a biocompatible environment for enzyme immobilization.[169,174–176,178,179,182,184,185,188,213–215] Heteroatom doped CNTs, both B-CNTs[192] and N-CNTs[149], have been shown to further decrease the oxidation overpotential compared to nondoped CNTs, without additional mediation. Although many reports have touted the benefits of CNTs for NADH oxidation, or demonstrated their use with dehydrogenases, the electron transfer kinetics of the electrochemical reaction are often neglected. This aspect is increasingly important since many reports are evaluating the enzymatic behavior of the bioelectrode by electrochemically measuring the enzyme kinetics.[177,183,193,216–223] Thus, it is important to ensure that the electron transfer kinetics at the electrode surface are not a limiting factor in the kinetic analysis of the enzyme. The physical distance of the catalytic redox site embedded in most enzymes prevents the direct electron transfer between the redox site and the electrode.[23,26,127] The electric field emanating from the electrode surface, then, should have a negligible influence on the enzymatic reaction, which is mainly dependent on the substrate concentration. The vast majority of electrochemically determined enzyme kinetics (e.g. K_M^{app} and V_{max}) are performed at a single potential, neglecting to demonstrate potential-independence of the enzymatic reaction, or attempting to identify the influence of potential on the

electrochemical reaction. Herein, we report a kinetic evaluation of NADH oxidation at electrocatalytic N-CNT electrodes. Additionally, we allow glucose dehydrogenase (GDH) to spontaneously adsorb onto the N-CNT surface and evaluate the enzyme kinetics via NADH oxidation. This study is beneficial to understanding the fundamental reactivity of N-CNTs since dispersing agents, binders, redox mediators, oxidizing acids, and immobilizing matrices (polymer, biopolymer, or hydrogel matrix) are not used. We identify a potential region where the electron transfer rate constant is too rapid to accurately measure by the rotating disk electrode technique, and should supply accurate enzyme kinetics, but find that the obtained measurements are still under the kinetic control of the electrochemical reaction. Beyond this potential region, application of the enzyme by spontaneous adsorption is limited due to the oxidation of the N-CNT electrode surface, which causes the adsorbed enzyme to detach from the electrode surface.

5.2 EXPERIMENTAL

5.2.1 Enzyme and Chemicals

Glucose Dehydrogenase (from *Pseudomonas sp*., E.C. 1.1.1.47, lyophilized powder ≥200 U/mg), β-nicotinamide adenine dinucleotide dipotassium salt, α-D-glucose, and *m*-xylene (anhydrous) were obtained from Sigma-Aldrich. Sodium phosphate monobasic (NaH_2PO_4, monohydrate), sodium phosphate dibasic (Na_2HPO_4, anhydrous), pyridine, pH calibration buffers (4.00, 7.00, 10.00), and sodium hydroxide were purchased from Fisher. Bis(cyclopentadienyl)iron (ferrocene) was obtained from Alfa Aesar. Hexaammineruthenium (III) chloride (99%) was purchased from Strem Chemicals.

5.2.2 N-CNT Synthesis

N-CNTs were synthesized by injecting a 20 mg mL^{-1} solution of ferrocene dissolved in pyridine at 0.1 ml min^{-1} via a glass syringe (Hamilton 81320) and an automated syringe pump (New Era Pump Systems NE-1000) into a quartz tube laid lengthwise across two identical tube furnaces (Carbolite Model HST 12/35/200/2416CG). The first furnace, where the solution entered the tube, was set at 130°C to ensure the catalyst solution entered the vapor phase. The second furnace was set at 800°C to cause the vapor to deposit multiwalled N-CNTs on the inside lining of the quartz tube via a floating catalyst chemical vapor deposition (CVD) process. Argon was used as a carrier gas (532 sccm) to direct the flow of the catalyst solution from the first tube furnace to the second, with the coinjection of ammonia (43 sccm), controlled by two gas mass flow controllers (MKS type 1179A) for a total gas flow of 575 sccm. N-CNTs made by this process contain 7.4 at.% N.

5.2.3 Electrochemistry, Electrode Preparation, and Spectrophotometry

Electrochemical information is presented with a positive cathodic current and a negative anodic current. Ultramicroelectrode (UME) cyclic voltammograms were obtained with a CH Instruments 700A potentiostat in conjunction with a SCE reference electrode, and a platinum wire counter electrode, all inside a CH Instruments Faraday cage. All other electrochemical measurements were performed with an Autolab PGSTAT30 potentiostat (GPES software version 4.9) in coordination with a five-neck glass cell (125 ml), a Hg/Hg_2SO_4 reference electrode (CH Instruments, +0.64 V vs SHE; +0.44 V vs Ag/AgCl; +0.40 V vs SCE), and a coiled Au counter electrode. Potentials are reported vs. Hg/Hg_2SO_4 unless noted otherwise (such as in the UME section). Rotating disk electrode (RDE) experiments were performed on a Pine Instruments AFMSRX

rotator. N-CNT electrodes were prepared by drop casting a 12 μl aliquot of a 2 mg ml^{-1} solution of N-CNTs in absolute ethanol (sonicated for 2 hours) onto a 0.5 cm diameter glassy carbon RDE (Pine Instruments AFE2M050GC). GC electrodes which were polished with a 0.05 μm alumina slurry on microcloth (Buehler) and briefly sonicated in 18 MΩ cm water to remove adsorbed alumina prior to use or N-CNT application. N-CNT electrodes were "wet" in a mixture of ethanol and 0.1 M sodium phosphate buffer (SPB) to ensure complete surface contact with the electrolyte solution. N-CNT electrodes were also cycled between 0 and -1.2 V to passivate electroactive iron remaining from the CVD synthesis.[55] NADH concentrations for electrochemical experiments were calculated based on weight, which may underestimate the actual concentration. Spectrophotometric analysis was performed on an Agilent 8453 UV-visible (UV-sis) spectrophotometer (photodiode array) using quartz cuvettes (path length of 1 cm). Glucose dehydrogenase and NAD^+ were added to the cuvette prior to the introduction of glucose for all UV-vis measurements. NADH concentrations via UV-vis absorbance at 340 nm were calculated with an molar extinction coefficient of 6200 M^{-1} cm^{-1}, a value similar to other reports.[177,224] Nonlinear Michaelis-Menten enzyme kinetics were fit using IGOR Pro 6.12.

5.3 Results and Discussion

5.3.1 Oxidation of NADH at Carbon Fiber Ultramicroelectrodes: A Qualitative Study

Ultramicroelectrodes (UMEs) are a useful tool for evaluating the electron transfer kinetics of redox molecules due to their increased mass transport via radial diffusion. Figure 5.1 presents a cyclic voltammogram (CV) of a 8 μm carbon fiber electrode in the presence of 1.0 mM NADH or 1.0 mM ruthenium hexamine ($Ru(NH_3)^{3+}$) in 0.1 M sodium phosphate buffer (SPB) at a pH of 7.0. The reduction of $Ru(NH_3)^{3+}$ displays a

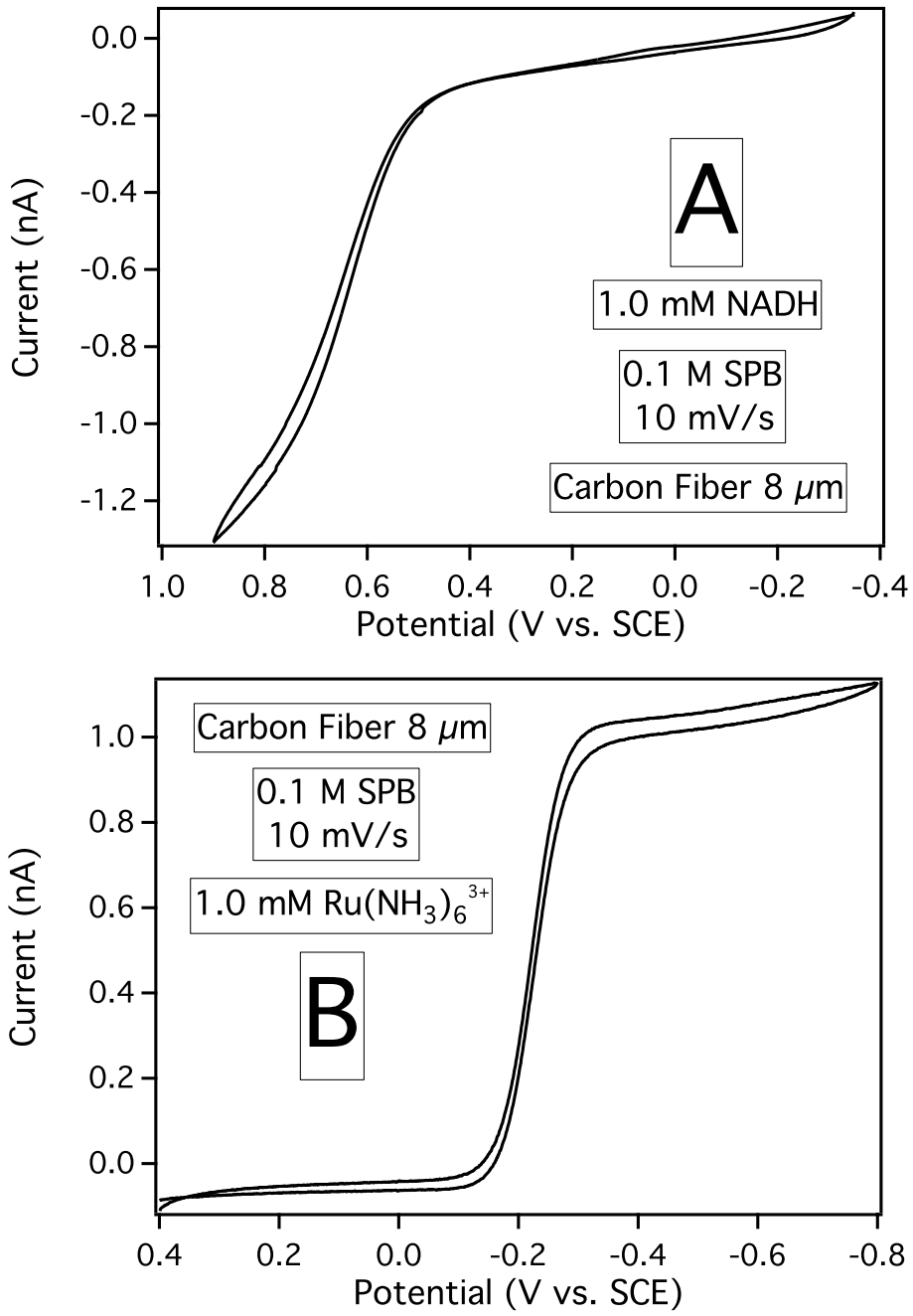

Figure 5.1. Oxidation of 1.0 mM NADH (A) or the reduction of 1.0 mM $Ru(NH_3)^{3+}$ (B) at an 8 μm carbon fiber UME (0.1 M SPB, pH 7.0, scan rate 10 mV/s).

typical sigmoidal shape with a mass transfer limited plateau, not seen in the NADH oxidation CV. The missing plateau can be explained if the electron transfer reaction for NADH oxidation is kinetically limited, rather than mass transfer limited like the $Ru(NH_3)^{3+}$. More importantly, the ideal outer sphere redox couple $Ru(NH_3)^{3+}$ displays a nearly flat baseline with an $E_{1/2}$ at -0.2 (V vs. SCE), with a rapid attainment of a mass transfer controlled plateau. NADH, on the other hand, displays a sloping background before the E_p, close to 0.6 (V vs. SCE), and does not attain a limiting current. Furthermore, the reduction of $Ru(NH_3)^{3+}$ is a one electron reaction while the oxidation of NADH is a 2-electron oxidation, even though the current magnitude for both reactions is similar (diffusion will be slightly slower for the larger NADH molecule). Qualitatively, the data suggests that NADH oxidation is kinetically limited rather than mass transport limited.

5.3.2 The Potential Dependent Observed Electron Transfer Rate Constant (k_{obs})

Our prior report identified the E_p for the oxidation of NADH at N-CNTs (7.4 at.% N) and GC at -0.32 and 0.22 (V vs. Hg/Hg_2SO_4), respectively, in 0.1 M SPB (pH 7.0) at a scan rate of 10 mV/s in the presence of 2.0 mM NADH.[149] In order to further quantify the electron transfer kinetics of the NADH reaction, five potentials where chosen to perform Koutecky-Levich rotating disk electrode (RDE) analysis, which is capable of differentiating a kinetically limited process from a mass transport limited process. The mass transfer limiting current at a RDE is defined by the Levich equation, shown below[113]:

$$i_{mt} = 0.62nFAD^{2/3}\omega^{1/2}\nu^{-1/6}C \qquad (5.3)$$

where i_{mt} is the mass transfer limiting current, *n* is the number of electrons transferred (*n* = 2), F is Faraday's constant (96,485 C/mol), A is the electrode area, ω is the angular velocity ($\omega = 2\pi f$; f is frequency), ν is the kinematic viscosity of the solvent (water in this case, 0.01 cm^2/s), C is the concentration of NADH, and D is the diffusion coefficient. The diffusion coefficient was selected as 3.0×10^{-6} cm^2/s based on literature references.[47,189,214,225,226] The measured current (i) may not align with i_{mt} if the reaction is limited by the electron transfer kinetics rather than mass transport. In this case, a plot of i vs. $\omega^{1/2}$ should yield an asymptote approaching the kinetically limiting current i_K. The kinetically limiting current is also a function of potential (E), shown below[113]:

$$i_K = nFAk_{obs}(E)C \tag{5.4}$$

where i_K is the kinetically limited current, k_{obs} is the observed electron transfer rate constant (a function of E) and F, A, *n,* and C are the same as mentioned above. A plot of 1/i vs $1/\omega^{1/2}$ allows one to determine the asymptote i_K, which will be the y-intercept (a mass transport limited plot will theoretically intercept the y-axis at 0). The measured current (i) can be expressed from the Koutecky-Levich equation shown below:

$$1/i = 1/i_K + 1/i_{mt} \tag{5.5}$$

where the measured current (i) is a function of both the mass transport limited current (i_{mt}) and the kinetically limited current (i_K). Likewise, one can use nonlinear fitting to approximate the asymptote directly from the plot of i vs. $\omega^{1/2}$. The nonlinear method will avoid errors introduced from linearization, which will be discussed later. Practically, one must be able to rotate at high rates in order to observe the asymptotic behavior for relatively fast k_{obs}, setting an upper limit on our measuring capabilities. Nonetheless, we

used RDE amperometry to ascertain the k_{obs} as a function of potential and concentration with both a conventional GC electrode, or an electrocatalytic material, N-CNTs. Figure 5.2A presents CV of a GC and a N-CNT electrode in the presence of 2.0 mM NADH, and includes the potentials chosen to perform RDE analysis. Figure 5.2C and B present representative chronoamperograms of the RDE analysis for a series of N-CNT electrodes at 1.0 mM NADH (5.2B) and a series of GC electrodes at 0.5 mM NADH (5.2C). According to the CV in Figure 5.2A, the rate constant for N-CNTs should by relatively fast, since they are all at or past the observed E_p. At GC, the selected potentials span the entire range. The negative potentials are before the reaction begins, 0.10 V is near the onset of E_p, and the most positive two potentials are at and beyond the E_p. Since the overpotential for NADH oxidation is much lower on N-CNTs than on GC, we expect the rate constant to be faster at all potentials for the N-CNTs. The initial spike at 300 s in Figure 5.2B and 5.2C is where the NADH was introduced into solution at the lowest rotation rate of 250 rpm. Subsequent current steps are due to an increase in the rotation rate. The spike was used to minimize NADH contact prior to obtaining a measurement, since NADH is known to foul the electrode surface.[160,164,211] Table 5.1 and Table 5.2 presents the calculated k_{obs} values as a function of potential and concentration for GC and N-CNT electrodes, repectively, using nonlinear fitting to determine i_K (and hence, k_{obs}). Table 5.3 and 5.4 present the k_{obs} values for GC and N-CNT electrodes, respectively, determined from the traditional Koutecky-Levich linear analysis. It is clear from the CVs in Figure 5.2 and the k_{obs} values in Table 5.1 and 5.2 that N-CNTs catalyze the oxidation of NADH at much lower potentials. The oxidation reaction is not observed at GC below 0.10 V, while above 0.10 V the reaction at N-CNTs is too fast to measure using the RDE technique (highest rotation rate of 5000 rpm). The k_{obs} values show a concurrent increase

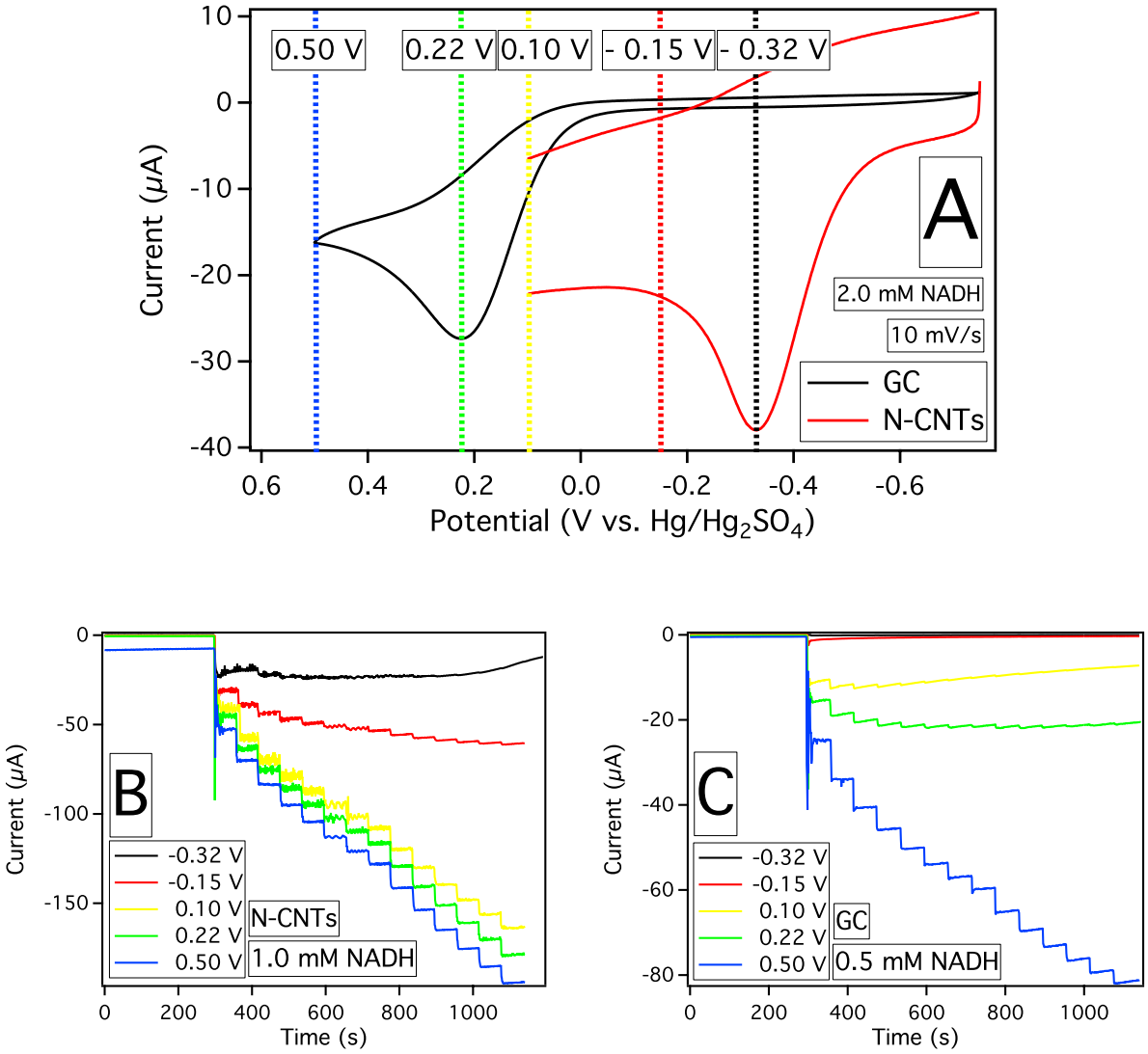

Figure 5.2. (A) CVs of a GC or a N-CNT electrode in the presence of 2.0 mM NADH in 0.1 M SPB (colored dashed lines mark the selected potentials for RDE measurements). Chronoamperograms for a series of N-CNT electrodes in the presence of (B) 1.0 mM NADH or a series of GC electrodes in the presence of (C) 0.5 mM NADH as the rotation rate is increased (from 250 rpm to 5000 rpm).

Table 5.1. k_{obs} (cm/s) values as a function of potential and concentration at GC (nonlinear analysis)

Potential (V vs. Hg/Hg_2SO_4)	-0.32	-0.15	0.10	0.22	0.50
0.1 mM NADH	No reaction	No reaction	0.0048	0.0051	0.038
0.5 mM NADH	No reaction	No reaction	0.0010	0.0019	0.016
1.0 mM NADH	No reaction	No reaction	0.0003	0.0018	0.0059

Table 5.2. k_{obs} (cm/s) values as a function of potential and concentration at N-CNTs (nonlinear analysis)

Potential (V vs. Hg/Hg_2SO_4)	-0.32	-0.15	0.10	0.22	0.50
0.1 mM NADH	0.0028	0.0089	NM	NM	NM
0.5 mM NADH	0.0013	0.0041	NM	NM	NM
1.0 mM NADH	0.0009	0.0027	NM	NM	NM

*NM = Not Measured. This indicates that for the rotation rates used here, an asymptote was not observed and the reaction is apparently mass transfer limited.

Table 5.3. k_{obs} (cm/s) values as a function of potential and concentration at GC electrodes (linear analysis)

Potential (V vs. Hg/Hg_2SO_4)	-0.32	-0.15	0.10	0.22	0.50
0.1 mM NADH	No reaction	No reaction	0.0007	0.0016	0.038
0.5 mM NADH	No reaction	No reaction	0.0009	0.0017	0.017
1.0 mM NADH	No reaction	No reaction	0.0003	0.0017	0.0060

Table 5.4. k_{obs} (cm/s) values as a function of potential and concentration at N-CNT electrodes (linear analysis)

Potential (V vs. Hg/Hg_2SO_4)	-0.32	-0.15	0.10	0.22	0.50
0.1 mM NADH	0.0027	0.0093	NM	NM	NM
0.5 mM NADH	0.0013	0.0041	NM	NM	NM
1.0 mM NADH	0.0008	0.0026	NM	NM	NM

*NM = Not Measured. This indicates that for the rotation rates used here, an asymptote was not observed and the reaction is apparently mass transfer limited.

with potential at any given concentration, but a decreasing k_{obs} with increasing NADH concentration at the same potential. The inverse relationship of the rate constant to NADH concentration at constant potential has also been observed at MWCNT electrodes modified with 2,3,5,6-tetrachloro-1,4-benzoquinone[172], poly-xanthurenic acid[214], and 3,5-dinitrobenzoic acid[227], or SWCNT electrodes modified with Nile Blue[228] or poly(phenosafranin)[229]. The aforementioned electrodes all used mediators, often called chemically modified or mediator modified electrodes. The inverse relationship of the rate constant to the NADH concentration at these mediator modified electrodes has been characterized by Gorton, who identifies the rate limiting step as a charge transfer complex between NADH and the surface bound mediator.[164,211] The complex essentially mimics the Michaelis-Menten kinetics of an enzyme, where the substrate-bound enzyme limits the enzymatic turnover. Although there is not an observable surface wave indicating an electroactive mediator at our N-CNTs, they still may include a mediating surface site, since nitrogen incorporated into an all carbon lattice significantly influences the electron distribution and can also introduce nitrogen functional groups.[52,57,59,197] The data presented here precludes an accurate analysis of the type characterized by Gorton, but it should be further investigated, taking note that unmodified GC also displays a similar effect.

Response currents from the introduction of NADH at a constant rotation rate can also be used to show the potential dependence of the NADH oxidation current. Figure 5.3 presents a series of chronoamperograms for N-CNT electrodes obtained at the five selected potentials as 0.5 mM NADH was introduced into solution. Table 5.5 and 5.6 present the current as a percent of the theoretical current, calculated from eq. 5.3, using

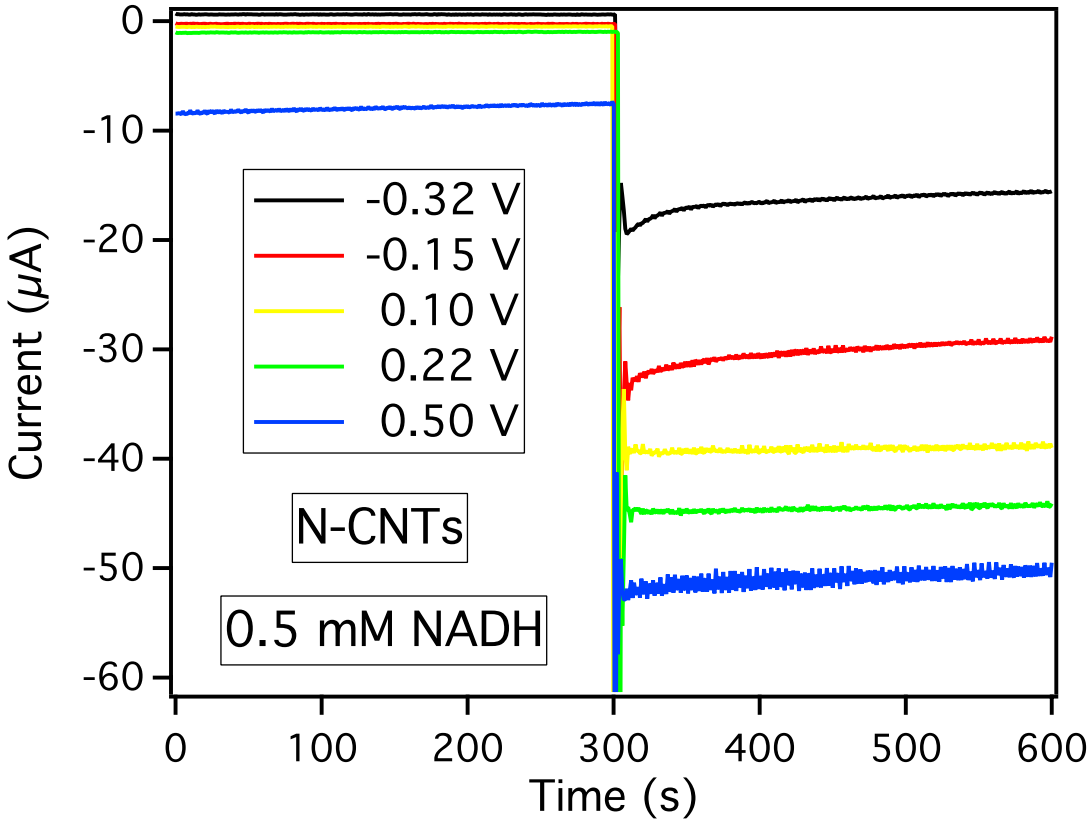

Figure 5.3. Chronoamperograms of the oxidation of (A) 0.5 mM NADH at N-CNT electrodes and (B) 1.0 mM NADH at GC electrodes it they are rotated at 1000 rpm (0.1 M SPB, pH 7.0).

Table 5.5. Percent of theoretical current as a function of potential and concentration at GC

Potential (V vs. Hg/Hg_2SO_4)	-0.32	-0.15	0.10	0.22	0.50
0.1 mM NADH	0.23 %	1.7 %	37 %	78 %	86 %
0.5 mM NADH	0.05 %	0.43 %	24 %	63 %	86 %
1.0 mM NADH	0.05 %	0.06 %	44 %	75 %	84 %

Table 5.6. Percent of theoretical current as a function of potential and concentration at N-CNTs

Potential (V vs. Hg/Hg_2SO_4)	-0.32	-0.15	0.10	0.22	0.50
0.1 mM NADH	61 %	65 %	75 %	83 %	84 %
0.5 mM NADH	35 %	60 %	73 %	81 %	83 %
1.0 mM NADH	31 %	49 %	69 %	75 %	79 %

the geometric area of the GC electrode for both the GC and N-CNT electrodes (0.196 cm^2), since solution based electroactive species interact with the same effective area on both electrodes.[230] The current response for GC is not as monotonic as the N-CNTs, which display an increase in the current response concurrent with potential and inversely related to NADH concentration. For GC, there is almost no current response before 0.10 V,expected since it is before the onset of NADH oxidation at GC. Both GC and N-CNTs tend towards a limit of about 85% at high potentials, verifying that the same effective surface area is utilized by NADH at both electrodes. The limit also suggests that either the initial surface fouling at higher potentials is similar, and/or the diffusion coefficient is underestimated. It should be noted that the anodic background current at 0.50 V on N-CNTs is significantly higher than the other potentials, or the GC electrode. The background current at both GC and N-CNT electrodes increases slightly (more anodic) concomitant with potential, shown in Figure 5.4 for the smaller 0.1 mM NADH current responses. The jump at 0.50 V and subsequent decay suggests that at this potential (and beyond) the carbon is being oxidized. This phenomenon will have a significant impact when enzymes are adsorbed on the N-CNT surface, where the oxidizing carbon will cause the adsorbed enzyme to disengage from the electrode surface.

5.3.3 Spectrophotometric Enzyme Kinetics

The standard method to measure the activity of glucose dehydrogenase, and many other NAD^+-dependent dehydrogenase enzymes, is to monitor the appearance of NADH from the enzymatic turnover of NAD^+ and glucose (or an appropriate substrate for other NAD^+-dependent dehydrogenase enzymes). NADH absorbs at 340 nm, due to the pyridinic ring in nicotinamide, with an molar extinction coefficient of about 6200 $M^{-1} cm^{-1}$.[224] For enzymes purchased from a reputable company, and usually for the sake of time,

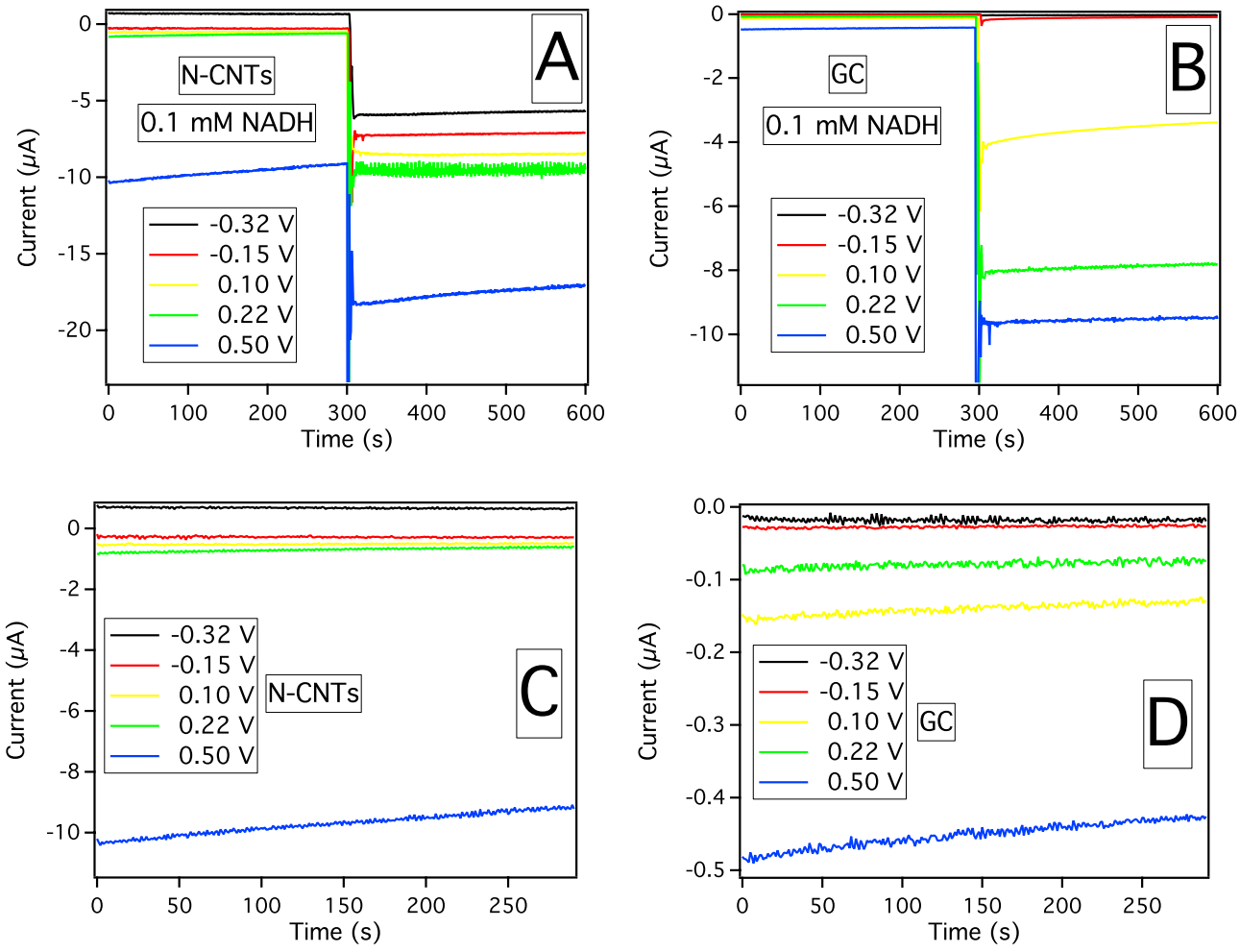

Figure 5.4. Chronoamperograms of (A) N-CNT electrodes or (B) GC electrodes rotating at 1000 rpm as 0.1 mM NADH is introduced into the solution at 300 s. Chronoamperograms of the background current for (C) N-CNT electrodes or (D) GC electrodes before NADH injection (0.1 M SPB, pH 7.0).

only one very high substrate concentration is performed at a high temperature (37°C) and optimal pH to obtain the unit activity which is defined by the company. In order to obtain a more comprehensive kinetic analysis, a series of concentrations must be characterized, where the initial enzyme activity increases with the concentration of substrate until it reaches an asymptote, where the rate is nearly independent of concentration. Figure 5.5(A-E) presents the series of spectrophotometric analyses for GDH in 0.1 M SPB with 2.0 mM NAD^+. The kinetic parameters K_M and V_{max} can be calculated from the y-intercept and the slope of the Lineweaver Burk plot (shown in Figure 5.5D) or by nonlinear fitting (shown in Figure 5.5E). Due to linearization errors from the double reciprocal plot, where the low concentration rates in the bottom left corner of Figure 5.5C become the most influential points in the top right corner of Figure 5.5D, we chose to present the data from the nonlinear analysis shown in Figure 5.5E. Figure 5.6 presents the UV-visible spectra of the increasing peak at 340 nm as a function of glucose concentration. Table 5.7 presents the Lineweaver-Burk linear analysis of K_M and V_{max} along with a modified data set to minimize errors from linearization. Note that even after the data was modified to eliminate linearization errors, the standard deviation for both K_M and V_{max} are smaller for the nonlinear analysis, compared to the linear analysis. The nonlinear values were determined to be 2.9 ± 0.3 mM for K_M and 4.4 ± 0.8 x 10^{-7} M/s for V_{max}. To ensure the 2.0 mM NAD^+ concentration did not limit the enzymatic reaction, analysis was also performed in 10.0 mM NAD^+. The kinetic parameters were not statistically differentiable, and actually displayed a slightly smaller K_M and V_{max}. Given that 8 nM of GDH was present in solution (based on weight) the k_{cat} can be calculated ($k_{cat} = V_{max}/[GDH]$) at 55 s^{-1}. Over a 74 day period, K_M and V_{max} were

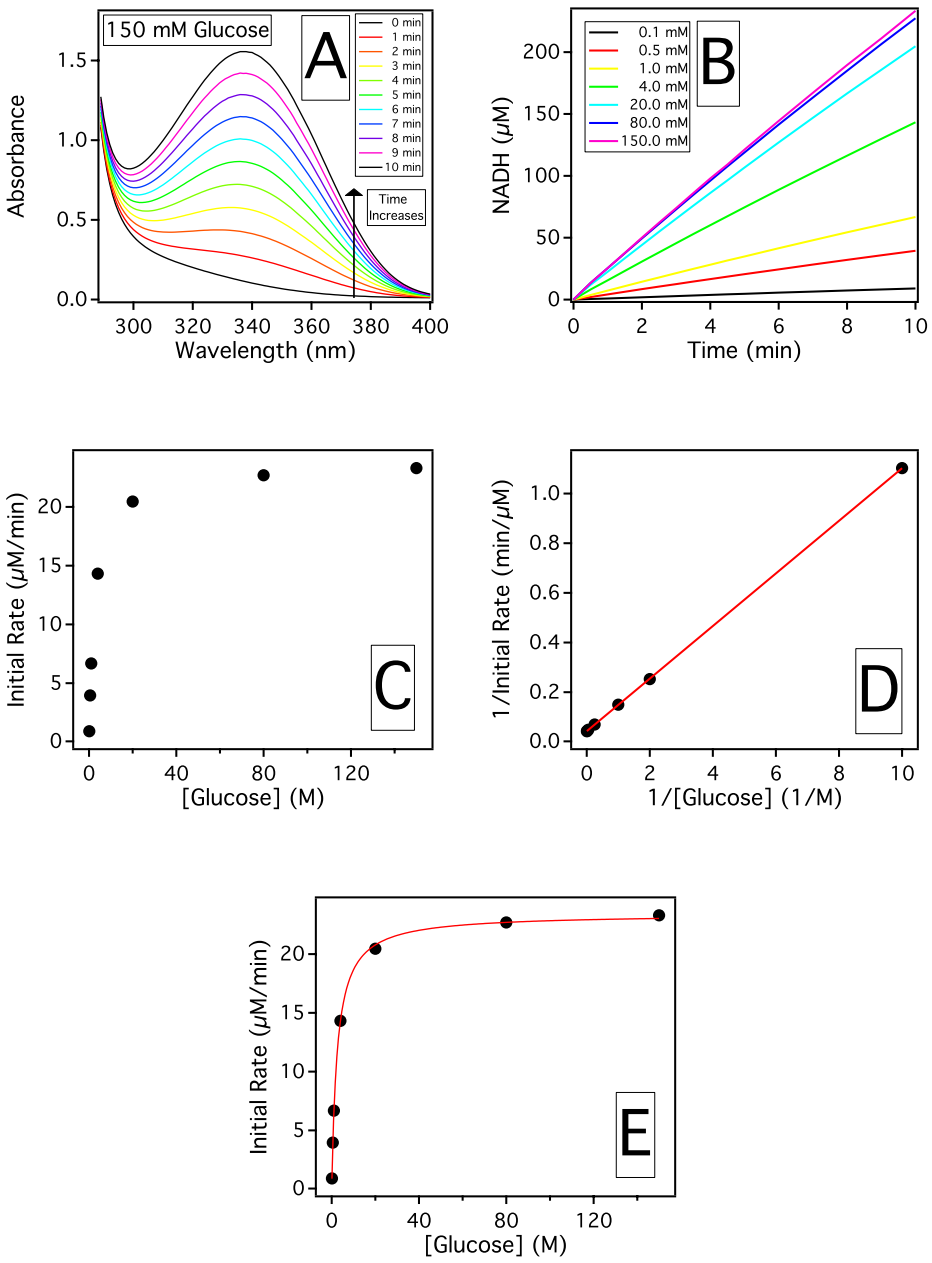

Figure 5.5. (A) UV-vis spectra displaying the increase in absorbance as a function of time and concentration of glucose. (B) Increase in NADH concentration as a function glucose concentration displaying linearity in the 10 min timeframe. (C) Plot of glucose concentration versus initial rate (first 10 min). (D) Lineweaver-Burk plot of the inverse glucose concentration versus the inverse initial rate. (E) Nonlinear fitting of the substrate saturation curve.

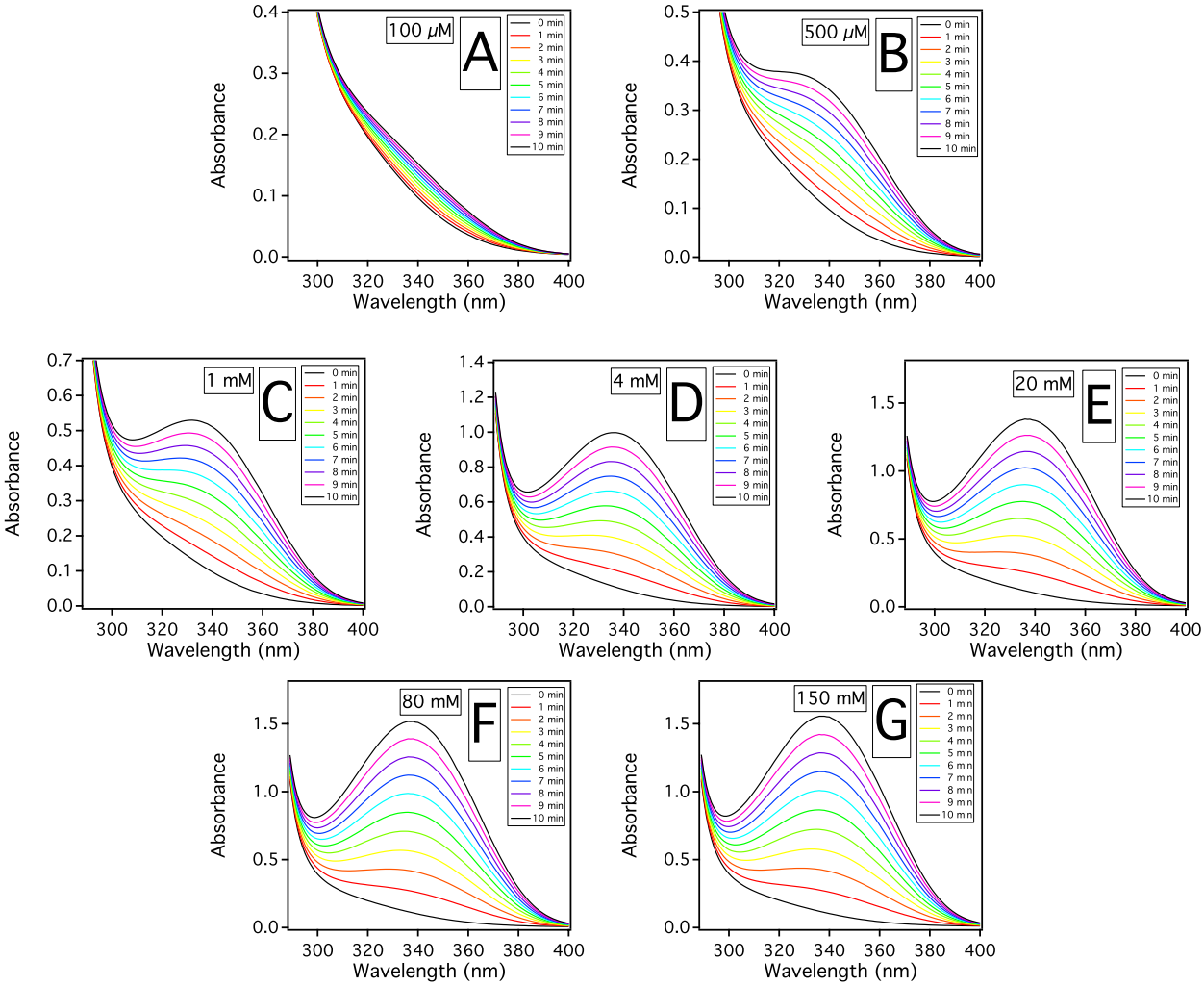

Figure 5.6. UV-visible spectra displaying the increase in absorbance at 340 nm over 10 minutes as a function of glucose concentration. (A = 100 μM, B = 500 μM, C = 1 mM, D = 4 mM, E = 20 mM, F = 80 mM, G = 150 mM; GDH 8 nM, 2.0 mM NAD^+, 0.1 M SPB, pH 7.0)

Table 5.7. Spectrophotometrically determined K_M and V_{max} calculated by the Lineweaver-Burk linear analysis using the full data set, or a modified data set to minimize linearization errors.

Full Data Set K_M (mM)	Full Data Set V_{max} ($1x10^{-7}$ M/s)	Modified Data Set K_M (mM)	Modified Data Set V_{max} ($1x10^{-7}$ M/s)
4 ± 3	6 ± 3	2.9 ± 0.8	5 ± 1

not seen to appreciably change, indicating that enzyme was quite stable in solution. Table 5.8 presents a chart of the K_M and V_{max} over the 74 day period.

5.3.4 Electrochemical Enzyme Kinetics

Electrochemically measured enzyme kinetics are actually quite a bit easier to perform than the standard spectrophotometric analysis. The enzymatic rate for each glucose concentration is simply the steady-state current of the bioelectrode at each glucose concentration. The entire saturation curve can be obtained in a single experiment, rather than multiple experiments at different substrate concentrations. The measured signal, however, is now created from the electrochemical oxidation of the enzymatically generated NADH at the N-CNT surface. This is a current density (A/cm^2), rather than a concentration measurement (M), since the measured current is coming from an area, not a volume. Herein lies the fundamental problem of matching up enzyme kinetics obtained electrochemically or spectrophotometrically, since the V_{max} will be in different units. The K_M values can be compared directly, since they are both in identical units (M).[231] The k_{cat} can be calculated if the concentration of enzyme is known or the surface coverage of the enzyme on the electrode is known. If adsorbed GDH and free GDH operate identically (have the same k_{cat}) then k_{cat} determined spectrophotometrically can be used to determine the amount of enzyme on the electrode surface. Enzyme kinetics were measured electrochemically by allowing GDH to adsorb onto the surface of N-CNTs, and subsequently performing substrate saturation curves by amperometric detection. A prior report showed that allowing GDH to adsorb onto the N-CNT surface for 20 min in a 20 μM GDH solution (0.1 M SPB, pH 7.0) gave the bioelectrode the highest current sensitivity ($A\ M^{-1}\ cm^{-2}$) to glucose.[149] Thus, N-CNT electrodes were allowed to adsorb GDH from a 20 μM solution for 20 min. Figure 5.7 presents

Table 5.8. K_M and V_{max} spectrophotometrically determined over 74 days (Nonlinear Analysis)

Day	K_M (mM)	V_{max} ($1x10^{-7}$ M/s)
2	3.4	6.9
7	2.6	4.5
14	2.9	4.4
21	2.8	4.4
29	3.0	4.4
38	3.2	4.4
42	2.4	3.7
50	2.7	4.0
74	2.6	3.8

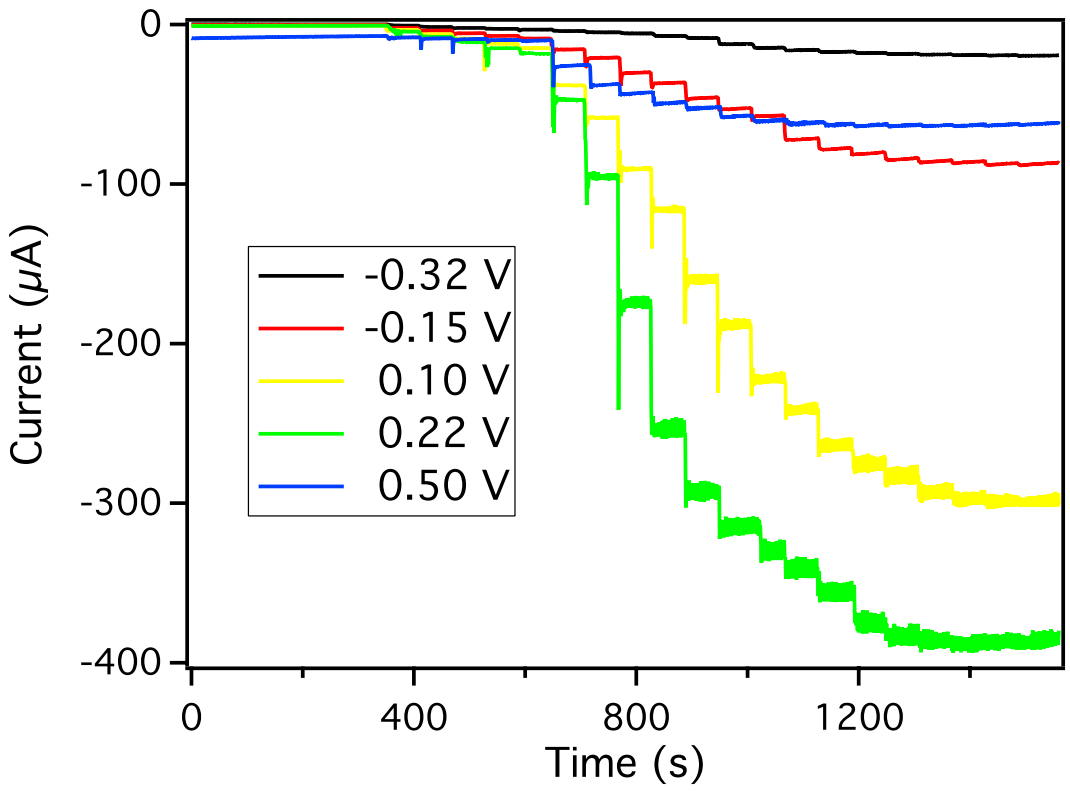

Figure 5.7. Chronoamperograms of the GDH loaded N-CNT electrodes at increasing potentials as glucose is introduced into solution (0.1 M SPB, pH 7.0, 1000 rpm)

chronoamperograms of the electrochemically measured enzyme substrate saturation curves at the five selected potentials for the GDH loaded N-CNT electrodes. Table 5.9 presents the electrochemically determined K_M^{app} and V_{max} (by nonlinear analysis) as well as the bioelectrode's sensitivity to glucose at each poised potential. Figure 5.8 displays representative plots of the Lineaweaver-Burk linear fitting versus the nonlinear fitting for each of the selected potentials. The residuals of each fit, included in Figure 5.8, show that the majority of the error in the linear fit comes from the initial points of the original (non-linearized) data whereas the error in the nonlinear fit are more evenly distributed. Table 5.10 presents K_M^{app} and V_{max} determined from the Lineweaver-Burk linear analysis from the full data set, or a modified data set to minimize linearization errors. As mentioned before, the enzyme should be unaffected by the electrode potential, and thus, only controlled by the concentration of substrate in solution. Figure 5.7 and Table 5.9 clearly show an increase in both K_M^{app} and V_{max} concurrent with increasing potential until 0.50, which breaks from the increasing trend. Since the amount of enzyme on every electrode is similar, and the enzyme should not be influenced by the potential, the increasing kinetic parameters indicate that the electrochemical reaction of NADH, even at an electrocatalyst like N-CNTs, is the rate limiting reaction. Thus, electrochemically measured enzyme kinetics obtained from the oxidation of NADH created from the enzymatic turnover of NAD^+-dependent dehydrogenases are not independent of potential. It is simply circumstance that the K_M obtained spectrophotometrically and the electrochemical K_M^{app} at -0.32 V are identical.

In order to determine the root cause of the discrepancy at 0.50V, which was not observed to break trend during the RDE analysis, electrochemical enzyme substrate saturation curves were performed at 0.22 V, but after the normal 20 min of GDH

Table 5.9. K_M^{app} and V_{max} and the sensitivity of the GDH electrode to glucose

Potential (V vs. Hg/Hg_2SO_4)	Sensitivity ($A\ M^{-1}\ cm^{-2}$)	K_M^{app} (mM)	V_{max} (1×10^{-10} mol/s)
-0.32	0.029 ± 0.005	3.0 ± 0.2	1.0 ± 0.2
-0.15	0.074 ± 0.007	5.1 ± 0.7	4 ± 2
0.10	0.13 ± 0.01	12.6 ± 0.7	18 ± 1
0.22	0.14 ± 0.02	15.0 ± 0.9	22 ± 2
0.50	0.018 ± 0.009	20 ± 6	3 ± 1

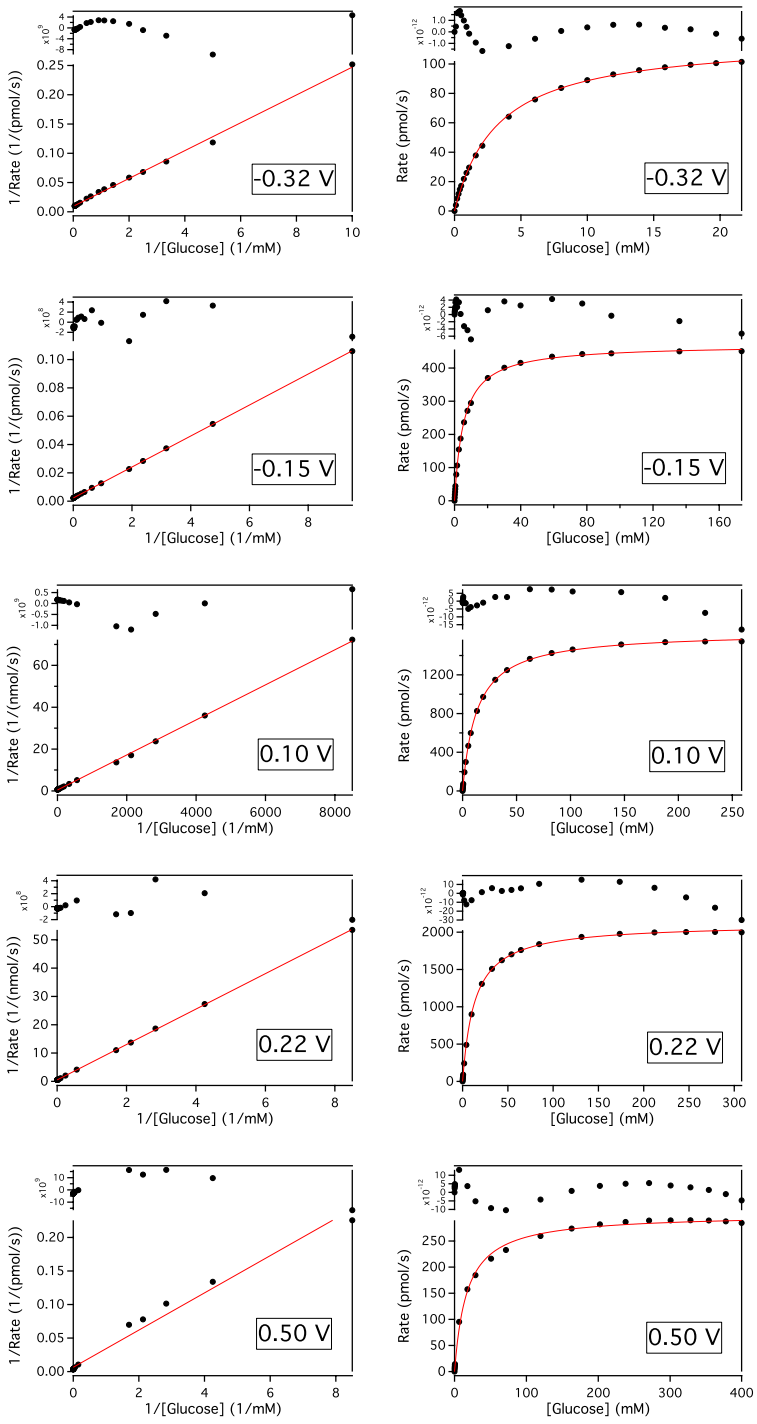

Figure 5.8. Lineweaver-Burk linear fitting compared to the nonlinear fitting for the electrochemical enzyme saturation curves (-0.32 V, -0.15 V, 0.10 V, 0.22 V, and 0.50 V vs. Hg/Hg_2SO_4; residuals included at the top of each fit).

Table 5.10. Lineweaver-Burk linear analysis of the K_M^{app} and V_{max} using the full data set, or a modified data set to minimize linearization errors.

Potential (V vs. Hg/Hg_2SO_4)	Full Data Set K_M^{app} (mM)	Full Data Set V_{max} (1×10^{-10} mol/s)	Modified Data Set K_M^{app} (mM)	Modified Data Set V_{max} (1×10^{-10} mol/s)
-0.32	2.2 ± 0.5	0.9 ± 0.2	2.3 ± 0.4	0.9 ± 0.2
-0.15	4.3 ± 0.8	3.7 ± 0.6	4.3 ± 0.8	3.7 ± 0.6
0.10	14 ± 5	19 ± 6	13 ± 3	18 ± 3
0.22	63 ± 120	94 ± 181	15 ± 2	23 ± 3
0.50	5 ± 2	1.5 ± 0.9	16 ± 6	3 ± 1

adsorption, the electrodes were then pretreated at 0.22 or 0.50 for 30 min (electrodes are under potential for 26 min during the normal electrochemical measurement). Additionally, GDH was only allowed to adsorb for 3 min or 30 s on two other N-CNT electrodes, as a comparison. Figure 5.9 presents the results of performing the substrate saturation curves on all four electrodes. The K_M^{app} for the various adsorption times (30 s, 3 min, and 20 min pretreated at 0.22V) were within the standard deviation of the normal K_M^{app} for 20 min of adsorption and analysis at 0.22 V. This data indicates that at a single potential (0.22 V), the K_M^{app} is independent of the amount of enzyme adsorbed on the surface, expected for a Michalis-Menten type behavior. Figure 5.9 clearly shows that the amount of enzyme remaining on the 0.50 V pretreated electrode has significantly decreased, less than the electrode with only 30 s of adsorption. The background anodic signal at 0.50 V is significantly higher, indicating that something is getting oxidized. Since the high anodic background current is observed without the presence of redox active species, the most likely source of the oxidation current is from the N-CNTs. This observation is corroborated by the low V_{max}, suggesting that GDH is disengaging from the surface as it is being oxidized.

5.4 CONCLUSION

The spontaneous adsorption of GDH onto the N-CNT surface provides a simple technique to create bioelectrodes without binders, dispersing agents, immobilizing matrices (polymers, biopolymers, hydrogel, etc.), or the inclusion of redox mediators. The elementary bioelectrodes allow for an unambiguous assessment of the intrinsic reactivity and/or limitations of the electrode/biomolecule system. In regards to NAD^+-dependent dehydrogenases, N-CNTs have been shown to be effective electrocatalysts for

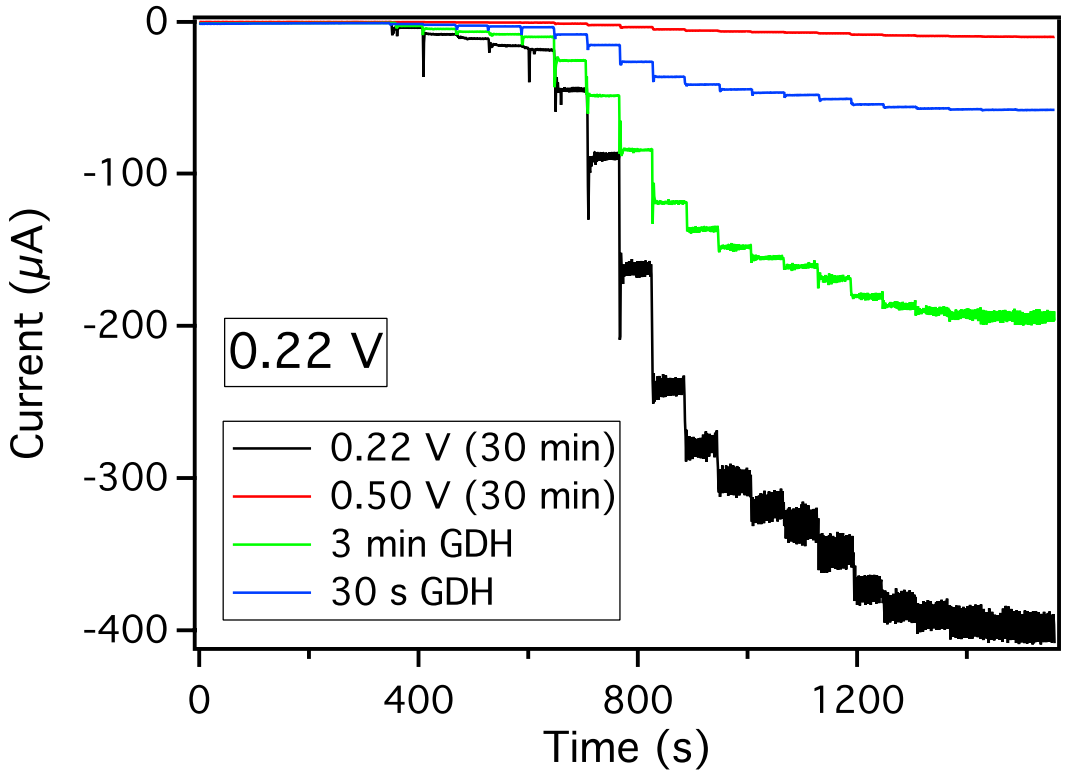

Figure 5.9. Chronoamperograms of the substrate saturation curves obtained at 0.22 V for the GDH loaded N-CNT electrodes pretreated at 0.50 V and 0.22 V, or allowed to adsorb GDH for only 3 min or 30 s (1000 rpm, 0.1 M SPB, pH 7.0)

NADH oxidation, but the observed rate constant is under potential control. Thus, electrochemically measured enzyme kinetics, which obtain their measurement by the oxidation of NADH, are not reliable indicators of the enzymatic behavior. Albeit, at a single potential, the measured enzyme kinetics can be used as a relative indicator, the obtained kinetic parameters are unique to each potential and are not directly comparable to the enzyme free in solution.

References

(1) Clark, L. C.; Lyons, C. *Ann. N.Y. Acad. Sci.* **1962**, *102*, 29–45.
(2) Salimi, A.; Miranzadeh, L.; Hallaj, R.; Mamkhezri, H. *Electroanalysis* **2008**, *20*, 1760–1768.
(3) Wang, J.; Musameh, M.; Lin, Y. *J. Am. Chem. Soc.* **2003**, *125*, 2408–2409.
(4) Lyon, J. L.; Stevenson, K. J. *Anal. Chem.* **2006**, *78*, 8518–8525.
(5) Wang, J. *Chem. Rev.* **2008**, *108*, 814–825.
(6) Gamburzev, S.; Atanassov, P.; Ghindilis, A. L.; Wilkins, E. *Sens. Actuators, B* **1997**, *43*, 70–77.
(7) Mulchandani, A.; Wang, C. *Electroanalysis* **1996**, *8*, 414–419.
(8) Ruzgas, T.; Csöregi, E.; Emnéus, J.; Gorton, L.; Marko-Varga, G. *Anal. Chim. Acta* **1996**, *330*, 123–138.
(9) Spohn, U.; Narasaiah, D.; Gorton, L.; Pfeiffer, D. *Anal. Chim. Acta* **1996**, *319*, 79–90.
(10) Tatsuma, T.; Okawa, Y.; Watanabe, T. *Anal. Chem.* **1989**, *61*, 2352–2355.
(11) Kulys, J.; Schmid, R. D. *Bioelectrochem. Bioenerg.* **1990**, *299*, 305–311.
(12) Gorton, L.; Jonsson-Pettersson, G.; Csoregi, E.; Johansson, K.; Dominguez, E.; Marko-Varga, G. *Analyst* **1992**, *117*, 1235–1241.
(13) Cass, A.; Davis, G.; Francis, G. *Anal. Chem.* **1984**, *56*, 667–671.
(14) Ikeda, T.; Katasho, I.; Kamei, M.; Senda, M. *Agric. Biol. Chem.* **1984**, *48*, 1969–1976.
(15) Jönsson, G.; Gorton, L.; Pettersson, L. *Electroanalysis* **1989**, *1*, 49–55.
(16) Kulys, J.; Hansen, H. E.; Buch-Rasmussen, T.; Wang, J.; Ozsoz, M. *Anal. Chim. Acta* **1994**, *288*, 193–196.
(17) Kulys, J.; Wang, L.; Maksimoviene, A. *Anal. Chim. Acta* **1993**, *274*, 53–58.
(18) Palleschi, G.; Turner, A. P. F. *Anal. Chim. Acta* **1990**, *234*, 459–463.
(19) Ghindilis, A. L.; Atanassov, P.; Wilkins, E. *Electroanalysis* **1997**, *9*, 661–674.
(20) Gorton, L.; Lindgren, a.; Larsson, T.; Munteanu, F. D.; Ruzgas, T.; Gazaryan, I. *Anal. Chim. Acta* **1999**, *400*, 91–108.
(21) Yaropolov, A. . I.; Tarasevich, M. R.; Varfolomeev, S. D. *Bioelectrochem. Bioenerg.* **1978**, *5*, 18–24.
(22) Schuhmann, W. *Rev. Mol. Biotechnol.* **2002**, *82*, 425–441.
(23) Heller, A. *Acc. Chem. Res.* **1990**, *23*, 128–134.
(24) Degani, Y.; Heller, A. *J. Am. Chem. Soc.* **1989**, *111*, 2357–2358.
(25) Gregg, B. a; Heller, a. *Anal. Chem.* **1990**, *62*, 258–263.
(26) Heller, A. *J. Phys. Chem.* **1992**, *96*, 3579–3587.
(27) Pishko, M. V; Michael, a C.; Heller, a. *Anal. Chem.* **1991**, *63*, 2268–2272.
(28) Cosnier, S. *Biosens. Bioelectron.* **1999**, *14*, 443–456.
(29) Ramanavicius, a; Habermuller, K.; Csöregi, E.; Laurinavicius, V.; Schuhmann, W. *Anal. Chem.* **1999**, *71*, 3581–3586.
(30) Schuhmann, W. *Biosens. Bioelectron.* **1995**, *10*, 181–193.
(31) Schuhmann, W. *Microchim. Acta* **1995**, *29*.
(32) Foulds, N. C.; Lowe, C. R. *Anal. Chem.* **1988**, *60*, 2473–2478.
(33) Raitman, O. a; Katz, E.; Bückmann, A. F.; Willner, I. *J. Am. Chem. Soc.* **2002**, *124*, 6487–6496.
(34) Zayats, M.; Willner, B.; Willner, I. *Electroanalysis* **2008**, *20*, 583–601.
(35) Lin, Y.; Yantasee, W.; Wang, J. *Front. Biosci.* **2005**, *2*, 492–505.
(36) Cai, C.; Chen, J. *Anal. Biochem.* **2004**, *332*, 75–83.
(37) Deng, S.; Jian, G.; Lei, J.; Hu, Z.; Ju, H. *Biosens. Bioelectron.* **2009**, *25*, 373–377.
(38) Gooding, J. J.; Wibowo, R.; Liu, J.; Yang, W.; Losic, D.; Orbons, S.; Mearns, F. J.; Shapter, J. G.; Hibbert, D. B. *J. Am. Chem. Soc.* **2003**, *125*, 9006–9007.

(39) Yu, X.; Chattopadhyay, D.; Galeska, I.; Papadimitrakopoulos, F.; Rusling, J. F. *Electrochem. Commun.* **2003**, *5*, 408–411.
(40) Vaze, A.; Hussain, N.; Tang, C.; Leech, D.; Rusling, J. *Electrochem. Commun.* **2009**, *11*, 2004–2007.
(41) Periasamy, A. P.; Chang, Y.-J.; Chen, S.-M. *Bioelectrochemistry* **2011**, *80*, 114–120.
(42) Liu, J.; Chou, A.; Rahmat, W.; Paddon-Row, M. N.; Gooding, J. J. *Electroanalysis* **2005**, *17*, 38–46.
(43) Guiseppi-Elie, A.; Lei, C.; Baughman, R. H. *Nanotechnol.* **2002**, *13*, 559 – 64.
(44) Wang, J.; Deo, R. P.; Poulin, P.; Mangey, M. *J. Am. Chem. Soc.* **2003**, *125*, 14706–14707.
(45) Wang, J.; Musameh, M. *Anal. Chem.* **2003**, *75*, 2075–2079.
(46) Musameh, M.; Wang, J.; Merkoci, A.; Lin, Y. *Electrochem. Commun.* **2002**, *4*, 743–746.
(47) Banks, C. E.; Compton, R. G. *Analyst* **2005**, *130*, 1232–1239.
(48) Banks, C. E.; Davies, T. J.; Wildgoose, G. G.; Compton, R. G. *Chem. Commun.* **2005**, 829–841.
(49) Biddinger, E. J.; Ozkan, U. S. *J. Phys. Chem. C* **2010**, *114*, 15306–15314.
(50) Landis, E. C.; Klein, K. L.; Liao, A.; Pop, E.; Hensley, D. K.; Melechko, A. V.; Hamers, R. J. *Chem. Mater.* **2010**, *22*, 2357–2366.
(51) Rice, R. J.; McCreery, R. L. *Anal. Chem.* **1989**, *61*, 1637–1641.
(52) Maldonado, S.; Morin, S.; Stevenson, K. J. *Carbon N. Y.* **2006**, *44*, 1429–1437.
(53) Tang, Y.; Allen, B. L.; Kauffman, D. R.; Star, A. *J. Am. Chem. Soc.* **2009**, *131*, 13200–13201.
(54) Xu, X.; Jiang, S.; Hu, Z.; Liu, S. *ACS Nano* **2010**, *4*, 4292–4298.
(55) Lyon, J. L.; Stevenson, K. J. *Langmuir* **2007**, *23*, 11311–11318.
(56) Lyon, J.; Stevenson, K. *Electrochim. Acta* **2008**, *53*, 6714–6721.
(57) Maldonado, S.; Morin, S.; Stevenson, K. J. *Analyst* **2006**, *131*, 262–267.
(58) Maldonado, S.; Stevenson, K. J. *J. Phys. Chem. B* **2004**, *108*, 11375–11383.
(59) Wiggins-Camacho, J. D.; Stevenson, K. J. *J. Phys. Chem. C* **2009**, *113*, 19082–19090.
(60) Maldonado, S.; Stevenson, K. J. *J. Phys. Chem. B* **2005**, *109*, 4707–4716.
(61) Wiggins-Camacho, J. D.; Stevenson, K. J. *J. Phys. Chem. C* **2011**, *115*, 20002–20010.
(62) Lyon, J. L.; Stevenson, K. J. *ECS Trans.* **2009**, *16*, 1–12.
(63) Schrenk, M.; Villigram, R. *J. Membr. Sci.* **2002**, *205*, 3–10.
(64) Thomas, T. J.; Ponnusamy, K. E.; Chang, N. M.; Galmore, K.; Minteer, S. D. *J. Membr. …* **2003**, *213*, 55–66.
(65) Yu, X.; Sotzing, G. A.; Papadimitrakopoulos, F.; Rusling, J. F. *Anal. Chem.* **2003**, *75*, 9265–9271.
(66) Huang, J.; Song, Z.; Li, J.; Yang, Y.; Shi, H.; Wu, B.; Anzai, J.; Osa, T.; Chen, Q. *Mater. Sci. Eng. C* **2007**, *27*, 29–34.
(67) Cui, X.; Li, C. M.; Zang, J.; Yu, S. *Biosens. Bioelectron.* **2007**, *22*, 3288–3292.
(68) Huang, J.; Li, J.; Yang, Y.; Wang, X.; Wu, B.; Anzai, J.; Osa, T.; Chen, Q. *Mater. Sci. Eng. C* **2008**, *28*, 1070–1075.
(69) Male, K. B.; Hrapovic, S.; Luong, J. H. T. *Analyst* **2007**, *132*, 1254–1261.
(70) Yamamoto, K.; Shi, G.; Zhou, T.; Xu, F.; Xu, J.; Kato, T.; Jin, J.-Y.; Jin, L. *Analyst* **2003**, *128*, 249–254.
(71) Rubianes, M.; Rivas, G. *Electroanalysis* **2005**, *17*, 73–78.
(72) Fortier, G.; Vaillancourt, M.; Bélanger, D. *Electroanalysis* **1992**, *4*, 275–283.
(73) Harrison, D. J.; Turner, R. F.; Baltes, H. P. *Anal. Chem.* **1988**, *60*, 2002–2007.
(74) Manowitz, P.; Stoecker, P. W.; Yacynych, a M. *Biosens. Bioelectron.* **1995**, *10*, 359–370.
(75) Vaidya, R.; Atanasov, P.; Wilkins, E. *Med. Eng. Phys.* **1995**, *17*, 416–424.
(76) Wang, J.; Tuzhi, P. *Anal. Chem.* **1986**, *58*, 3257–3261.
(77) Aydın, G.; Çelebi, S.; Özyörük, H.; Yıldız, A. *Sensors Actuators B …* **2002**, *87*, 8–12.
(78) Ges, I. A.; Baudenbacher, F. *Biosens. Bioelectron.* **2010**, *26*, 828–833.
(79) Haccoun, J.; Piro, B.; Tran, L. D.; Dang, L. a.; Pham, M. C. *Biosens. Bioelectron.* **2004**, *19*, 1325–1329.

(80) Kataky, R.; Zawawi, R. M. *Phys. Chem. Chem. Phys.* **2010**, *12*, 9183–9187.
(81) Palmisano, F.; Benedetto, G. De; Zambonin, C. *Analyst* **1997**, *122*, 365–369.
(82) Birss, V. I.; Elzanowska, H.; Turner, R. A. *Can. J. Chem.* **1988**, *66*, 86–96.
(83) Xiao, Y.; Patolsky, F.; Katz, E.; Hainfeld, J. F.; Willner, I. *Science (80-.).* **2003**, *299*, 1877–1881.
(84) Jacobs, C. B.; Peairs, M. J.; Venton, B. J. *Anal. Chim. Acta* **2010**, *662*, 105–127.
(85) Vashist, S. K.; Zheng, D.; Al-Rubeaan, K. *Biotechnol. Adv.* **2011**, *29*, 169–188.
(86) Yáñez-Sedeño, P.; Pingarrón, J. M.; Riu, J.; Rius, F. X. *Trends Anal. Chem.* **2010**, *29*, 939–953.
(87) Lin, Y.; Lu, F.; Tu, Y.; Ren, Z. *Nano Lett.* **2004**, *4*, 191–195.
(88) Balasubramanian, K.; Burghard, M. *Anal. Bioanal. Chem.* **2006**, *385*, 452–468.
(89) Katz, E.; Willner, I. *ChemPhysChem* **2004**, *5*, 1084–1104.
(90) Patolsky, F.; Weizmann, Y.; Willner, I. *Angew. Chem. Int. Ed.* **2004**, *43*, 2113–2117.
(91) Luong, J. H. T.; Hrapovic, S.; Wang, D.; Bensebaa, F.; Simard, B. *Electroanalysis* **2004**, *16*, 132–139.
(92) Gutierrez, F.; Rubianes, M. D.; Rivas, G. A. *Sens. Actuators, B* **2012**, *161*, 191–197.
(93) Janegitz, B. C.; Pauliukaite, R.; Ghica, M. E.; Brett, C. M. A.; Fatibello-Filho, O. *Sens. Actuators, B* **2011**, *158*, 411–417.
(94) Deng, C.; Chen, J.; Nie, Z.; Si, S. *Biosens. Bioelectron.* **2010**, *26*, 213–219.
(95) Ivnitski, D.; Branch, B.; Atanassov, P.; Apblett, C. *Electrochem. Commun.* **2006**, *8*, 1204–1210.
(96) Deng, C.; Chen, J.; Chen, X.; Xiao, C.; Nie, L.; Yao, S. *Biosens. Bioelectron.* **2008**, *23*, 1272–1277.
(97) Wang, Y.; Yuan, R.; Chaia, Y.; Li, W.; Zhuo, Y.; Yuan, Y.; Li, J. *J. Mol. Catal. B Enzym.* **2011**, *71*, 146–151.
(98) Zhao, H.-Z.; Sun, J.-J.; Song, J.; Yang, Q.-Z. *Carbon N. Y.* **2010**, *48*, 1508–1514.
(99) Jose, M. V.; Marx, S.; Murata, H.; Koepsel, R. R.; Russell, A. J. *Carbon N. Y.* **2012**, *50*, 4010–4020.
(100) Wilson, R.; Turner, A. P. F. *Biosens. Bioelectron.* **1992**, *7*, 165–185.
(101) Honeychurch, M. J.; Ridd, M. J. *Electroanalysis* **1996**, *8*, 362–369.
(102) Kamal, M. M.; Elzanowska, H.; Gaur, M.; Kim, D.; Birss, V. I. *J. Electroanal. Chem.* **1991**, *318*, 349–367.
(103) Wei, H.; Omanovic, S. *Chem. Biodivers.* **2008**, *5*, 1622–1639.
(104) Verghagen, M. F. J. M.; Hagen, W. R. *J. Electroanal. Chem.* **1992**, *334*, 339–350.
(105) Wei, H. Z.; van de Ven, T. G. M.; Omanovic, S.; Zeng, Y. W. *Langmuir* **2008**, *24*, 12375–12384.
(106) Wang, Y.; Zhu, G.; Wang, E. *Anal. Chim. Acta* **1997**, 97–101.
(107) Garjonyte, R.; Malinauskas, A.; Gorton, L. *Bioelectrochem.* **2003**, *61*, 39–49.
(108) Shinohara, H.; Gratzel, M. *Bioelectrochem. Bioenerg.* **1991**, *26*, 307–320.
(109) Gorton, L.; Johansson, G. *J. Electroanal. Chem.* **1980**, *113*, 151–158.
(110) Miyawaki, O.; Wingard, L. B. J. *Biotechnol. Bioeng.* **1984**, *26*, 1364–1371.
(111) Nejadnik, M. R.; Deepak, F. L.; Garcia, C. D. *Electroanalysis* **2011**, *23*, 1462–1469.
(112) Birss, V. I.; Guha-Thakurta, S.; McGarvey, C. E.; Quach, S.; Vanysek, P. *J. Electroanal. Chem.* **1997**, *423*, 13–21.
(113) Bard, A. J.; Faulkner, L. R. *Electrochemical methods: Fundamentals and applications*; 2nd Ed.; John Wiley and Sons: New York, 2001.
(114) Laviron, E. *J. Electroanal. Chem.* **1979**, *100*, 263–270.
(115) Laviron, E. *J. Electroanal. Chem.* **1974**, *52*, 395–402.
(116) Clark, R. A.; Bowden, E. F. *Langmuir* **1997**, *13*, 559–565.
(117) Stiles, R. L.; Balasubramanian, R.; Feldberg, S. W.; Murray, R. W. *J. Am. Chem. Soc.* **2008**, *130*, 1856–1865.
(118) Laviron, E. *J. Electroanal. Chem.* **1979**, *101*, 19–28.
(119) Feldberg, S. W. *J. Electroanal. Chem.* **2008**, *624*, 45–51.
(120) Feldberg, S. W.; Rubinstein, I. *J. Electroanal. Chem.* **1988**, *240*, 1–15.
(121) Goran, J. M.; Lyon, J. L.; Stevenson, K. J. *Anal. Chem.* **2011**, *83*, 8123–8129.

(122) Wang, Y.; Yao, Y. *Microchim. Acta* **2012**, *176*, 271–277.
(123) McCreery, R. L. *Chem. Rev.* **2008**, *108*, 2646–2687.
(124) Gooding, J. J. *Electrochim. Acta* **2005**, *50*, 3049–3060.
(125) Rao, C. N. R.; Satishkumar, B. C.; Govindaraj, A.; Nath, M. *ChemPhysChem* **2001**, *2*, 78–105.
(126) Merkoçi, A.; Pumera, M.; Llopis, X.; Pérez, B.; del Valle, M.; Alegret, S. *Trends Anal. Chem.* **2005**, *24*, 826–838.
(127) Willner, I.; Yan, Y.-M.; Willner, B.; Tel-Vered, R. *Fuel Cells (Weinheim, Ger.)* **2009**, *9*, 7–24.
(128) Meredith, M. T.; Minteer, S. D. *Annu. Rev. Anal. Chem.* **2012**, *5*, 157–179.
(129) Ksenzhek, O.; Petrova, S. *Bioelectrochem. Bioenerg.* **1983**, *11*, 105–127.
(130) Tzedakis, T.; Cheikhou, K.; Jerôme, R.; Karine, G. S.; Olivier, R. *Electrochim. Acta* **2010**, *55*, 2286–2294.
(131) Ashok Kumar, S.; Lo, P.-H.; Chen, S.-M. *Nanotechnology* **2008**, *19*, 255501.
(132) Salimi, A.; Noorbakhsh, A.; Semnani, A. *J. Solid State Electrochem.* **2011**, *15*, 2041–2052.
(133) Yamashita, M.; Rosatto, S. S.; Kubota, L. T. *J. Braz. Chem. Soc.* **2002**, *13*, 635–641.
(134) Marafon, E.; Kubota, L. T.; Gushikem, Y. *J. Solid State Electrochem.* **2009**, *13*, 377–383.
(135) Salimi, A.; Hallaj, R.; Mamkhezri, H.; Hosaini, S. M. T. *J. Electroanal. Chem.* **2008**, *619-620*, 31–38.
(136) Kumar, S. A.; Chen, S.-M. *Sens. Actuators, B* **2007**, *123*, 964–977.
(137) Li, Y.; Umasankar, Y.; Chen, S.-M. *Talanta* **2009**, *79*, 486–492.
(138) Li, T.; Lin, C.; Balamurugan, A.; Kung, C. *Anal. Chim. Acta* **2012**, *737*, 55–63.
(139) Ivanova, Y. N.; Karyakin, A. a. *Electrochem. Commun.* **2004**, *6*, 120–125.
(140) Karyakin, A. A.; Ivanova, Y. N.; Revunova, K. V; Karyakina, E. E. *Anal. Chem.* **2004**, *76*, 2004–2009.
(141) Miyawaki, O.; Wingard, L. B. J. *Biochim. Biophys. Acta* **1985**, *838*, 60–68.
(142) Wei, H.; Tan, H.; Zeng, Y. *Phys. Chem. Liq.* **2010**, *48*, 708–722.
(143) Liang, W.; Zhuobin, Y. *Sensors* **2003**, *3*, 544–554.
(144) Xue, C.-H.; Zhou, R.-J.; Shi, M.-M.; Wu, G.; Zhang, X.-B.; Wang, M.; Chen, H.-Z. *J. Electroanal. Chem.* **2010**, *642*, 92–97.
(145) Abiman, P.; Crossley, A.; Wildgoose, G. G.; Jones, J. H.; Compton, R. G. *Langmuir* **2007**, 7847–7852.
(146) Heald, C. G. R.; Wildgoose, G. G.; Jiang, L.; Jones, T. G. J.; Compton, R. G. *ChemPhysChem* **2004**, *5*, 1794–1799.
(147) Goran, J. M.; Mantilla, S. M.; Stevenson, K. J. *Anal. Chem.* **2013**, *85*, 1571–1581.
(148) Carrero-Sanchez, J. C.; Elías, a L.; Mancilla, R.; Arrellín, G.; Terrones, H.; Laclette, J. P.; Terrones, M. *Nano Lett.* **2006**, *6*, 1609–1616.
(149) Goran, J. M.; Favela, C. A.; Stevenson, K. J. *Anal. Chem.* **2013**, *85*, 9135–9141.
(150) Holloway, A. F.; Craven, D. a.; Xiao, L.; Campo, J. Del; Wildgoose, G. G. *J. Phys. Chem. C* **2008**, *112*, 13729–13738.
(151) Brunauer, S.; Emmett, P.; Teller, E. *J. Am. Chem. Soc.* **1938**, *60*, 309–319.
(152) Vijayaraghavan, G.; Stevenson, K. J. *Langmuir* **2007**, *23*, 5279–5282.
(153) Lin, C.; Zhang, R. *J. Phys. Chem. C* **2007**, *111*, 4069–4073.
(154) Banks, C. E.; Compton, R. G. *Analyst* **2006**, *131*, 15–21.
(155) Robinson, R.; Sternitzke, K.; McDermott, M.; McCreery, R. *J. Electrochem. Soc.* **1991**, *138*, 2412–2418.
(156) Lowe, H. J.; Clark, W. M. *J. Biol. Chem.* **1956**, *221*, 983–992.
(157) Müller, F. *Chemistry and Biochemistry of Flavoenzymes*; Volume 1.; CRC Press: Boca Raton, 1991.
(158) Zhang, J.; Chi, Q.; Dong, S.; Wang, E. *J. Chem. Soc. Faraday Trans.* **1996**, *92*, 1913.
(159) Lobo, M.; Miranda, A.; Tuñón, P. *Electroanalysis* **2005**, *9*, 191–202.
(160) Radoi, A.; Compagnone, D. *Bioelectrochemistry* **2009**, *76*, 126–134.

(161) Wang, J. *Electroanalysis* **2005**, *17*, 7–14.
(162) Katakis, I.; Domínguez, E. *Microchim. Acta* **1997**, *32*, 11–32.
(163) Barton, S. C.; Gallaway, J.; Atanassov, P. *Chem. Rev.* **2004**, *104*, 4867–4886.
(164) Gorton, L.; Domínguez, E. *Rev. Mol. Biotechnol.* **2002**, *82*, 371–392.
(165) Gründig, B.; Wittstock, G.; Rüdel, U.; Strehlitz, B. *J. Electroanal. Chem.* **1995**, *395*, 143–157.
(166) Wang, J.; Angnes, L.; Martinez, T. *Bioelectrochemistry Bioenerg.* **1992**, *29*, 215–221.
(167) Chen, J.; Bao, J.; Cai, C.; Lu, T. *Anal. Chim. Acta* **2004**, *516*, 29–34.
(168) Filip, J.; Sefčovičová, J.; Tomčík, P.; Gemeiner, P.; Tkac, J. *Talanta* **2011**, *84*, 355–361.
(169) Zhang, M.; Smith, A.; Gorski, W. *Anal. Chem.* **2004**, *76*, 5045–5050.
(170) Zhu, L.; Zhai, J.; Yang, R.; Tian, C.; Guo, L. *Biosens. Bioelectron.* **2007**, *22*, 2768–2773.
(171) Radoi, A.; Compagnone, D.; Valcarcel, M. A.; Placidi, P.; Materazzi, S.; Moscone, D.; Palleschi, G. *Electrochim. Acta* **2008**, *53*, 2161–2169.
(172) De Cássia Silva Luz, R.; Damos, F. S.; Tanaka, A. A.; Kubota, L. T.; Gushikem, Y. *Electrochim. Acta* **2008**, *53*, 4706–4714.
(173) Lawrence, N. S.; Wang, J. *Electrochem. Commun.* **2006**, *8*, 71–76.
(174) Zhang, M.; Gorski, W. *J. Am. Chem. Soc* **2005**, *127*, 2058–2059.
(175) Zeng, J.; Wei, W.; Wu, L.; Liu, X.; Liu, K.; Li, Y. *J. Electroanal. Chem.* **2006**, *595*, 152–160.
(176) Li, H.; Wen, H.; Calabrese Barton, S. *Electroanalysis* **2012**, *24*, 398–406.
(177) Narváez Villarrubia, C. W.; Rincón, R. a; Radhakrishnan, V. K.; Davis, V.; Atanassov, P. *ACS Appl. Mater. Interfaces* **2011**, *3*, 2402–2409.
(178) Zhang, M.; Gorski, W. *Anal. Chem.* **2005**, *77*, 3960–3965.
(179) Meredith, M. T.; Giroud, F.; Minteer, S. D. *Electrochim. Acta* **2012**, *72*, 207–214.
(180) Gao, Q.; Sun, M.; Peng, P.; Qi, H.; Zhang, C. *Microchim. Acta* **2010**, *168*, 299–307.
(181) Raj, C. R.; Chakraborty, S. *Biosens. Bioelectron.* **2006**, *22*, 700–706.
(182) Lin, K. C.; Yin, C. Y.; Chen, S. M. *Analyst* **2012**, *137*, 1378–1383.
(183) Mao, X.; Wu, Y.; Xu, L.; Cao, X.; Cui, X.; Zhu, L. *Analyst* **2011**, *136*, 293–298.
(184) Karra, S.; Zhang, M.; Gorski, W. *Anal. Chem.* **2012**, *85*, 1208–1214.
(185) Agüí, L.; Peña-Farfal, C.; Yáñez-Sedeño, P.; Pingarrón, J. M. *Electrochim. Acta* **2007**, *52*, 7946–7952.
(186) You, J.-M.; Jeon, S. *Electrochim. Acta* **2011**, *56*, 10077–10082.
(187) Liu, J.; Tian, S.; Knoll, W. *Langmuir* **2005**, *21*, 5596–5599.
(188) Gasnier, A.; Pedano, M. L.; Gutierrez, F.; Labbé, P.; Rivas, G. A.; Rubianes, M. D. *Electrochim. Acta* **2012**, *71*, 73–81.
(189) Prasannakumar, S.; Manjunatha, R.; Nethravathi, C.; Suresh, G. S.; Rajamathi, M.; Venkatesha, T. V. *J. Solid State Electrochem.* **2012**, *16*, 3189–3199.
(190) Sun, Y.; Ren, Q.; Liu, X.; Zhao, S.; Qin, Y. *Biosens. Bioelectron.* **2013**, *39*, 289–295.
(191) Wooten, M.; Gorski, W. *Anal. Chem.* **2010**, *82*, 1299–1304.
(192) Deng, C.; Chen, J.; Chen, X.; Xiao, C.; Nie, Z.; Yao, S. *Electrochem. Commun.* **2008**, *10*, 907–909.
(193) Pelster, L. N.; Meredith, M. T.; Minteer, S. D. *Electroanalysis* **2012**, *24*, 1011–1018.
(194) Lawrence, N.; Deo, R.; Wang, J. *Electroanalysis* **2005**, *17*, 65–72.
(195) Banks, C. E.; Compton, R. G. *Analyst* **2005**, *130*, 1232–1239.
(196) Moore, R. R.; Banks, C. E.; Compton, R. G. *Anal. Chem.* **2004**, *76*, 2677–2682.
(197) Zhao, L.; He, R.; Rim, K. T.; Schiros, T.; Kim, K. S.; Zhou, H.; Gutiérrez, C.; Chockalingam, S. P.; Arguello, C. J.; Pálová, L.; Nordlund, D.; Hybertsen, M. S.; Reichman, D. R.; Heinz, T. F.; Kim, P.; Pinczuk, A.; Flynn, G. W.; Pasupathy, A. N. *Science (80-.).* **2011**, *333*, 999–1003.
(198) Cline, K.; McDermott, M.; McCreery, R. *J. Phys. Chem.* **1994**, *98*, 5314–5319.
(199) Güell, A. G.; Ebejer, N.; Snowden, M. E.; McKelvey, K.; Macpherson, J. V; Unwin, P. R. *Proc. Natl. Acad. Sci. USA* **2012**, *109*, 11487–11492.
(200) Moiroux, J.; Elving, P. J. *Anal. Chem.* **1978**, *50*, 1056–1062.
(201) Moiroux, J.; Elving, P. J. *Anal. Chem.* **1979**, *51*, 346–350.

(202) Moiroux, J.; Elving, P. J. *J. Am. Chem. Soc.* **1980**, *1337*, 6533–6538.
(203) Blaedel, W.; Jenkins, R. *Anal. Chem.* **1975**, *47*, 1337–1343.
(204) Blankespoor, R.; Miller, L. *J. Electroanal. Chem.* **1984**, *171*, 231–241.
(205) Jaegfeldt, H. *Bioelectrochem. Bioenerg.* **1981**, *128*, 355–370.
(206) Rover, L. J.; Fernandes, J. C.; de Oliveira Neto, G.; Kubota, L. T.; Katekawa, E.; Serrano, S. H. *Anal. Biochem.* **1998**, *260*, 50–55.
(207) Walcarius, A.; Minteer, S. D.; Wang, J.; Lin, Y.; Merkoçi, A. *J. Mater. Chem. B* **2013**, *1*, 4878–4908.
(208) Yang, W.; Ratinac, K. R.; Ringer, S. P.; Thordarson, P.; Gooding, J. J.; Braet, F. *Angew. Chem. Int. Ed.* **2010**, *49*, 2114–2138.
(209) Zhu, Z.; Garcia-Gancedo, L.; Flewitt, A. J.; Xie, H.; Moussy, F.; Milne, W. I. *Sensors* **2012**, *12*, 5996–6022.
(210) Holzinger, M.; Le Goff, A.; Cosnier, S. *Electrochim. Acta* **2012**, *82*, 179–190.
(211) Gorton, L. *J. Chem. Soc. Faraday Trans. 1* **1986**, *82*, 1245–1258.
(212) Neto, S. A.; Almeida, T. *Electroanalysis* **2013**, *25*, 2394–2402.
(213) Gao, Q.; Sun, M.; Peng, P.; Qi, H.; Zhang, C. *Microchim. Acta* **2010**, *168*, 299–307.
(214) De Assis dos Santos Silva, F.; Lopes, C. B.; de Oliveira Costa, E.; Lima, P. R.; Kubota, L. T.; Goulart, M. O. F. *Electrochem. Commun.* **2010**, *12*, 450–454.
(215) Kumar, S.; Chen, S. *Sensors* **2008**, *8*, 739–766.
(216) Du, P.; Liu, S.; Wu, P.; Cai, C. *Electrochim. Acta* **2007**, *53*, 1811–1823.
(217) Moehlenbrock, M. J.; Meredith, M. T.; Minteer, S. D. *ACS Catal.* **2012**, *2*, 17–25.
(218) Hoshino, T.; Sekiguchi, S.; Muguruma, H. *Bioelectrochemistry* **2012**, *84*, 1–5.
(219) Kowalewska, B.; Kulesza, P. J. *Anal. Chem.* **2012**, *84*, 9564–9571.
(220) Villarrubia, C. W. N.; Garcia, S. O.; Lau, C.; Atanassov, P. *ECS J. Solid State Sci. Technol.* **2013**, *2*, M3156–M3159.
(221) Liu, S.; Cai, C. *J. Electroanal. Chem.* **2007**, *602*, 103–114.
(222) Tsai, Y.-C.; Chen, S.-Y.; Liaw, H.-W. *Sensors Actuators B Chem.* **2007**, *125*, 474–481.
(223) Meng, L.; Wu, P.; Chen, G.; Cai, C.; Sun, Y.; Yuan, Z. *Biosens. Bioelectron.* **2009**, *24*, 1751–1756.
(224) Li, H.; Worley, K. E.; Calabrese Barton, S. *ACS Catal.* **2012**, *2*, 2572–2576.
(225) Aizawa, M.; Coughlin, R.; Charles, M. *Biochim. Biophys. Acta* **1975**, *385*, 362–370.
(226) Zare, H.; Golabi, S. *J. Solid State Electrochem.* **2000**, *4*, 87–94.
(227) Santhiago, M.; Lima, P. R.; Santos, W. D. J. R.; Oliveira, A. B. De; Kubota, L. T. *Electrochim. Acta* **2009**, *54*, 6609–6616.
(228) Saleh, F. S.; Rahman, M. R.; Kitamura, F.; Okajima, T.; Mao, L.; Ohsaka, T. *Electroanalysis* **2011**, *23*, 409–416.
(229) Saleh, F. S.; Okajima, T.; Kitamura, F.; Mao, L.; Ohsaka, T. *Electrochim. Acta* **2011**, *56*, 4916–4923.
(230) Goran, J. M.; Stevenson, K. J. *Langmuir* **2013**, *29*, 13605–13613.
(231) Ciolkosz, M.; Jordan, J. *Anal. Chem.* **1993**, *65*, 164–168.